WESTINGHOUSE CLASS 3 (Non-Proprietary)

Westinghouse Energy Systems

WESTINGHOUSE CLASS 3 (Non-Proprietary)

Westinghouse Energy Systems

WESTINGHOUSE CLASS 3 (NON-PROPRIETARY)

WCAP-13545

ANALYSIS OF CAPSULE X FROM THE TENNESSEE VALLEY AUTHORITY SEQUOYAH UNIT 2 REACTOR VESSEL RADIATION SURVEILLANCE PROGRAM

M .A. Ramirez
S. L. Anderson
A. Madeyski

November 1992

Work Performed Under Shop Order TJIP-S003C

Prepared by Westinghouse Electric Corporation
for the Tennessee Valley Authority

Approved by: T. A. Meyer
T. A. Meyer, Manager
Structural Reliability and
Plant Life Optimization

WESTINGHOUSE ELECTRIC CORPORATION
Nuclear and Advanced Technology Division
P.O. Box 355
Pittsburgh, Pennsylvania 15230-0355

PREFACE

This report has been technically reviewed and verified.

	Reviewer:	
Sections 1 through 5, 7, 8 and	E. Terek	E. Terek
Section 6	E. P. Lippincott	E. Lippincott

TABLE OF CONTENTS

LIST OF TABLES

LIST OF TABLES

LIST OF TABLES

LIST OF ILLUSTRATIONS

SECTION 1.0
SUMMARY OF RESULTS

The analysis of the reactor vessel materials contained in surveillance capsule X, the third capsule to be removed from the Sequoyah Unit 2 reactor pressure vessel, led to the following conclusions:

- The capsule received an average fast neutron fluence (E > 1.0 MeV) of $1.11 \times 10^{19} n/cm^2$ after 5.36 EFPY of plant operation.

- Irradiation of the reactor vessel intermediate shell forging 05 to $1.11 \times 10^{19} n/cm^2$ (E > 1.0 MeV) resulted in 30 ft-lb and 50 ft-lb transition temperature increases of 115°F and 90°F, respectively, for Charpy specimens oriented with the longitudinal axis normal to the major working direction of the forging (axial orientation). This results in a 30 ft-lb transition temperature of 115°F and a 50 ft-lb transition temperature of 150°F for axially oriented specimens.

- Irradiation of the reactor vessel intermediate shell forging 05 Charpy specimens to $1.11 \times 10^{19} n/cm^2$ (E > 1.0 MeV) resulted in 30 ft-lb and 50 ft-lb transition temperature increases of 105°F and 95°F, respectively, for Charpy specimens oriented with the longitudinal axis parallel to the major working direction of the forging (tangential orientation). This results in a 30 ft-lb transition temperature of 35°F and a 50 ft-lb transition temperature of 70°F for tangentially oriented specimens.

- The weld metal Charpy specimens irradiated to $1.11 \times 10^{19} n/cm^2$ (E > 1.0 MeV) resulted in 30 ft-lb and 50 ft-lb transition temperature increases of 55°F and 75°F, respectively. This results in a 30 ft-lb transition temperature of -20°F and a 50 ft-lb transition temperature of 35°F for the weld metal.

- Irradiation of the reactor vessel weld Heat-Affected-Zone (HAZ) metal Charpy specimens to $1.11 \times 10^{19} n/cm^2$ ($E > 1.0$ MeV) resulted in 30 and 50 ft-lb transition temperature increases of 25°F and 35°F, respectively. This results in a 30 ft-lb transition temperature of -35°F and a 50 ft-lb transition temperature of 5°F for the weld HAZ metal.

- The average upper shelf energy of intermediate shell forging 05 (axial orientation) resulted in an energy decrease of 2 ft-lb after irradiation to $1.11 \times 10^{19} n/cm^2$ ($E > 1.0$ MeV). This results in an upper shelf energy of 86 ft-lb for axially oriented specimens.

- The average upper shelf energy of intermediate shell forging 05 (tangential orientation) resulted in an energy decrease of 11 ft-lb after irradiation to $1.11 \times 10^{19} n/cm^2$ ($E > 1.0$ MeV). This results in an upper shelf energy of 123 ft-lb for tangentially oriented specimens.

- The average upper shelf energy of the weld metal decreased 39 ft-lb after irradiation to $1.11 \times 10^{19} n/cm^2$ ($E > 1.0$ MeV). This results in an upper shelf energy of 73 ft-lb for the weld metal.

- The average upper shelf energy of the weld HAZ metal decreased 23 ft-lb after irradiation to $1.11 \times 10^{19} n/cm^2$ ($E > 1.0$ MeV). This results in an upper shelf energy of 99 ft-lb for the weld HAZ metal.

- Comparison of the 30 ft-lb transition temperature increases for the Sequoyah Unit 2 Capsule X surveillance material with predicted increases using the methods of NRC Regulatory Guide 1.99, Revision 2, demonstrated that the weld metal transition temperature increase of 55°F was lower than predicted. However, the intermediate shell forging 05 transition temperature increases of 115°F and 105°F for axially and tangentially oriented specimens, respectively, were greater than predicted. NRC Regulatory Guide

1.99, Revision 2, requires a 2 sigma allowance of 34°F, for base metal, to be added to the predicted reference transition temperature to obtain a conservative upper bound value. Thus, the reference transition temperature increases for the intermediate shell forging 05 material are bounded by the 2 sigma allowance for shift prediction.

o The surveillance capsule materials exhibit a more than adequate upper shelf energy level for continued safe plant operation and are expected to maintain an upper shelf energy of no less than 50 ft-lb throughout the life (32 EFPY) of the vessel as required by 10CFR50, Appendix G.

o The calculated end-of-life (32 EFPY) maximum neutron fluence (E > 1.0 MeV) for the Sequoyah Unit 2 reactor vessel is as follows:

Vessel inner radius * - 1.94×10^{19} n/cm^2
Vessel 1/4 thickness - 1.02×10^{19} n/cm^2
Vessel 3/4 thickness - 2.03×10^{18} n/cm^2

* Clad/base metal interface

SECTION 2.0
INTRODUCTION

This report presents the results of the examination of Capsule X, the third capsule to be removed from the reactor in the continuing surveillance program which monitors the effects of neutron irradiation on the Sequoyah Unit 2 reactor pressure vessel materials under actual operating conditions.

The surveillance program for the Sequoyah Unit 2 reactor pressure vessel materials was designed and recommended by the Westinghouse Electric Corporation. A description of the surveillance program and the preirradiation mechanical properties of the reactor vessel materials is presented in WCAP-8513 entitled "Tennessee Valley Authority Sequoyah Unit No. 2 Reactor Vessel Radiation Surveillance Program"[1]. The surveillance program was planned to cover the 40-year design life of the reactor pressure vessel and was based on ASTM E185-73, "Standard Recommended Practice for Surveillance Tests for Nuclear Reactor Vessels". Westinghouse Power Systems personnel were contracted to aid in the preparation of procedures for removing capsule "X" from the reactor and its shipment to the Westinghouse Science and Technology Center Hot Cell Facility, where, the postirradiation mechanical testing of the Charpy V-notch impact and tensile surveillance specimens was performed.

This report summarizes the testing of and the postirradiation data obtained from surveillance capsule "X" removed from the Sequoyah Unit 2 reactor vessel and discusses the analysis of the data.

SECTION 3.0
BACKGROUND

The ability of the large steel pressure vessel containing the reactor core and its primary coolant to resist fracture constitutes an important factor in ensuring safety in the nuclear industry. The beltline region of the reactor pressure vessel is the most critical region of the vessel because it is subjected to significant fast neutron bombardment. The overall effects of fast neutron irradiation on the mechanical properties of low alloy, ferritic pressure vessel steels such as SA508 Class 2 forging (base material of the Sequoyah Unit 2 reactor pressure vessel beltline) are well documented in the literature. Generally, low alloy ferritic materials show an increase in hardness and tensile properties and a decrease in ductility and toughness under certain conditions of irradiation.

A method for performing analyses to guard against fast fracture in reactor pressure vessels has been presented in "Protection Against Nonductile Failure," Appendix G to Section III of the ASME Boiler and Pressure Vessel Code[4]. The method uses fracture mechanics concepts and is based on the reference nil-ductility temperature (RT_{NDT}).

RT_{NDT} is defined as the greater of either the drop weight nil-ductility transition temperature (NDTT per ASTM E-208) or the temperature 60°F less than the 50 ft-lb (and 35-mil lateral expansion) temperature as determined from Charpy specimens oriented normal (axial) to the major working direction of the forging. The RT_{NDT} of a given material is used to index that material to a reference stress intensity factor curve (K_{IR} curve) which appears in Appendix G to the ASME Code. The K_{IR} curve is a lower bound of dynamic, crack arrest, and static fracture toughness results obtained from several heats of pressure vessel steel. When a given material is indexed to the K_{IR} curve, allowable stress intensity factors can be obtained for this material as a function of temperature. Allowable operating limits can then be determined using these allowable stress intensity factors.

RT_{NDT} and, in turn, the operating limits of nuclear power plants can be adjusted to account for the effects of radiation on the reactor vessel material properties. The radiation embrittlement changes in mechanical properties of a given reactor pressure vessel steel can be monitored by a reactor vessel surveillance program, such as the Sequoyah Unit 2 Reactor Vessel Radiation Surveillance Program[1], in which a surveillance capsule is periodically removed from the operating nuclear reactor and the encapsulated specimens tested. The increase in the average Charpy V-notch 30 ft-lb temperature (ΔRT_{NDT}) due to irradiation is added to the original RT_{NDT} to adjust the RT_{NDT} for radiation embrittlement. This adjusted RT_{NDT} (RT_{NDT} initial + ΔRT_{NDT}) is used to index the material to the K_{IR} curve and, in turn, to set operating limits for the nuclear power plant which take into account the effects of irradiation on the reactor vessel materials.

SECTION 4.0
DESCRIPTION OF PROGRAM

Eight surveillance capsules for monitoring the effects of neutron exposure on the Sequoyah Unit 2 reactor pressure vessel core region material were inserted in the reactor vessel prior to initial plant start-up. The eight capsules were positioned in the reactor vessel between the thermal shield and the vessel wall at locations shown in Figure 4-1. The vertical center of the capsules is opposite the vertical center of the core.

Capsule X was removed after 5.36 Effective Full Power Years (EFPY) of plant operation. This capsule contained test specimens removed from sections of the 8-1/2-inch-thick intermediate shell forging 05, representative weld metal, and heat-affected-zone (HAZ) metal. The test specimens included forty-four Charpy V-notch, four tensile, and four WOL specimens (Figure 4-2) from the intermediate shell forging 05, heat no. 288757/981057, weldment made from sections of forging 05 and adjoining lower shell course forging 04 using weld representative of that used in the original fabrication and forging 05 HAZ metal supplied by Rotterdam Dockyard Company.

The test material was obtained from the intermediate shell course forging 05 after thermal heat treatment and forming of the forging. All test specimens were machined from the 1/4 thickness location of the forging after performing a simulated postweld stress-relieving treatment on the test material. The test specimens represented material taken at least one forging thickness from the quenched ends of the forging. The test material was also obtained from a weld and heat-affected zone metal of a stress-relieved weldment which joined sections of the intermediate and lower shell courses. All heat-affected zone specimens were obtained from the weld heat-affected zone of forging 05, heat no. 288757/981057.

Base metal Charpy V-notch impact specimens were machined with the longitudinal axis of the specimen parallel to the major working direction of the forging (tangential orientation) and with the longitudinal axis of the specimen normal to the major working direction (axial orientation). Charpy V-notch specimens from the weld metal were machined with the longitudinal axis of the specimens transverse to the welding direction. The notch was machined such that the direction of crack propagation in the specimen was in the weld direction.

Tensile specimens were machined with the longitudinal axis of the specimen perpendicular to the major working direction of the forging.

The chemistry and heat treatment history of the surveillance material are presented in Tables 4-1 and 4-2, respectively. The chemical analyses reported in Table 4-1 were the results of an independent analysis performed by Westinghouse on the unirradiated surveillance material and an analysis performed by Rotterdam Dockyard Company on the forging material.

Capsule X also contained dosimeter wires of pure iron, copper, nickel, and aluminum-cobalt (cadmium-shielded and unshielded). In addition, cadmium shielded dosimeters of neptunium (Np^{237}) and uranium (U^{238}) were placed in the capsule to measure the integrated flux at specific neutron energy levels.

Thermal monitors made from the two low-melting-point eutectic alloys and sealed in Pyrex tubes were included in the capsule. These thermal monitors were used to define the maximum temperature attained by the test specimens during irradiation. The composition of the two alloys and their melting points are as follows:

2.5% Ag, 97.5% Pb	Melting Point: 579°F (304°C)
1.75% Ag, 0.75% Sn, 97.5% Pb	Melting Point: 590°F (310°C)

Shown in Figure 4-1 is the arrangement of surveillance capsules in the Sequoyah Unit 2 reactor vessel and shown in Figure 2 is the arrangement of the various mechanical specimens, dosimeters and thermal monitors contained in capsule X.

TABLE 4-1

CHEMICAL COMPOSITION OF THE SEQUOYAH UNIT 2
REACTOR VESSEL SURVEILLANCE MATERIAL [1]

Element	Chemical Composition (wt%)		
	Intermediate shell Forging-05		Weld Metal
	(a)	(b)	(a)
C	0.180	0.190	0.950
S	0.018	0.013	0.013
N	0.009	--	0.012
Co	0.001	--	0.001
Cu	0.130	--	0.130
Si	0.270	0.220	0.410
Mo	0.640	0.570	0.530
Ni	0.740	0.780	0.110
Mn	0.720	0.700	1.500
Cr	0.330	0.340	0.085
V	0.022	< 0.010	0.002
P	0.018	0.014	0.016
Sn	0.002	--	0.002
Al	0.027	--	0.009

(a) Results of an analysis performed by Westinghouse.[1]

(b) Results of an analysis performed by Rotterdam Dockyard Analysis.[1]

TABLE 4-2

HEAT TREATMENT HISTORY OF THE SEQUOYAH UNIT 2

REACTOR VESSEL SURVEILLANCE MATERIAL[1]

Material	Temperature (°F)	Time (hrs)	Coolant
Intermediate Shell Forging 05 Heat No. 288757/981057	1675 ± 25	3 1/2	Water Quenched
	1225 ± 25	9	Furnace Cooled to 815°F
	1130 ± 25	20 1/2	Furnace Cooled
Weld metal	1130 ± 25	14 3/4	Furnace Cooled

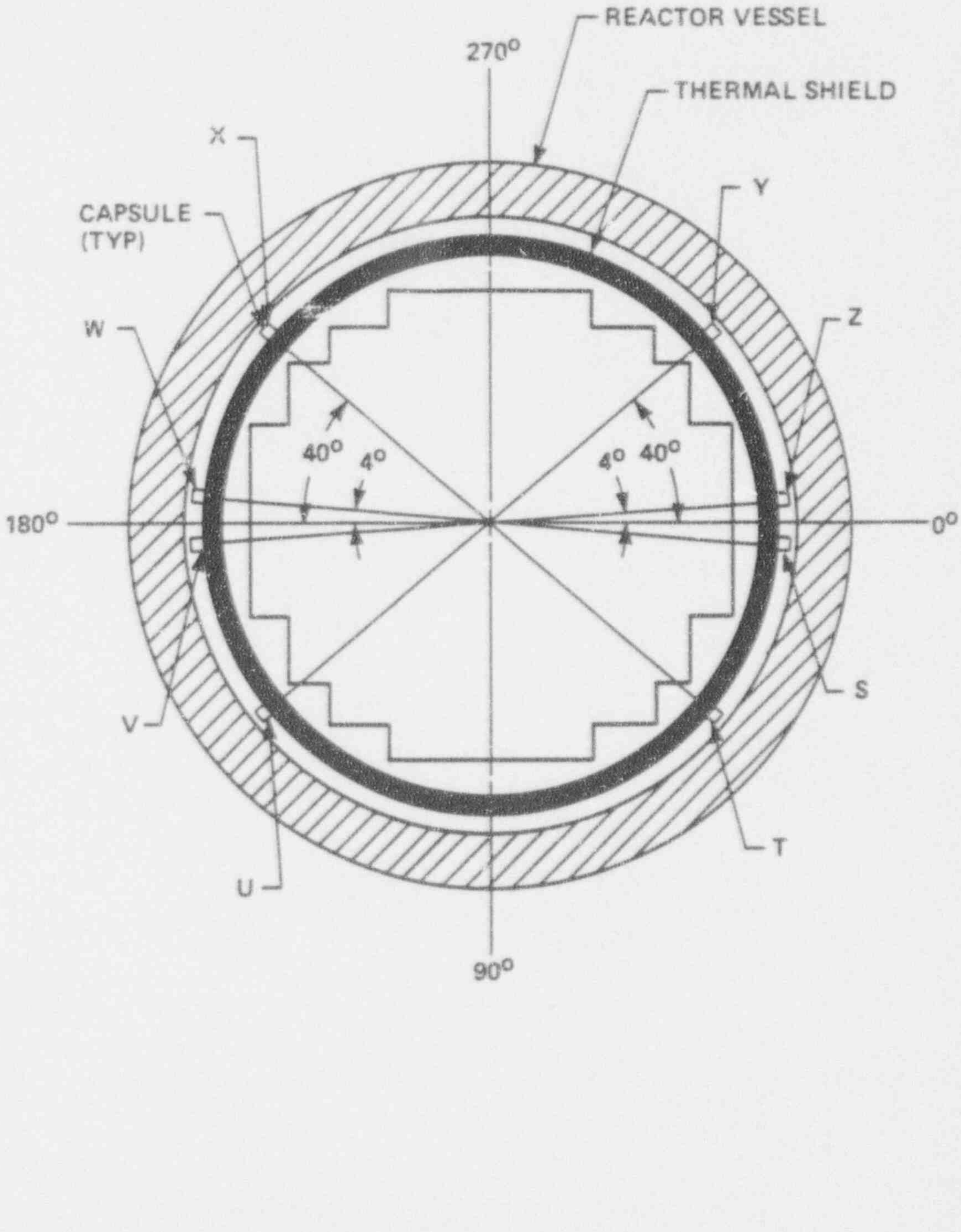

Figure 4-1. Arrangemen' of Surveillance Capsules in the Sequoyah Unit 2 Reactor Vessel

SURVEILLAN

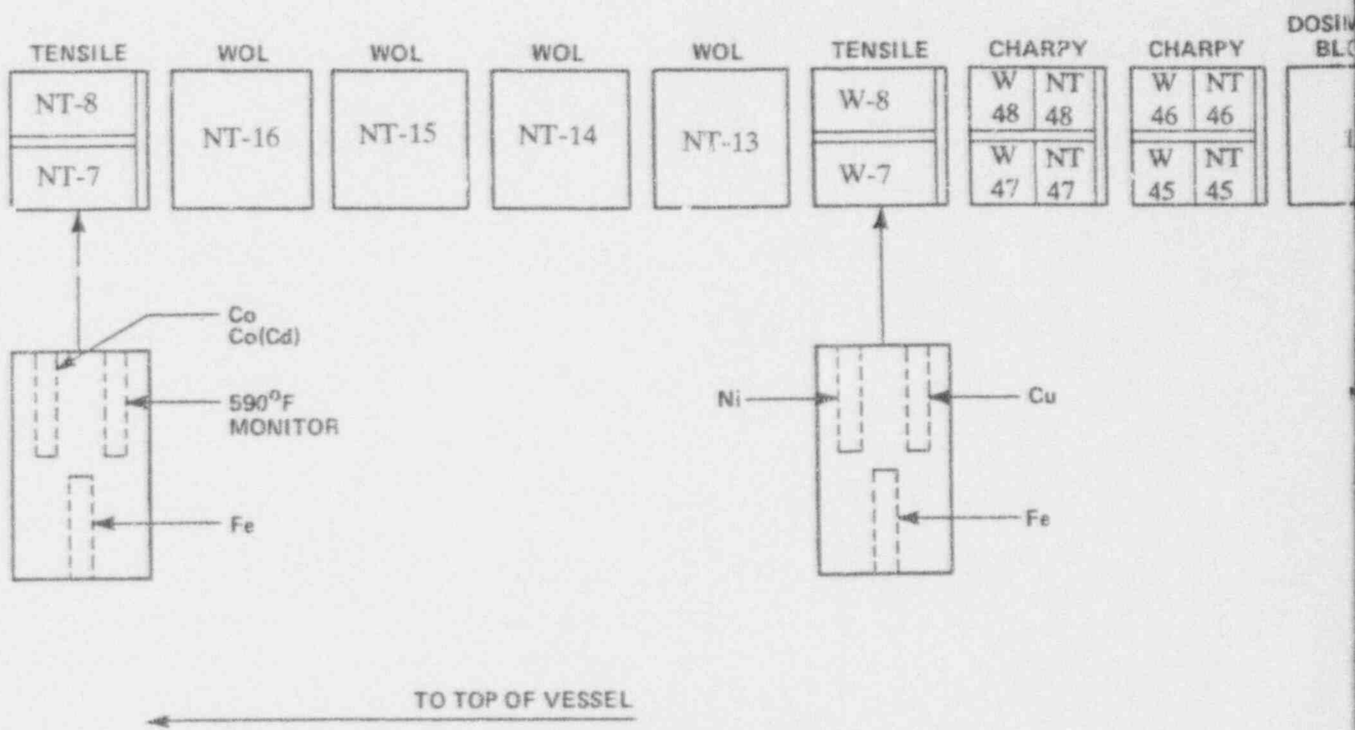

SPECIMEN NUMBERING CODE

NT – FORGING 05 (AXIAL ORIENTATION)
NL – FORGING 05 (TANGENTIAL ORIENTATION)

W = WELD METAL
H = HEAT AFFECTED ZONE

CE CAPSULE X

237

238

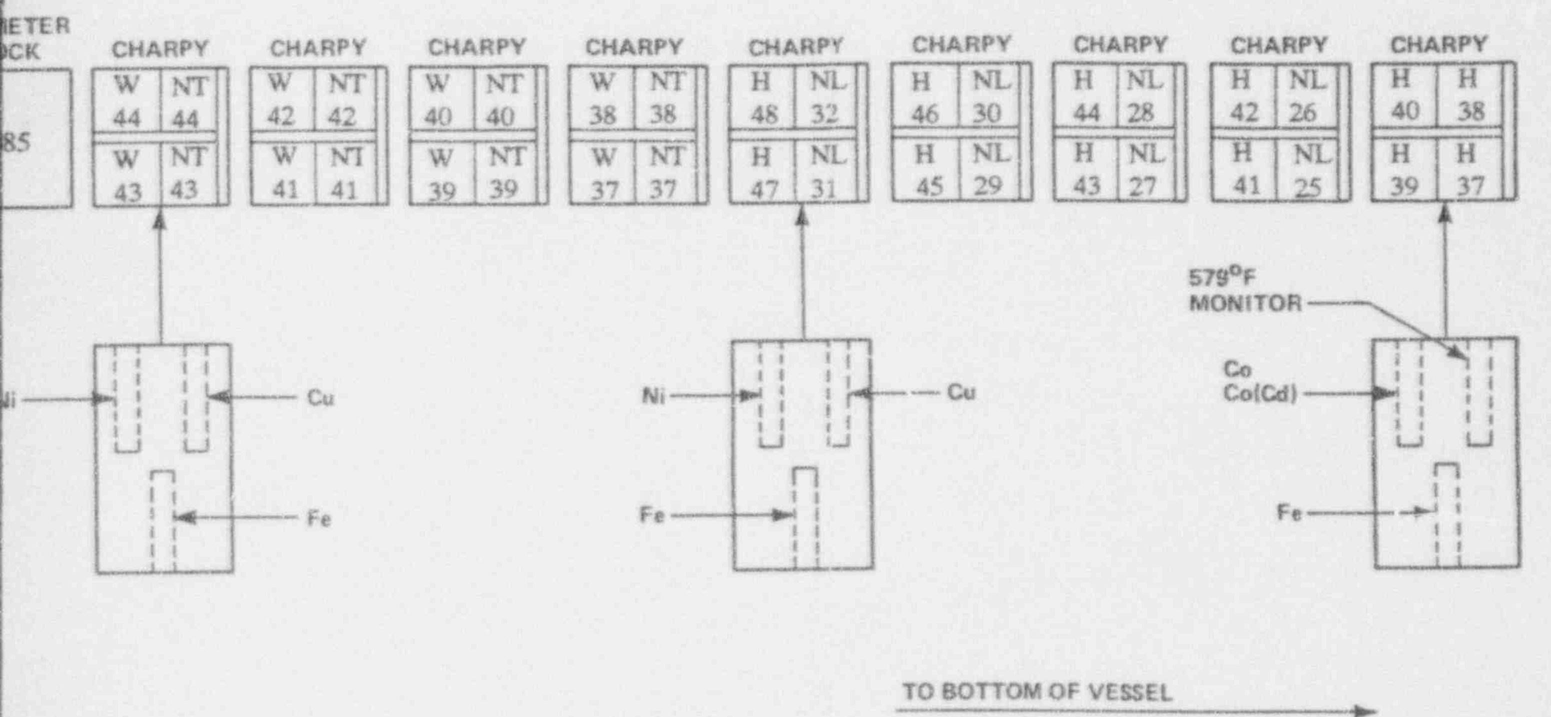

Figure 4-2 Capsule X Diagram Showing Location of Specimens, Thermal Monitors and Dosimeters

The energy at maximum load (E_M) was determined by comparing the energy-time record and the load-time record. The energy at maximum load is approximately equivalent to the energy required to initiate a crack in the specimen. Therefore, the propagation energy for the crack (E_p) is the difference between the total energy to fracture (E_D) and the energy at maximum load.

The yield stress (σ_Y) was calculated from the three-point bend formula having the following expression:

$$\sigma_Y = P_{GY} * \{L/[B*(W-a)^2*C]\} \qquad (1)$$

where L = distance between the specimen supports in the impact testing machine; B = the width of the specimen measured parallel to the notch; W = height of the specimen, measured perpendicularly to the notch; a = notch depth. The constant C is dependent on the notch flank angle (ϕ), notch root radius (ρ), and the type of loading (i.e., pure bending or three-point bending).

In three-point bending a Charpy specimen in which ϕ = 45° and ρ = 0.010", Equation 1 is valid with C = 1.21. Therefore (for L = 4W),

$$\sigma_Y = P_{GY} * \{L/[B*(W-a)^2*1.21]\} = [3.3P_{GY}W]/[B(W-a)^2] \qquad (2)$$

For the Charpy specimens, B = 0.394 in., W = 0.394 in., and a = 0.079 in. Equation 2 then reduces to:

$$\sigma_Y = 33.3 \times P_{GY} \qquad (3)$$

where σ_Y is in units of psi and P_{GY} is in units of lbs. The flow stress was calculated from the average of the yield and maximum loads, also using the three-point bend formula.

Percent shear was determined from post-fracture photographs using the ratio-of-areas methods in compliance with ASTM Specification A370-89[8]. The lateral expansion was measured using a dial gage rig similar to that shown in the same specification.

SECTION 5.0
TESTING OF SPECIMENS FROM CAPSULE X

5.1 Overview

The post-irradiation mechanical testing of the Charpy V-notch and tensile specimens was performed at the Westinghouse Science and Technology Center Remote Metallographic Facility (RMF). Testing was performed in accordance with 10CFR50, Appendices G and H[2], ASTM Specification E185-82[6], and Westinghouse RMF Procedure 8402, Revision 2 as modified by Westinghouse RMF Procedures 8102, Revision 1 and 8103, Revision 1.

Upon receipt of the capsule at the laboratory, the specimens and spacer blocks were carefully removed, inspected for identification number, and checked against the master list in WCAP-8513[1]. No discrepancies were found.

Examination of the two low-melting point 579°F (304°C) and 590°F (310°C) eutectic alloys indicated no melting of either type of thermal monitor. Based on this examination, the maximum temperature to which the test specimens were exposed was less than 579°F (304°C).

The Charpy impact tests were performed per ASTM Specification E23-88[7] and RMF Procedure 8103, Revision 1, on a Tinius-Olsen Model 74, 358J machine. The tup (striker) of the Charpy machine is instrumented with a GRC 830I instrumentation system feeding information into an IBM XT computer. With this system, load-time and energy-time signals can be recorded in addition to the standard measurement of Charpy energy (E_D). From the load-time curve (Appendix A), the load of general yielding (P_{GY}), the time to general yielding (t_{GY}), the maximum load (P_M), and the time to maximum load (t_M) can be determined. Under some test conditions, a sharp drop in load indicative of fast fracture was observed. The load at which fast fracture was initiated is identified as the fast fracture load (P_F), and the load at which fast fracture terminated is identified as the arrest load (P_A).

Tensile tests were performed on a 20,000-pound Instron Model 1115, split-console test machine, per ASTM Specification E8-89b[9] and E21-79 (1988)[10], and RMF Procedure 8102, Revision 1. The upper pull rod of the test machine was connected through a universal joint to improve axiality of loading. The tests were conducted at a constant crosshead speed of 0.05 inches per minute throughout the test.

Extension measurements were made with a linear variable displacement transducer (LVDT) extensometer. The extensometer knife edges were spring-loaded to the specimen and operated through specimen failure. The extensometer gage length is 1.00 inch. The extensometer is rated as Class B-2 per ASTM E83-85[11].

Elevated test temperatures were obtained with a three-zone electric resistance split-tube furnace with a 9-inch hot zone. All tests were conducted in air.

Because of the difficulty in remotely attaching a thermocouple directly to the specimen, the following procedure was used to monitor specimen temperatures: Chromel-alumel thermocouples were inserted in shallow holes in the center and each end of the gage section of a dummy specimen and in each grip. In the test configuration, with a slight load on the specimen, a plot of specimen temperature versus upper and lower grip and controller temperatures was developed over the range of room temperature to 550°F (288°C). The upper grip was used to control the furnace temperature. During the actual testing the grip temperatures were used to obtain desired specimen temperatures. Experiments indicated that this method is accurate to ± 2°F.

The yield load, ultimate load, fracture load, total elongation, and uniform elongation were determined directly from the load-extension curve. The yield strength, ultimate strength, and fracture strength were calculated using the original cross-sectional area. The final diameter and final gage length were determined from post-fracture photographs. The fracture area used to calculate the fracture stress (true stress at fracture) and percent reduction in area was computed using the final diameter measurement.

5.2 Charpy V-Notch Impact Test Results

The results of the Charpy V-notch impact tests performed on the various materials contained in Capsule X, which was irradiated to 1.11 x 10^{19}n/cm^2 (E > 1.0 MeV), in 5.36 EFPY of operation, are presented in Tables 5-1 through 5-4 and are compared with unirradiated results[1] as shown in Figures 5-1 through 5-4. The transition temperature increases and upper shelf energy decreases for the Capsule X materials are summarized in Table 5-5.

Irradiation of the reactor vessel intermediate shell forging 05 Charpy specimens to 1.11 x 10^{19}n/cm^2 (E > 1.0 MeV) at 550°F (Figure 5-1), oriented with the longitudinal axis of the specimen perpendicular to the major working direction of the forging (axial orientation), resulted in 30 and 50 ft-lb transition temperature increases of 115°F and 90°F, respectively. This resulted in a 30 ft-lb transition temperature of 115°F and a 50 ft-lb transition temperature of 150°F (axial orientation).

The average upper shelf energy (USE) of the intermediate shell forging 05 Charpy specimens (axial orientation) resulted in an energy decrease of 2 ft-lb after irradiation to 1.11 x 10^{19}n/cm^2 (E > 1.0 MeV) at 550°F. This results in an average USE of 86 ft-lb (Figure 5-1).

Irradiation of the reactor vessel intermediate shell forging 05 Charpy specimens to 1.11 x 10^{19}n/cm^2 (E > 1.0 MeV) at 550°F (Figure 5-2), oriented with the longitudinal axis of the specimen parallel to the major working direction of the forging (tangential orientation), resulted in 30 and 50 ft-lb transition temperature increases of 105°F and 95°F, respectively. This resulted in a 30 ft-lb transition temperature of 35°F and a 50 ft-lb transition temperature of 70°F (tangential orientation).

The average upper shelf energy (USE) of the intermediate shell forging 05 Charpy specimens (axial orientation) resulted in an energy decrease of 11 ft-lb after irradiation to $1.11 \times 10^{19} n/cm^2$ (E > 1.0 MeV) at 550°F. This resulted in an average USE of 123 ft-lb (Figure 5-2).

Irradiation of the reactor vessel core region weld metal Charpy specimens to $1.11 \times 10^{19} n/cm^2$ (E > 1.0 MeV) at 550°F (Figure 5-3) resulted in 30 and 50 ft-lb transition temperature increases of 55°F and 75°F, respectively. This resulted in a 30 ft-lb transition temperature of -20°F and a 50 ft-lb transition temperature of 35°F.

The average upper shelf energy (USE) of the reactor vessel core region weld metal resulted in an energy decrease of 39 ft-lb after irradiation to $1.11 \times 10^{19} n/cm^2$ (E > 1.0 MeV) at 550°F. This resulted in an average USE of 73 ft-lb (Figure 5-3).

Irradiation of the reactor vessel weld Heat-Affected-Zone (HAZ) metal specimens to $1.11 \times 10^{19} n/cm^2$ (E > 1.0 MeV) at 550°F (Figure 5-4) resulted in 30 and 50 ft-lb transition temperature increases of 25°F and 35°F, respectively. This resulted in a 30 ft-lb transition temperature of -35°F and a 50 ft-lb transition temperature of 5°F.

The average upper shelf energy (USE) of the reactor vessel weld HAZ metal experienced an energy decrease of 23 ft-lb after irradiation to $1.11 \times 10^{19} n/cm^2$ (E > 1.0 MeV) at 550°F. This resulted in an average USE of 99 ft-lb (Figure 5-4).

The fracture appearance of each irradiated Charpy specimen from the various materials is shown in Figures 5-5 through 5-8 and show an increasing ductile or tougher appearance with increasing test temperature.

A comparison of the 30 ft-lb transition temperature increases and upper shelf energy decreases for the various Sequoyah Unit 2 surveillance materials with predicted values using the methods of NRC Regulatory Guide 1.99, Revision 2[3] is presented in Table 5-6. This comparison demonstrated that the weld metal specimens have a measured transition temperature increase of 55°F which is lower than the predicted value. However, the intermediate shell forging 05 specimens have transition temperature increases of 115°F and 105°F for axially and tangentially oriented specimens, respectively, which are greater than the predicted values. NRC Regulatory Guide 1.99, Revision 2 requires a 2 sigma allowance of 34°F, for base metal, to be added to the predicted reference transition temperature to obtain a conservative upper bound value. Thus, the reference transition temperature increase for the intermediate shell forging 05 material is bounded by the 2 sigma allowance for shift prediction.

The surveillance capsule materials exhibit a more than adequate upper shelf energy level for continued safe plant operation and are expected to maintain an upper shelf energy of no less than 50 ft-lb throughout the life (32 EFPY) of the vessel as required by 10CFR50, Appendix G.

The load-time records for the individual instrumented Charpy specimen tests are shown in Appendix A.

5.3 Tension Test Results

The results of the tension tests performed on the various materials contained in capsule X irradiated to $1.11 \times 10^{19} n/cm^2$ (E > 1.0 MeV) at 550°F are presented in Table 5-7 and are compared with unirradiated results[1] as shown in Figures 5-9 and 5-10.

The results of the tension tests performed on the intermediate shell forging 05 (axial orientation) indicated that irradiation to $1.11 \times 10^{19} n/cm^2$ (E > 1.0 MeV) at 550°F caused a 10 to 14 ksi increase in the 0.2 percent offset yield strength and an 9 to 16 ksi increase in the ultimate tensile strength when compared to unirradiated data[1] (Figure 5-9).

The results of the tension tests performed on the reactor vessel core region weld metal indicated that irradiation to 1.11 x 10^{19}n/cm^2 (E > 1.0 MeV) at 550°F caused an 8 to 11 ksi increase in the 0.2 percent offset yield strength and a 7 to 9 ksi increase in the ultimate tensile strength when compared to unirradiated data[1] (Figure 5-10).

The fractured tension specimens for the intermediate shell forging 05 material are shown in Figures 5-11 , while the fractured specimens for the weld metal are shown in Figure 5-12.

The engineering stress-strain curves for the tension tests are shown in Figures 5-13 through 5-14.

5.4 Wedge Opening Loading (WOL) Tests

Per the surveillance capsule testing program with Tennessee Valley Authority (TVA), the WOL fracture mechanics specimens will not be tested and will be stored at the Westinghouse Science and Technology Center.

TABLE 5-1

CHARPY V-NOTCH IMPACT DATA FOR THE SEQUOYAH UNIT 2
REACTOR VESSEL INTERMEDIATE SHELL FORGING 05
IRRADIATED AT 550°F, FLUENCE 1.11 x 10^{19} n/cm^2 (E > 1.0 MeV)

Sample No.	Temperature (°F)	(°C)	Impact Energy (ft-lb)	(J)	Lateral Expansion (mils)	(mm)	Shear (%)
			Tangential Orientation				
NL32	- 80	(- 62)	4	(5)	5	(0.13)	5
NL29	- 30	(- 34)	5	(7)	6	(0.15)	5
NL31	5	(- 15)	24	(33)	18	(0.46)	10
NL28	50	(10)	43	(58)	36	(0.91)	25
NL25	100	(38)	84	(114)	59	(1.50)	80
NL30	150	(66)	85	(115)	60	(1.52)	95
NL27	250	(121)	120	(163)	81	(2.06)	100
NL26	325	(163)	126	(171)	83	(2.11)	100
			Axial Orientation				
NT42	- 30	(- 34)	7	(9)	5	(0.13)	5
NT40	25	(- 4)	10	(14)	6	(0.15)	10
NT38	50	(10)	21	(28)	18	(0.46)	20
NT45	75	(24)	30	(41)	18	(0.46)	25
NT39	100	(38)	33	(45)	32	(0.81)	30
NT46	125	(52)	43	(58)	37	(0.94)	45
NT41	150	(66)	38	(52)	32	(0.81)	40
NT44	175	(79)	48	(65)	34	(0.86)	65
NT43	200	(93)	52	(71)	40	(1.02)	80
NT47	225	(107)	86	(117)	63	(1.60)	100
NT48	275	(135)	89	(121)	61	(1.55)	100
NT37	325	(163)	84	(114)	54	(1.37)	100

TABLE 5-2

CHARPY V-NOTCH IMPACT DATA FOR THE SEQUOYAH UNIT 2 REACTOR VESSEL WELD METAL AND HEAT-AFFECTED-ZONE (HAZ) METAL IRRADIATED AT 550°F, FLUENCE 1.11 x 10^{19} n/cm^2 (E > 1.0 MeV)

Sample No.	Temperature (°F)	(°C)	Impact Energy (ft-lb)	(J)	Lateral (mils)	Expansion (mm)	Shear (%)
			Weld Metal				
W45	- 90	(- 68)	11	(15)	7	(0.18)	10
W38	- 75	(- 59)	5	(7)	4	(0.10)	5
W47	- 60	(- 51)	17	(23)	14	(0.36)	15
W40	- 50	(- 46)	42	(57)	30	(0.76)	35
W39	- 25	(- 32)	50	(68)	43	(1.09)	50
W48	0	(- 18)	55	(75)	48	(1.22)	60
W37	75	(24)	58	(79)	42	(1.07)	70
W44	100	(38)	22	(30)	19	(0.48)	30
W43	150	(66)	108	(146)	85	(2.16)	100
W42	225	(107)	59	(80)	52	(1.32)	100
W46	250	(121)	58	(79)	50	(1.27)	100
W41	250	(121)	68	(92)	56	(1.42)	100
			HAZ Metal				
H38	- 75	(- 59)	15	(20)	7	(0.18)	15
H40	- 65	(- 54)	19	(26)	15	(0.38)	20
H43	- 50	(- 46)	35	(47)	16	(0.41)	30
H46	- 25	(- 32)	39	(53)	21	(0.53)	40
H47	0	(- 18)	52	(71)	34	(0.86)	45
H45	35	(2)	57	(77)	28	(0.71)	55
H48	75	(24)	109	(148)	60	(1.52)	85
H41	100	(38)	87	(118)	56	(1.42)	80
H37	150	(66)	92	(125)	62	(1.57)	95
H39	185	(85)	73	(99)	55	(1.40)	100
H44	225	(107)	114	(155)	68	(1.73)	100
H42	250	(121)	111	(150)	67	(1.70)	100

TABLE 5-3

INSTRUMENTED CHARPY IMPACT TEST RESULTS FOR THE SEQUOYAH UNIT 2 REACTOR VESSEL INTERMEDIATE SHELL FORGING 05 IRRADIATED AT 550°F, FLUENCE $1.11 \times 10^{19} n/cm^2$ (E > 1.0 MeV)

Sample Number	Test Temp (°F)	Charpy Energy (ft-lb)	Normalized Energies (ft-lb/in²): Charpy Ed/A	Maximum Em/A	Prop. Ep/A	Yield Load (lbs)	Time to Yield (msec)	Maximum Load (lbs)	Time to Maximum (msec)	Fracture Load (lbs)	Arrest Load (lbs)	Yield Stress (ksi)	Flow Stress (ksi)
						Tangential Orientation							
NL32	- 80	4	32	13	19	1987	0.09	2112	0.10	2112	–	66	68
NL29	- 30	5	40	21	19	3086	0.10	3216	0.11	3216	51	103	105
NL31	5	24	193	118	75	3542	0.14	3952	0.33	3802	58	118	124
NL28	50	43	346	246	100	3969	0.23	4747	0.55	4747	196	132	145
NL25	100	84	676	340	337	3351	0.60	4362	1.15	4362	887	111	128
NL30	150	85	684	264	420	2932	0.11	4526	0.66	3971	2321	97	124
NL27	250	120	966	332	635	2858	0.17	4187	0.80	*	*	95	117
NL26	325	126	1015	302	712	3223	0.31	4308	0.79	*	*	107	125
						Axial Orientation							
NT42	- 30	7	56	26	30	3128	0.10	3437	0.13	3437	–	104	109
NT40	25	10	81	26	54	3044	0.12	3161	0.13	3161	146	101	103
NT38	50	21	169	72	97	3507	0.14	4071	0.22	3887	301	116	126
NT45	75	30	242	165	76	3541	0.14	4454	0.38	4454	687	118	133
NT39	100	33	266	199	67	3223	0.13	4341	0.48	4341	493	107	126
NT46	125	43	346	203	143	3145	0.12	4218	0.50	4140	1272	104	122
NT41	150	38	306	185	121	2980	0.11	4363	0.45	4363	1699	99	122
NT44	175	48	387	213	174	314[illegible]	0.13	4259	0.51	4259	2460	104	123
NT43	200	52	419	210	209	3166	0.14	4215	0.52	4215	2662	105	123
NT47	225	86	692	231	462	3508	0.26	4338	0.16	*	*	117	130
NT48	275	89	717	298	419	356	0.28	4233	0.76	*	*	12	76
NT37	325	84	676	246	430	2804	0.20	4175	0.65	*	*	93	116

*Fully ductile fracture. No brittle fracture load and no arrest load.

TABLE 5-4

INSTRUMENTED CHARPY IMPACT TEST RESULTS FOR THE SEQUOYAH UNIT 2 WELD METAL AND HEAT-AFFECTED-ZONE (HAZ) METAL, IRRADIATED AT 550°F, FLUENCE 1.11 x 10^{19} n/cm^2 (E > 1.0 MeV)

Sample Number	Test Temp (°F)	Charpy Energy (ft-lb)	Normalized Energies (ft-lb/in^2) Charpy Ed/A	Maximum Em/A	Prop Ep/A	Yield Load (lbs)	Time to Yield (msec)	Maximum Load (lbs)	Time to Maximum (msec)	Fracture Load (lbs)	Arrest Load (lbs)	Yield Stress (ksi)	Flow Stress (ksi)
Weld Metal													
W45	- 90	11	89	56	33	3956	0.14	4108	0.19	4108	66	131	134
W38	- 75	5	40	22	18	3043	0.11	3185	0.12	3185	58	101	103
W47	- 60	17	137	107	30	3485	0.13	4100	0.30	4100	–	116	126
W40	- 50	42	338	244	94	3632	0.14	4687	0.53	4309	68	121	138
W39	- 25	50	403	217	186	3108	0.12	4321	0.54	3929	169	103	123
W48	0	55	443	304	138	3298	0.14	4432	0.69	2873	85	110	128
W37	75	58	467	328	139	3194	0.21	4401	0.82	4401	1149	106	126
W44	100	22	177	103	74	2970	0.12	3550	0.31	3550	902	99	108
W43	150	108	870	269	600	2710	0.14	4116	0.70	*	*	90	113
W42	225	59	475	179	296	2578	0.10	3902	0.50	*	*	86	108
W46	250	58	467	181	286	3537	0.24	3963	0.48	*	*	117	125
W41	250	68	548	210	337	3084	0.14	3944	0.52	*	*	102	117
HAZ Metal													
H38	- 75	15	121	84	37	4159	0.17	4603	0.23	4603	–	138	146
H40	- 65	19	153	**	**	**	**	**	**	**	**	**	**
H43	- 50	35	282	211	71	3743	0.13	5068	0.44	5068	74	124	146
H46	- 25	39	314	215	99	4315	0.25	4689	0.47	4689	698	143	150
H47	0	52	419	248	171	3835	0.14	4885	0.53	4774	1133	127	145
H45	35	57	459	256	203	3860	0.14	5037	0.54	4901	1760	128	148
H48	75	109	878	344	534	3708	0.14	4862	0.68	3380	2037	123	142
H41	100	87	701	328	373	3468	0.14	4768	0.68	3718	2569	115	137
H37	150	92	741	303	438	3316	0.14	4690	0.69	3211	1083	110	133
H39	185	73	588	221	367	2876	0.12	4092	0.54	*	*	96	116
H44	225	114	918	189	729	2791	0.13	3932	0.52	*	*	93	112
H42	250	111	894	377	517	3129	0.14	4698	0.80	*	*	104	130

*Fully ductile fracture. No arrest load.
**No data. Computer malfunction.

TABLE 5-5

EFFECT OF 550°F IRRADIATION TO 1.11×10^{19} n/cm^2 (E > 1.0 MeV)

ON THE NOTCH TOUGHNESS PROPERTIES OF THE SEQUOYAH UNIT 2 REACTOR VESSEL SURVEILLANCE MATERIALS

	Average 30 ft-lb[1] Transition Temperature (°F)			Average 35 mil[1] Lateral Expansion Temperature (°F)			Average 50 ft-lb[1] Transition Temperature (°F)			Average Energy[1] Absorption at Full Shear (ft-lb)		
Material	Unirradiated	Irradiated	ΔT	Unirradiated	Irradiated	ΔT	Unirradiated	Irradiated	ΔT	Unirradiated	Irradiated	Δ(ft-lb)
Forging 05 (Axial)	0	115	115	20	135	115	60	150	90	88	86	- 2
Forging 05 (Tangential)	-70	35	105	-45	60	105	-25	70	95	134	123	- 11
Weld Metal	- 75	-20	55	-50	-20	30	-40	35	75	112	73	- 39
HAZ Metal	- 60	-35	25	-25	40	65	-30	5	35	122	99	- 23

(1) "AVERAGE" is defined as the value read from the curve fitted through the data points of the Charpy tests (Figures 5-1 through 5-4).

TABLE 5-6

COMPARISON OF THE SEQUOYAH UNIT 2 SURVEILLANCE MATERIAL 30 FT-LB TRANSITION

TEMPERATURE SHIFTS AND UPPER SHELF ENERGY DECREASES WITH REGULATORY GUIDE 1.99 REVISION 2 PREDICTIONS

			30 ft-lb Transition Temp.Shift		Upper Shelf Energy Decrease	
Material	Capsule[b]	Fluence 10^{19} n/cm^2	R.G. 1.99 Rev. 2 (Predicted)[a] (°F)	Measured (°F)	R.G. 1.99 Rev. 2 (Predicted) (%)	Measured (%)
Forging 05	T	0.220	56	25	15	7
(Axial)	U	0.643	83	62	20	9
	X	1.110	98	115	24	2
Forging 05	T	0.220	56	60	15	12
(Tangential)	U	0.643	83	93	20	18
	X	1.110	98	105	24	8
Weld Metal	T	0.220	40	80	19	2
	U	0.643	60	130	24	3
	X	1.110	70	55	30	35
HAZ Metal	T	0.220	--	50	--	2
	U	0.643	--	58	--	14
	X	1.110	--	25	--	19

(a) Mean wt. % values of Cu and Ni were used to calculate the chemistry factors for the forging surveillance material.

(b) Values presented here for capsules T and U were determined based on test results given in References [36] and [37].

TABLE 5-7

TENSILE PROPERTIES OF THE SEQUOYAH UNIT 2 REACTOR VESSEL SURVEILLANCE MATERIALS IRRADIATED AT 550°F TO 1.11 X 10^{19} n/cm^2 (E > 1.0 MeV)

Material	Sample Number	Test Temp. (°F)	0.2% Yield Strength (ksi)	Ultimate Strength (ksi)	Fracture Load (kip)	Fracture Stress (ksi)	Fracture Strength (ksi)	Uniform Elongation (%)	Total Elongation (%)	Reduction in Area (%)
Forging 05, Heat No. 388757/981057, (Axial)	NT7	115	74.9	94.7	3.30	189.5	67.2	10.5	20.0	65
	NT8	550	65.2	91.7	4.01	146.3	81.6	9.6	12.7	44
Weld	W7	50	73.3	89.1	2.90	194.5	59.1	10.5	21.9	70
	W8	550	66.2	82.5	2.96	186.3	60.3	7.5	17.3	68

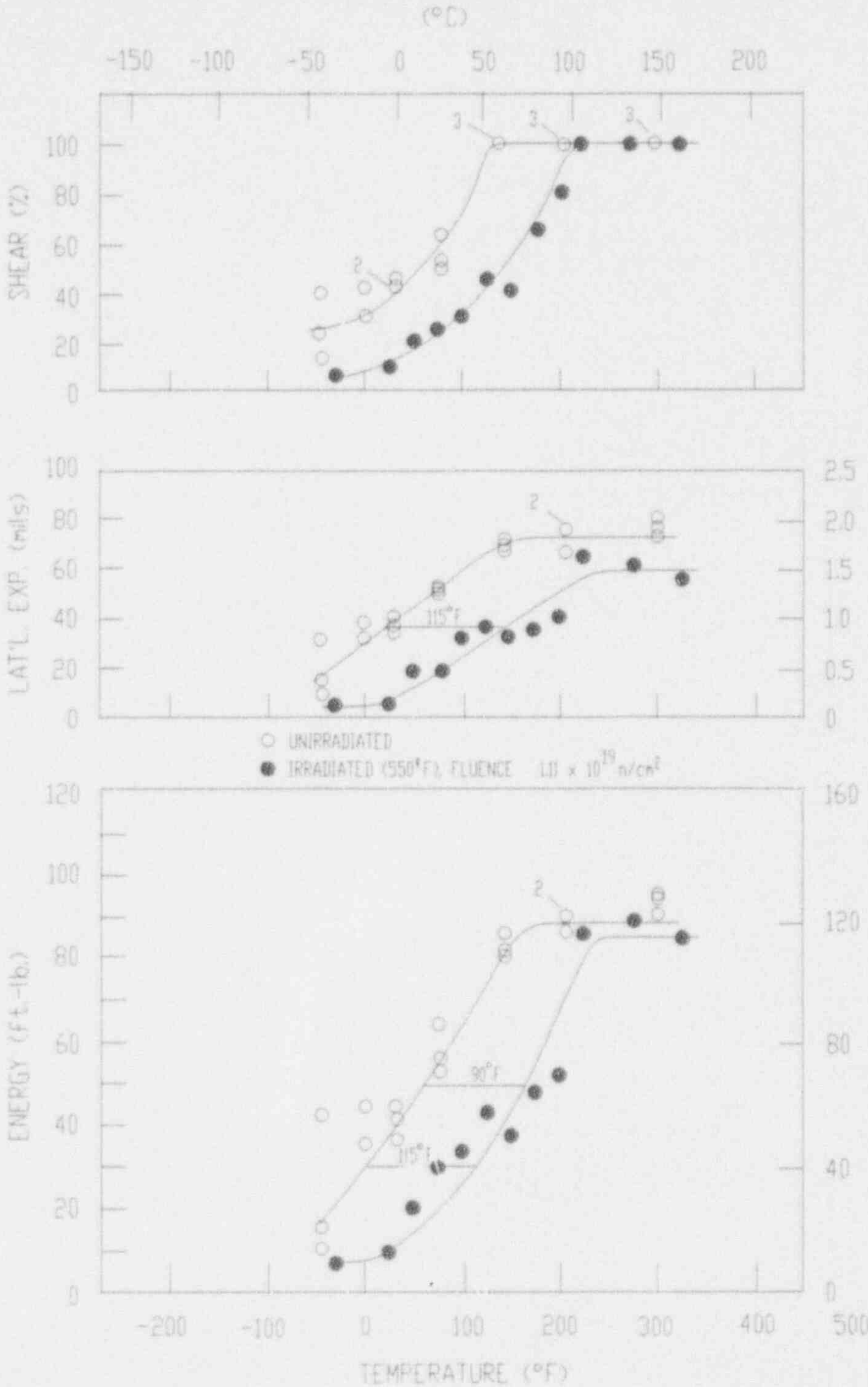

Figure 5-1. Charpy V-Notch Impact Properties for Sequoyah Unit 2 Reactor Vessel Intermediate Shell Forging 05 (Axial Orientation)

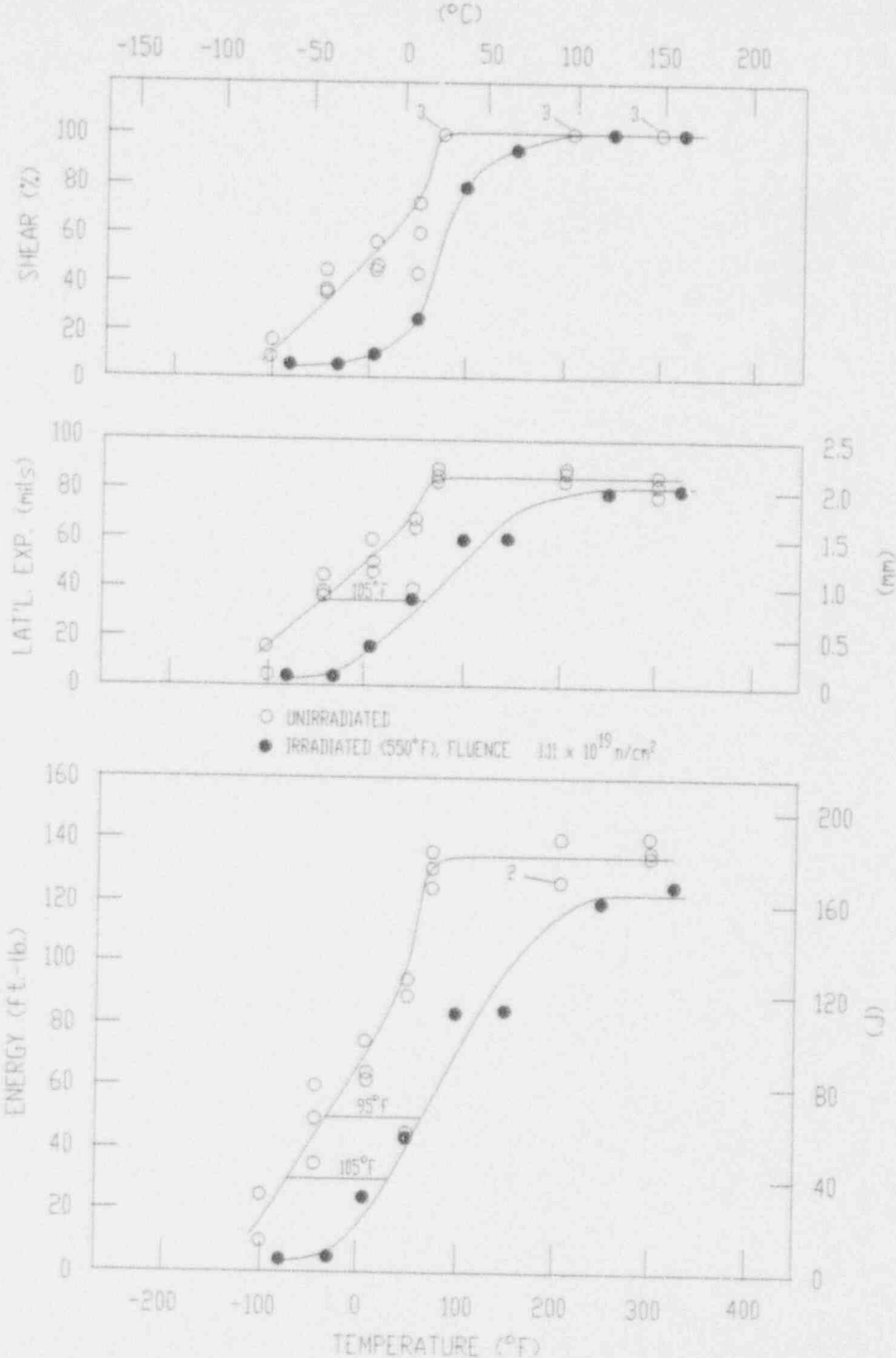

Figure 5-2. Charpy V-Notch Impact Properties for Sequoyah Unit 2 Reactor Vessel Intermediate Shell Forging 05 (Tangential Orientation)

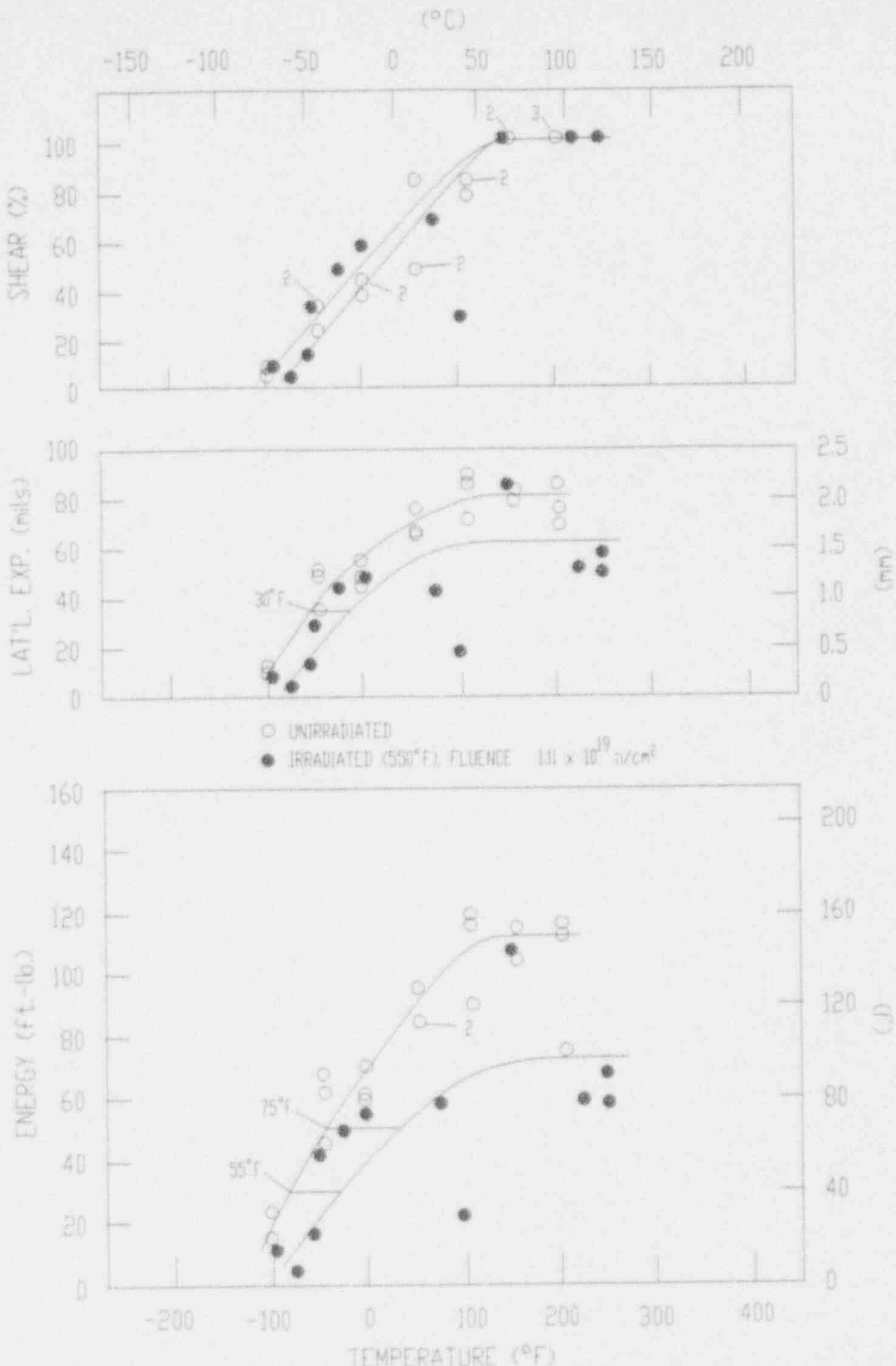

Figure 5-3. Charpy V-Notch Impact Properties for Sequoyah Unit 2 Reactor Vessel Surveillance Weld Metal

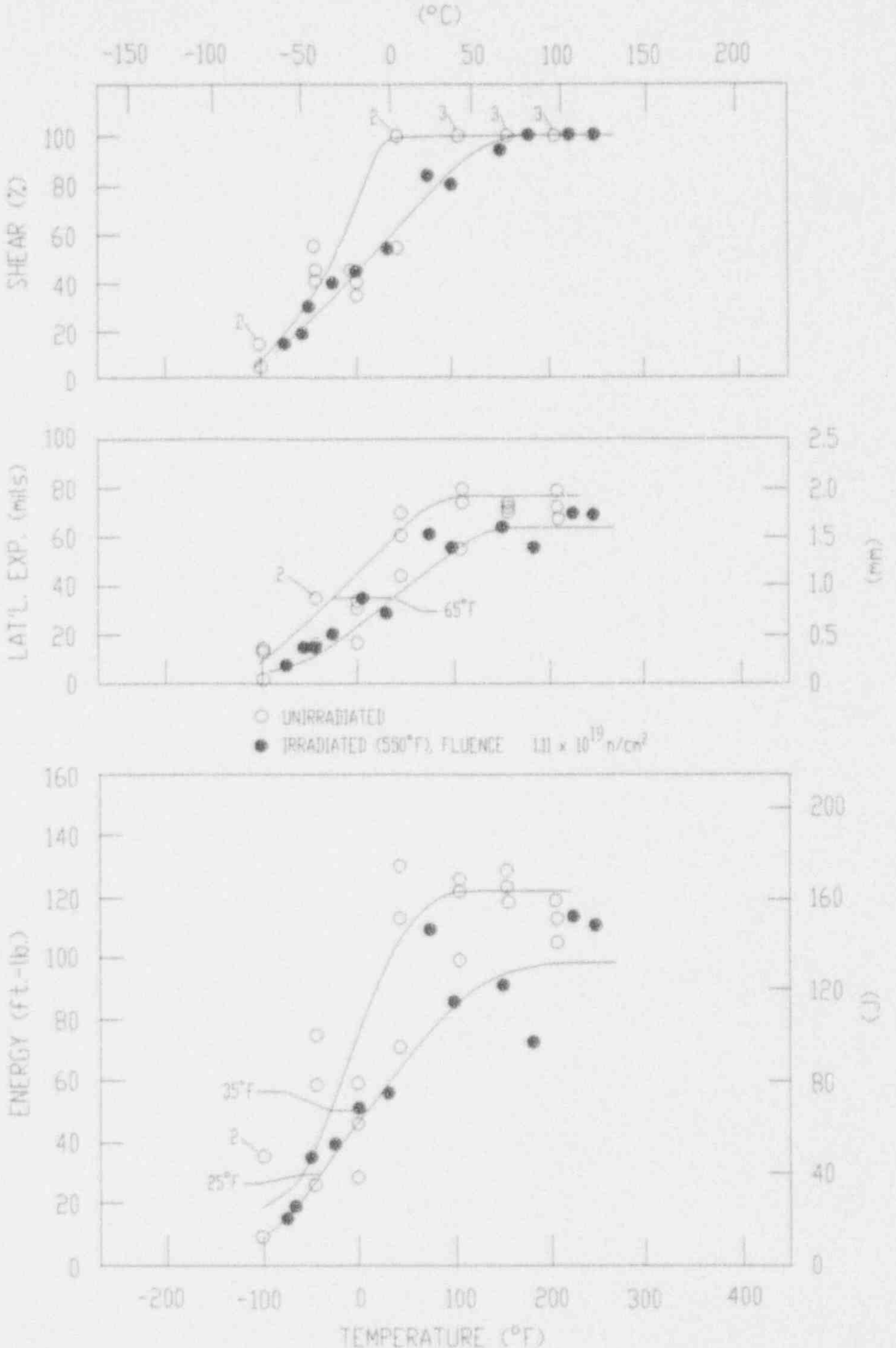

Figure 5-4. Charpy V-Notch Impact Properties for Sequoyah Unit 2 Reactor Vessel Weld Heat-Affected-Zone Metal

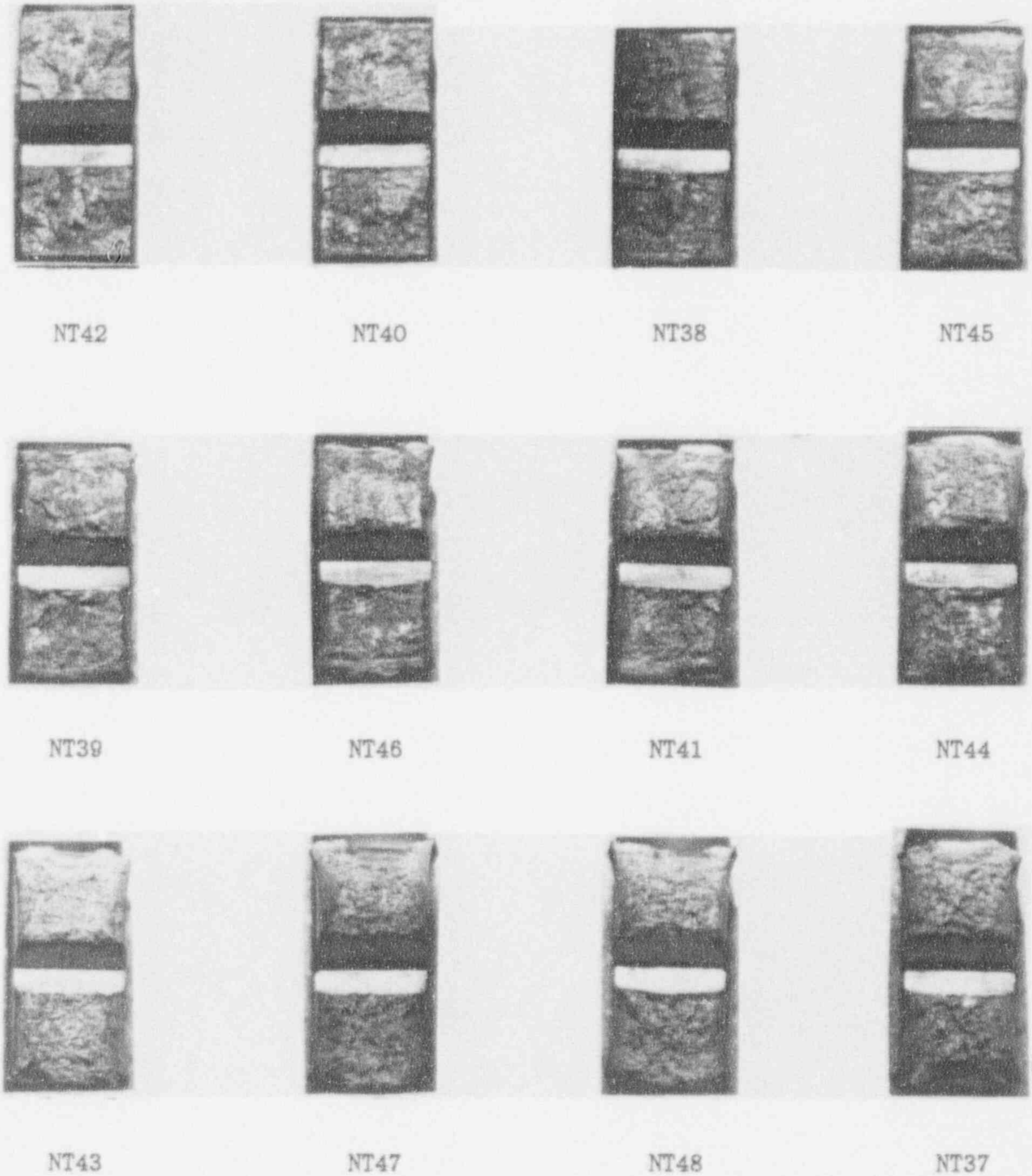

Figure 5-5. Charpy Impact Specimen Fracture Surfaces for Sequoyah Unit 2 Reactor Vessel Intermediate shell Forging 05 (Axial Orientation)

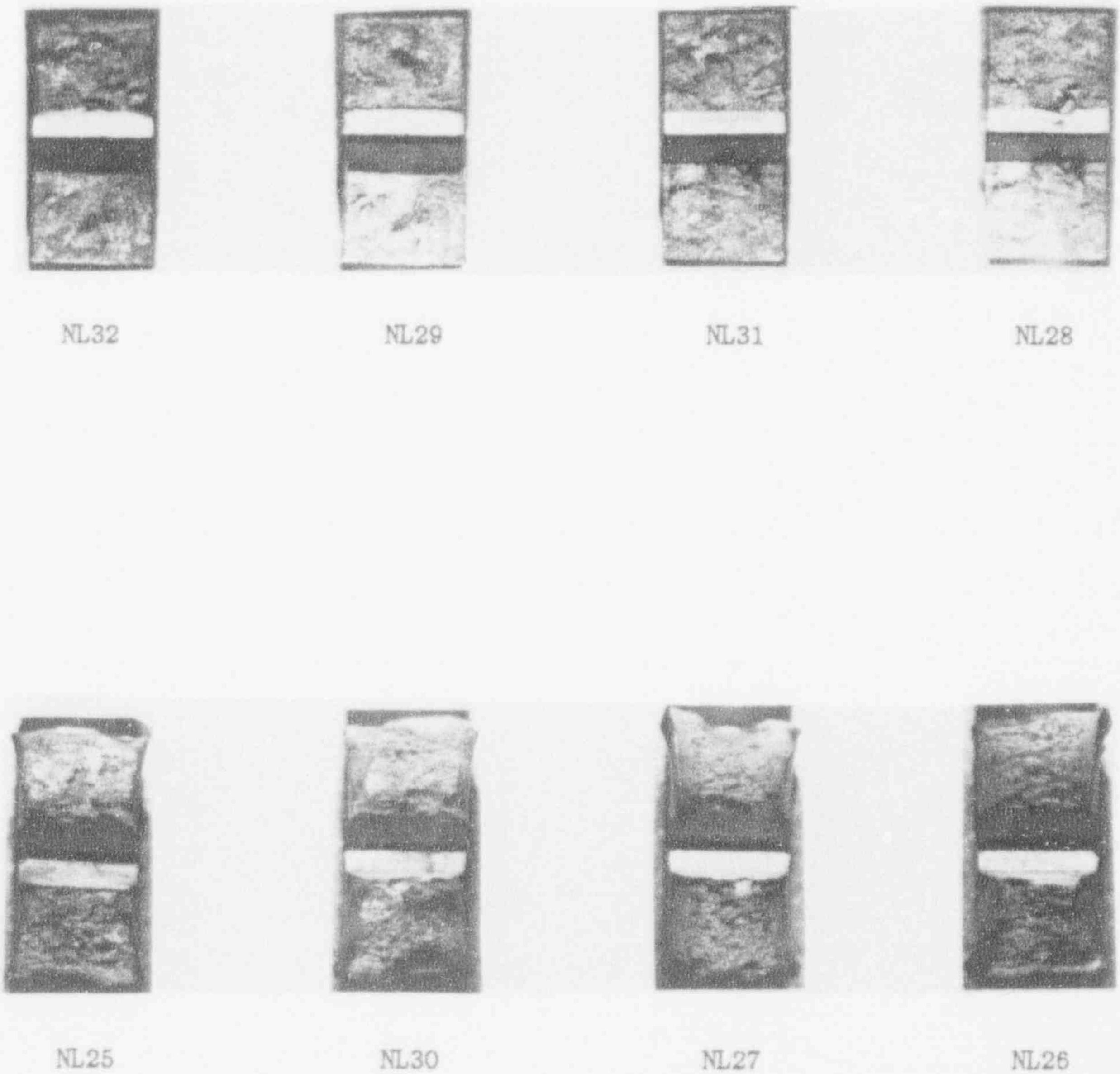

Figure 5-6. Charpy Impact Specimen Fracture Surfaces for Sequoyah Unit 2 Reactor Vessel Intermediate Shell Forging 05 (Tangential Orientation)

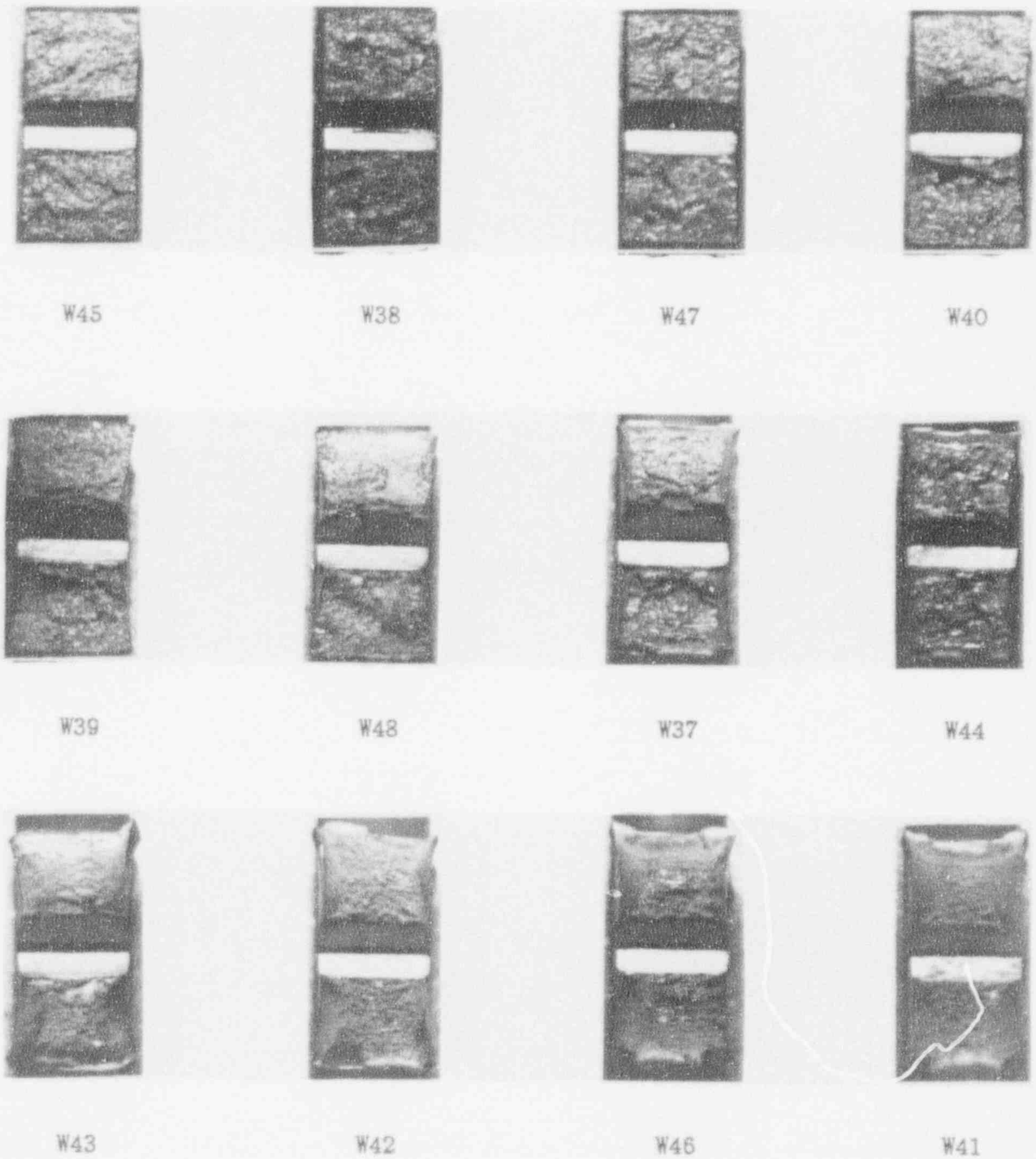

Figure 5-7. Charpy Impact Specimen Fracture Surfaces for Sequoyah Unit 2 Reactor Vessel Surveillance Weld Metal

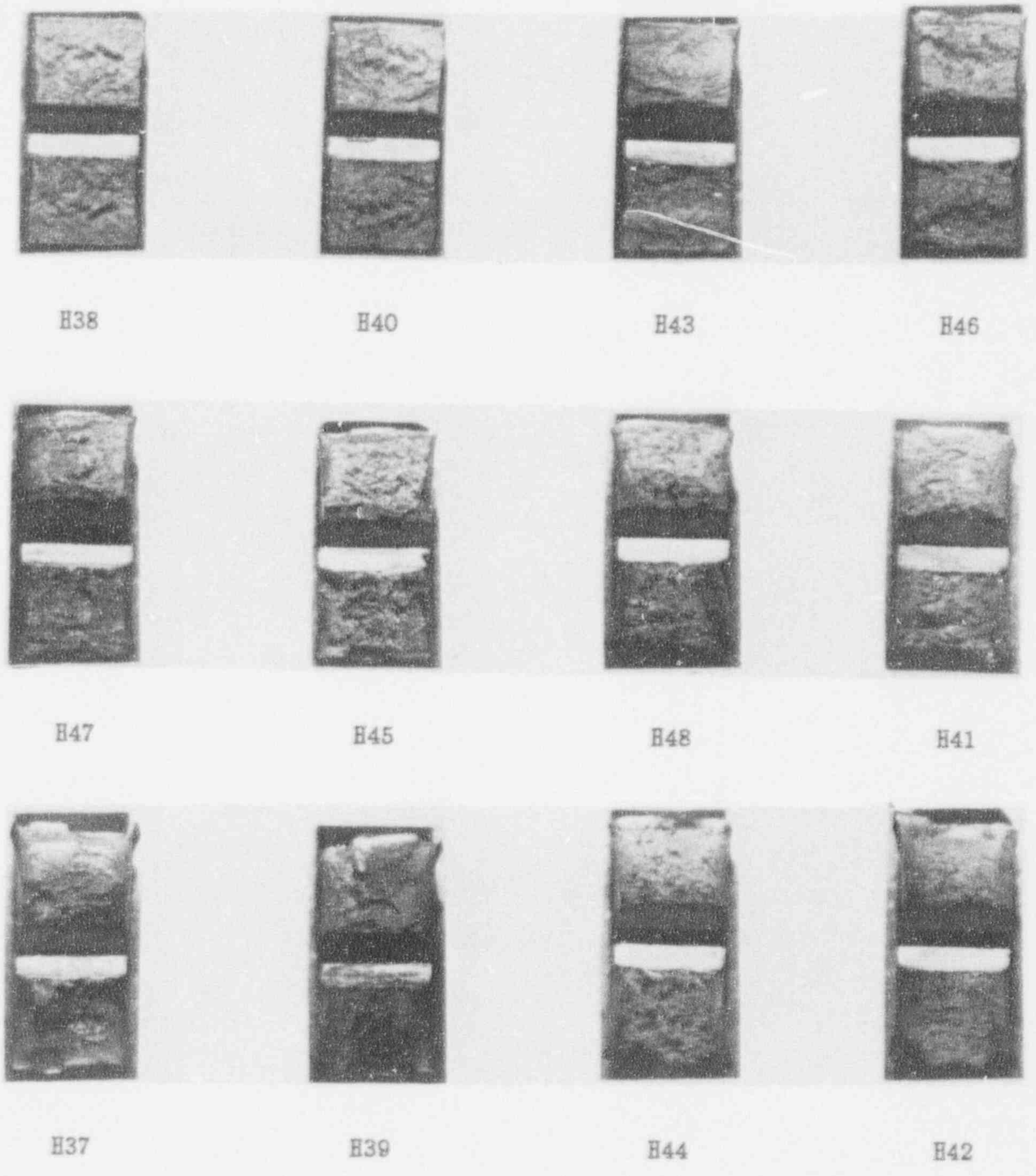

Figure 5-8. Charpy Impact Specimen Fracture Surfaces for Sequoyah Unit 2 Reactor Vessel Weld Heat-Affected-Zone Metal

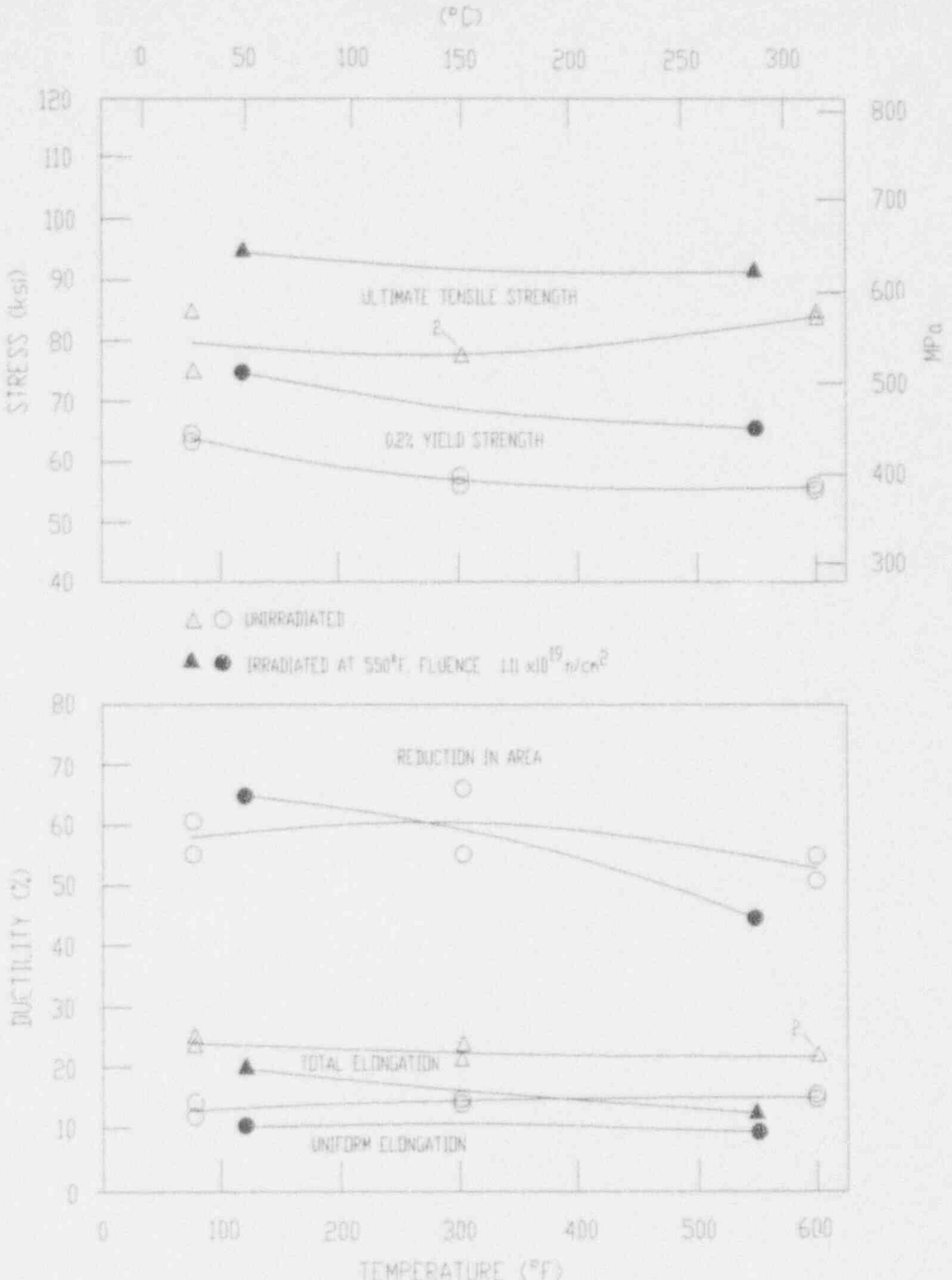

Figure 5-9. Tensile Properties for Sequoyah Unit 2 Reactor Vessel Intermediate Shell Forging 05 (Axial Orientation)

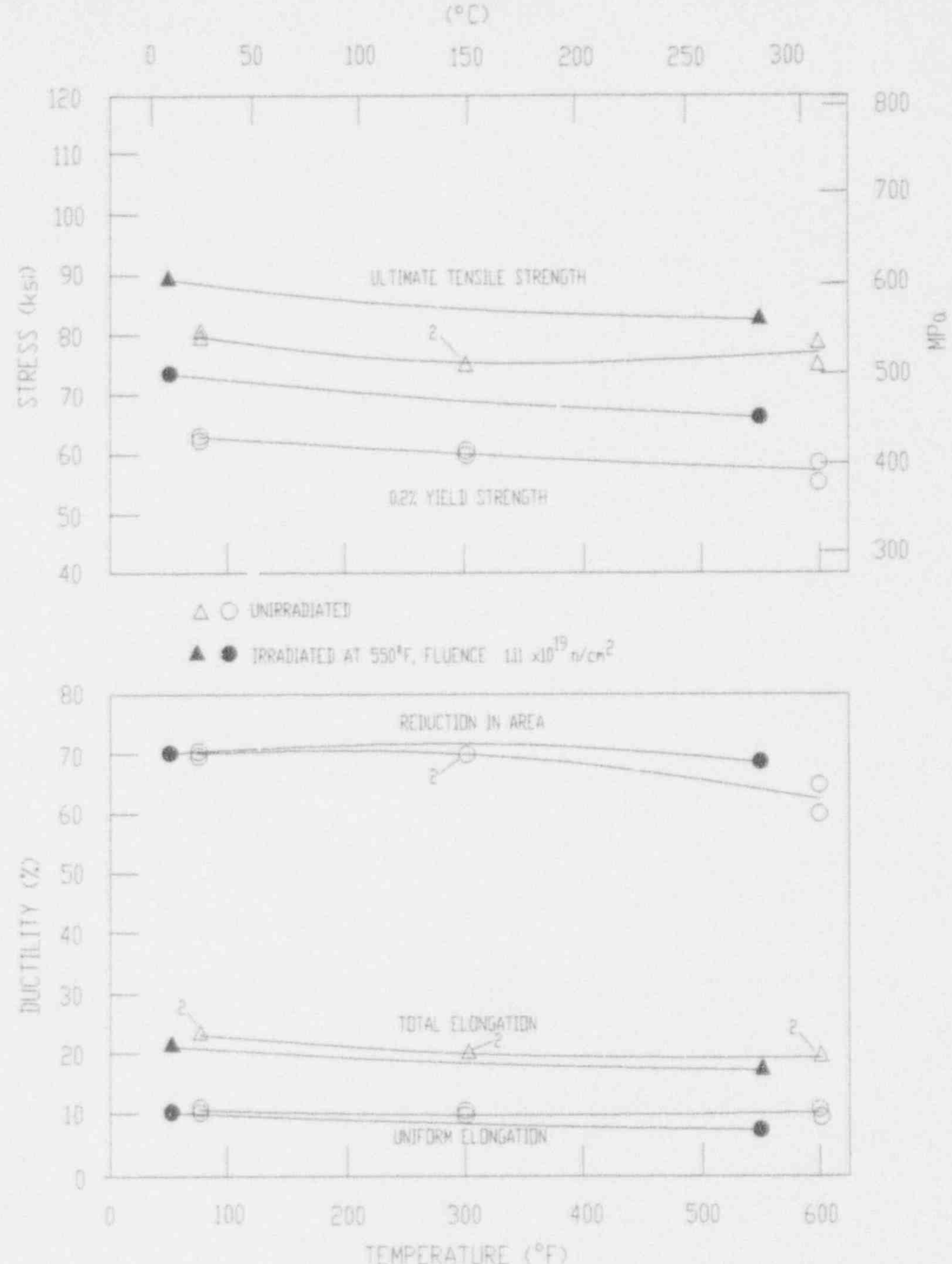

Figure 5-10. Tensile Properties for Sequoyah Unit 2 Reactor Vessel Surveillance Weld Metal

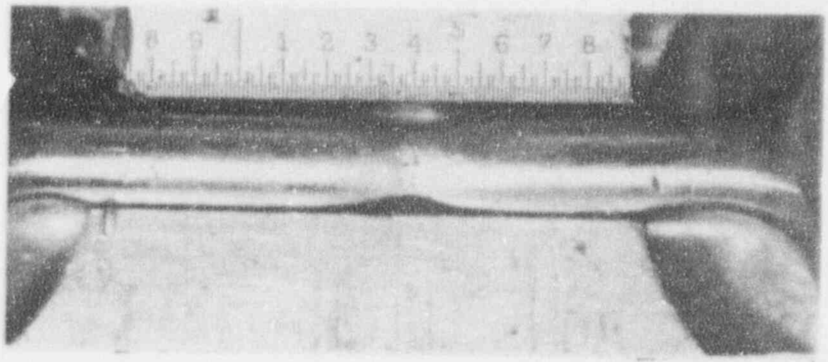

Specimen NT7 115°F

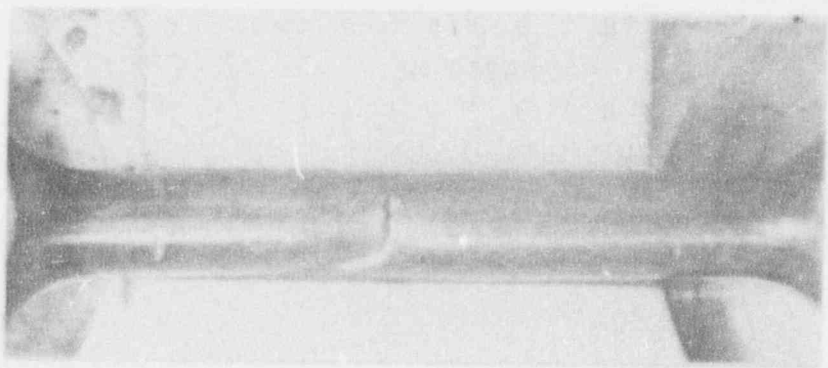

Specimen NT8 550°F

Figure 5-11. Fractured Tensile Specimens from Sequoyah Unit 2 Reactor Vessel Intermediate Shell Forging 05 (Axial Orientation)

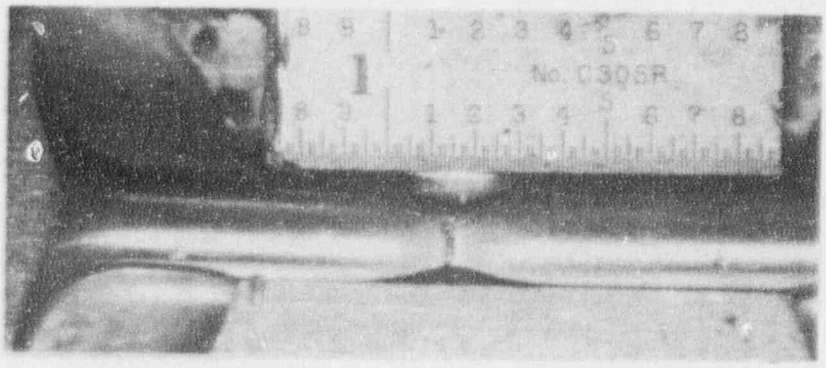

Specimen W7 50°F

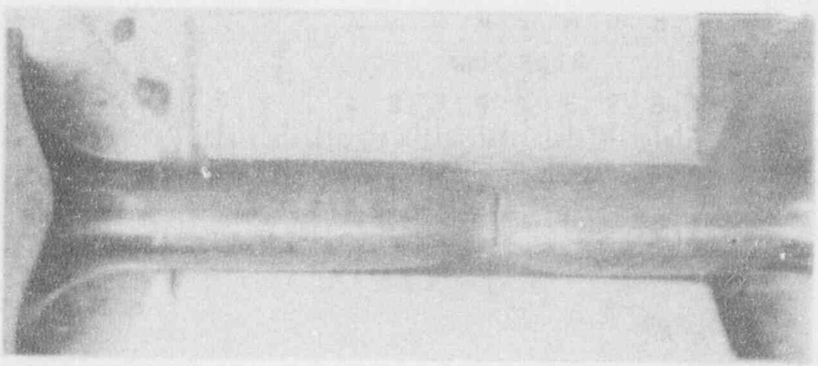

Specimen W8 550°F

Figure 5-12. Fractured Tensile Specimens from Sequoyah Unit 2 Reactor Vessel Surveillance Weld Metal

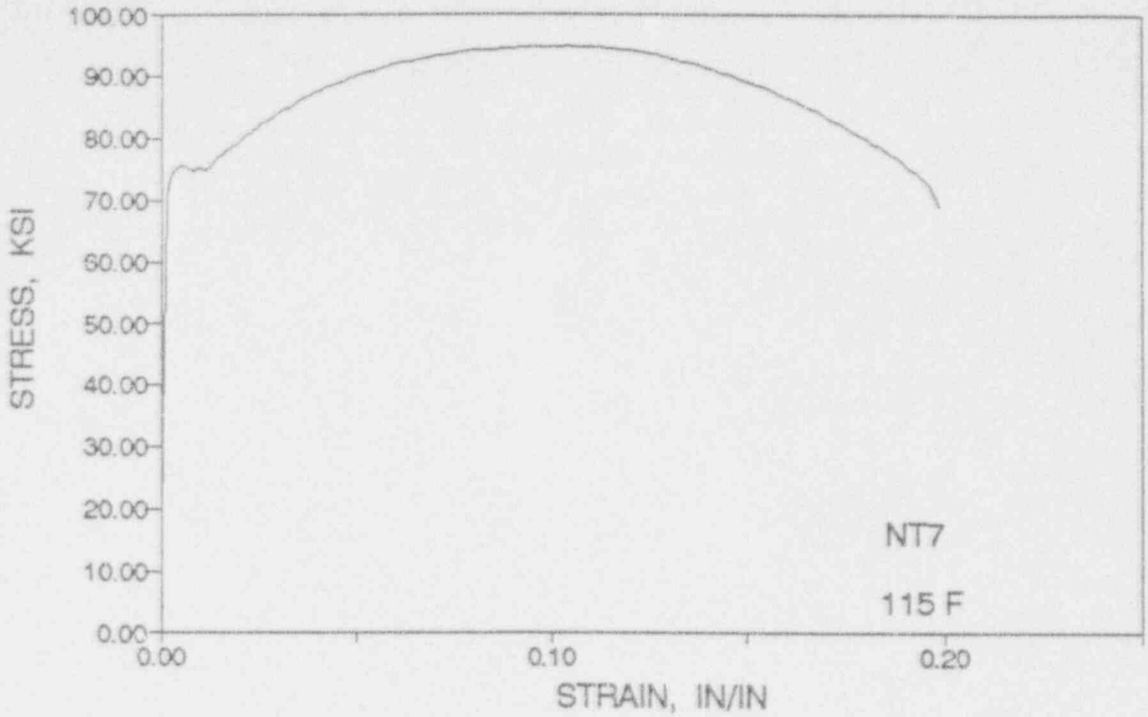

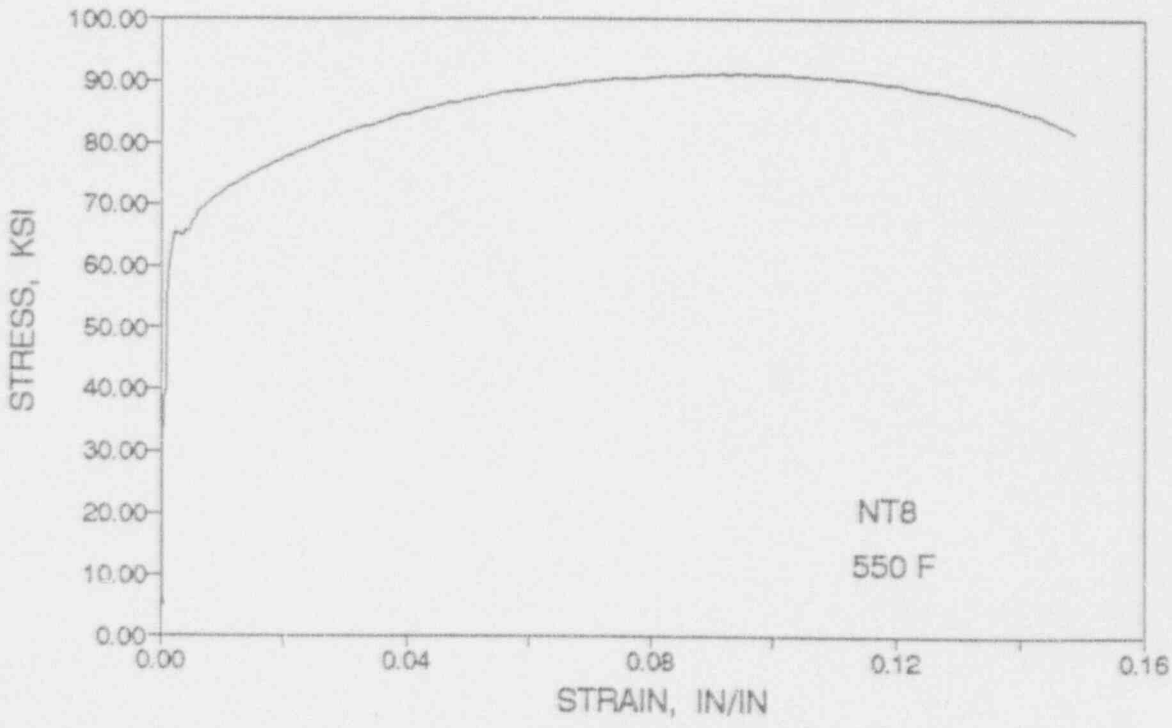

Figure 5-13. Engineering Stress-Strain Curves for Forging 05 Tensile Specimens NT7 and NT8

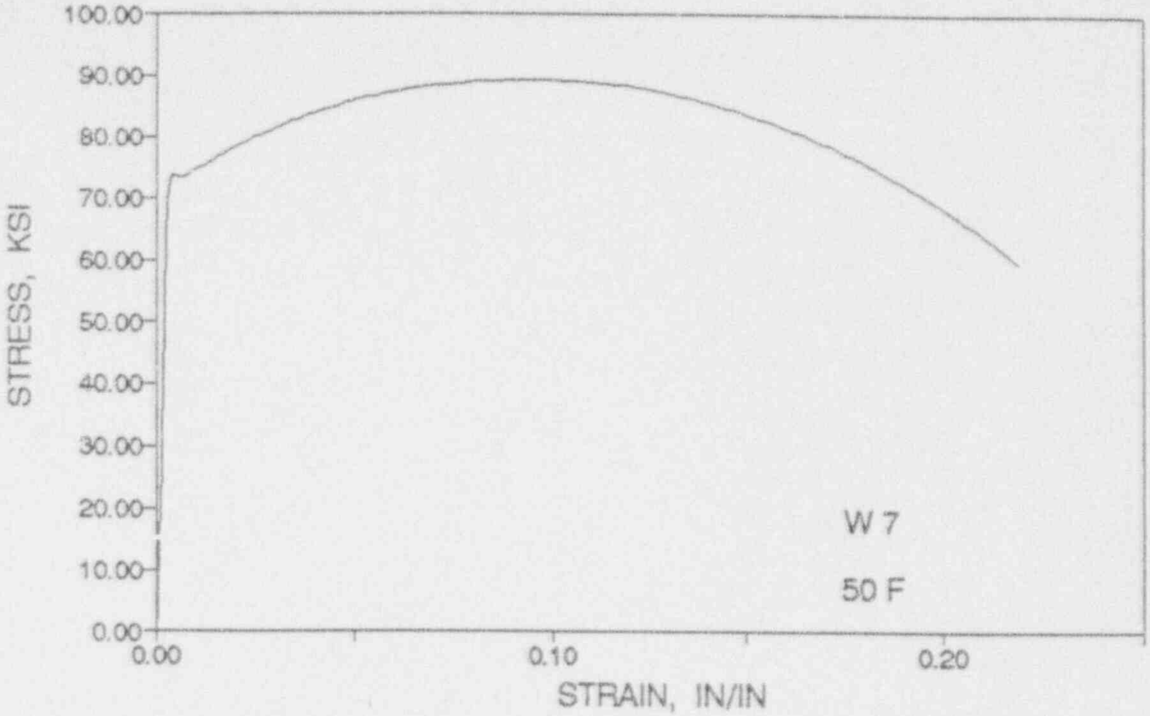

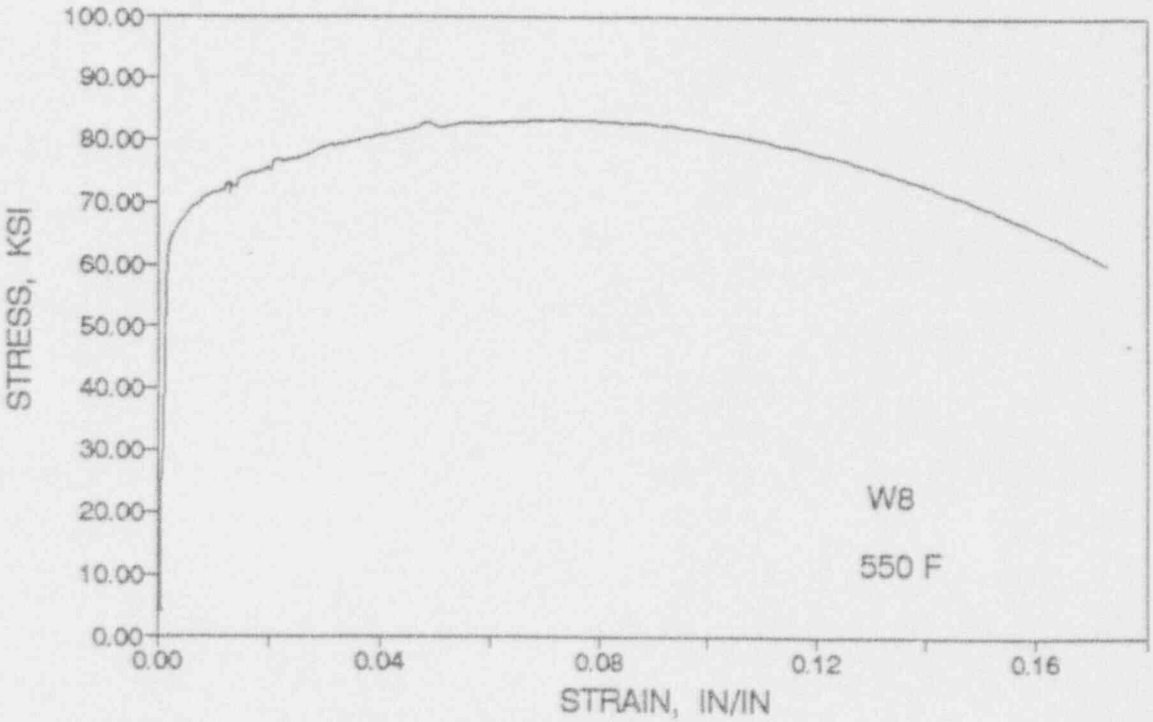

Figure 5-14. Engineering Stress-Strain Curve for Weld Metal Tensile Specimens W7 and W8

SECTION 6.0
RADIATION ANALYSIS AND NEUTRON DOSIMETRY

6.1 Introduction

Knowledge of the neutron environment within the reactor pressure vessel and surveillance capsule geometry is required as an integral part of LWR reactor pressure vessel surveillance programs for two reasons. First, in order to interpret the neutron radiation-induced material property changes observed in the test specimens, the neutron environment (energy spectrum, flux, fluence) to which the test specimens were exposed must be known. Second, in order to relate the changes observed in the test specimens to the present and future condition of the reactor vessel, a relationship must be established between the neutron environment at various positions within the reactor vessel and that experienced by the test specimens. The former requirement is normally met by employing a combination of rigorous analytical techniques and measurements obtained with passive neutron flux monitors contained in each of the surveillance capsules. The latter information is derived solely from analysis.

The use of fast neutron fluence ($E > 1.0$ MeV) to correlate measured materials properties changes to the neutron exposure of the material for light water reactor applications has traditionally been accepted for development of damage trend curves as well as for the implementation of trend curve data to assess vessel condition. In recent years, however, it has been suggested that an exposure model that accounts for differences in neutron energy spectra between surveillance capsule locations and positions within the vessel wall could lead to an improvement in the uncertainties associated with damage trend curves as well as to a more accurate evaluation of damage gradients through the pressure vessel wall.

Because of this potential shift away from a threshold fluence toward an energy dependent damage function for data correlation, ASTM Standard Practice E853, "Analysis and Interpretation of Light Water Reactor Surveillance Results," recommends reporting displacements per iron atom (dpa) along with fluence (E > 1.0 MeV) to provide a data base for future reference. The energy dependent dpa function to be used for this evaluation is specified in ASTM Standard Practice E693, "Characterizing Neutron Exposures in Ferritic Steels in Terms of Displacements per Atom." The application of the dpa parameter to the assessment of embrittlement gradients through the thickness of the pressure vessel wall has already been promulgated in Revision 2 to the Regulatory Guide 1.99, "Radiation Damage to Reactor Vessel Materials."[3]

This section provides the results of the neutron dosimetry evaluations performed in conjunction with the analysis of test specimens contained in surveillance Capsule X. Fast neutron exposure parameters in terms of fast neutron fluence (E > 1.0 MeV), fast neutron fluence (E > 0.1 Mev), and iron atom displacements (dpa) are established for the capsule irradiation history. The analytical formalism relating the measured capsule exposure to the exposure of the vessel wall is described and used to project the integrated exposure of the vessel itself. Also uncertainties associated with the derived exposure parameters at the surveillance capsule and with the projected exposure of the pressure vessel are provided.

6.2 Discrete Ordinates Analysis

A plan view of the reactor geometry at the core midplane is shown in Figure 4-1. Eight irradiation capsules attached to the thermal shield are included in the reactor design to constitute the reactor vessel surveillance program. The capsules are located at azimuthal angles of 4.0°, 40.0°, 140.0°, 176.0°, 184.0°, 220.0°, 320.0°, and 356.0° relative to the core cardinal axes as shown in Figure 4-1.

A plan view of a surveillance capsule holder attached to the thermal shield is shown in Figure 6-1. The stainless steel specimen containers are 1.0 inch square and approximately 38 inches in height. The containers are positioned axially such that the specimens are centered on the core midplane, thus spanning the central 3 feet of the 12-foot high reactor core.

From a neutron transport standpoint, the surveillance capsule structures are significant. They have a marked effect on both the distribution of neutron flux and the neutron energy spectrum in the water annulus between the thermal shield and the reactor vessel. In order to properly determine the neutron environment at the test specimen locations, the capsules themselves must be included in the analytical model.

In performing the fast neutron exposure evaluations for the surveillance capsules and reactor vessel, two distinct sets of transport calculations were carried out. The first, a single computation in the conventional forward mode, was used primarily to obtain relative neutron energy distributions throughout the reactor geometry as well as to establish relative radial distributions of exposure parameters {$\phi(E > 1.0$ Mev), $\phi(E > 0.1$ Mev), and dpa} through the vessel wall. The neutron spectral information was required for the interpretation of neutron dosimetry withdrawn from the surveillance capsule as well as for the determination of exposure parameter ratios; i.e., dpa/$\phi(E > 1.0$ MeV), within the pressure vessel geometry. The relative radial gradient information was required to permit the projection of measured exposure parameters to locations interior to the pressure vessel wall; i.e., the 1/4T, 1/2T, and 3/4T locations.

The second set of calculations consisted of a series of adjoint analyses relating the fast neutron flux ($E > 1.0$ MeV) at surveillance capsule positions, and several azimuthal locations on the pressure vessel inner radius to neutron source distributions within the reactor core. The importance functions generated from these adjoint analyses provided the basis for all absolute exposure projections and comparison with measurement. These importance functions, when combined with cycle specific neutron source distributions, yielded absolute predictions of neutron exposure at the locations of interest for each cycle of irradiation; and established the means to perform similar predictions and dosimetry evaluations for all subsequent fuel cycles. It is important to note that the cycle specific neutron source distributions utilized in these analyses included not only spatial variations of fission rates within the reactor core; but, also accounted for the effects of varying neutron yield per fission and fission spectrum introduced by the build-in of plutonium as the burnup of individual fuel assemblies increased.

The absolute cycle specific data from the adjoint evaluations together with relative neutron energy spectra and radial distribution information from the forward calculation provided the means to:

1. Evaluate neutron dosimetry obtained from surveillance capsule locations.

2. Extrapolate dosimetry results to key locations at the inner radius and through the thickness of the pressure vessel wall.

3. Enable a direct comparison of analytical prediction with measurement.

4. Establish a mechanism for projection of pressure vessel exposure as the design of each new fuel cycle evolves.

The forward transport calculation for the reactor model summarized in Figures 4-1 and 6-1 was carried out in R, θ geometry using the DOT two-dimensional discrete ordinates code[12] and the SAILOR cross-section library[13]. The SAILOR library is a 47 group ENDFB-IV based data set produced specifically for light water reactor applications. In these analyses anisotropic scattering was treated with a P_3 expansion of the cross-sections and the angular discretization was modeled with an S_8 order of angular quadrature.

The reference core power distribution utilized in the forward analysis was derived from statistical studies of long-term operation of Westinghouse 4-loop plants. Inherent in the development of this reference core power distribution is the use of an out-in fuel management strategy; i.e., fresh fuel on the core periphery. Furthermore, for the peripheral fuel assemblies, a 2σ uncertainty derived from the statistical evaluation of plant to plant and cycle to cycle variations in peripheral power was used. Since it is unlikely that a single reactor would have a power distribution at the nominal $+2\sigma$

level for a large number of fuel cycles, the use of this reference distribution is expected to yield somewhat conservative results.

All adjoint analyses were also carried out using an S_8 order of angular quadrature and the P_3 cross-section approximation from the SAILOR library. Adjoint source locations were chosen at several azimuthal locations along the pressure vessel inner radius as well as the geometric center of each surveillance capsule. Again, these calculations were run in R, θ geometry to provide neutron source distribution importance functions for the exposure parameter of interest; in this case, ϕ (E > 1.0 MeV). Having the importance functions and appropriate core source distributions, the response of interest could be calculated as:

$$R(r, \theta) = \int_r \int_\theta \int_E I(r, \theta, E)\, S(r, \theta, E)\, r\, dr\, d\theta\, dE$$

where: $R(r, \theta)$ = ϕ (E > 1.0 MeV) at radius r and azimuthal angle θ

$I(r, \theta, E)$ = Adjoint importance function at radius, r, azimuthal angle θ, and neutron source energy E.

$S(r, \theta, E)$ = Neutron source strength at core location r, θ and energy E.

Although the adjoint importance functions used in the analysis were based on a response function defined by the threshold neutron flux (E > 1.0 MeV), prior calculations have shown that, while the implementation of low leakage loading patterns significantly impact the magnitude and the spatial distribution of the neutron field, changes in the relative neutron energy spectrum are of second order. Thus, for a given location the ratio of dpa/ϕ (E > 1.0 MeV) is insensitive to changing core source distributions. In the application of these adjoint importance functions to the Sequoyah Unit 2 reactor, therefore, the iron displacement rates (dpa) and the neutron flux (E > 0.1 MeV) were computed on a cycle specific basis by using dpa/ϕ (E > 1.0 MeV) and ϕ (E > 0.1 MeV)/ϕ (E > 1.0 MeV) ratios from the forward analysis in conjunction with the cycle specific ϕ (E > 1.0 MeV) solutions from the individual adjoint evaluations.

The reactor core power distribution used in the plant specific adjoint calculations was taken from the fuel cycle design reports for the first five operating cycles of Sequoyah Unit 2[14 through 18].

Selected results from the neutron transport analyses are provided in Tables 6-1 through 6-5. The data listed in these tables establish the means for absolute comparisons of analysis and measurement for the capsule irradiation period and provide the means to correlate dosimetry results with the corresponding neutron exposure of the pressure vessel wall.

In Table 6-1, the calculated exposure parameters [ϕ (E > 1.0 MeV), ϕ(E > 0.1 MeV), and dpa] are given at the geometric center of the two symmetric surveillance capsule positions for both the design basis and the plant specific core power distributions. The plant specific data, based on the adjoint transport analysis, are meant to establish the absolute comparison of measurement with analysis. The design basis data derived from the forward calculation are provided as a point of reference against which plant specific fluence evaluations can be compared. Similar data is given in Table 6-2 for the pressure vessel inner radius. Again, the three pertinent exposure parameters are listed for both the design basis and the Cycles 1 through 5 plant specific power distributions. It is important to note that the data for the vessel inner radius were taken at the clad/base metal interface; and, thus, represent the maximum exposure levels of the vessel wall itself.

Radial gradient information for neutron flux (E > 1.0 MeV), neutron flux (E > 0.1 MeV), and iron atom displacement rate is given in Tables 6-3, 6-4, and 6-5, respectively. The data, obtained from the forward neutron transport calculation, are presented on a relative basis for each exposure parameter at several azimuthal locations. Exposure parameter distributions within the wall may be obtained by normalizing the calculated or projected exposure at the vessel inner radius to the gradient data given in Tables 6-3 through 6-5.

For example, the neutron flux (E > 1.0 MeV) at the 1/4T position on the 45° azimuth is given by:

$$\phi_{1/4T}(45°) = \phi(220.27, 45°)\ F\ (225.75, 45°)$$

where: $\phi_{1/4T}(45°)$ = Projected neutron flux at the 1/4T position on the 45° azimuth

ϕ (220.27,45°) = Projected or calculated neutron flux at the vessel inner radius on the 45° azimuth.

F (225.75, 45°) = Relative radial distribution function from Table 6-3.

Similar expressions apply for exposure parameters in terms of ϕ (E > 0.1 MeV) and dpa/sec.

6.3 Neutron Dosimetry

The passive neutron sensors included in the Sequoyah Unit 2 surveillance program are listed in Table 6-6. Also given in Table 6-6 are the primary nuclear reactions and associated nuclear constants that were used in the evaluation of the neutron energy spectrum within the capsule and the subsequent determination of the various exposure parameters of interest [ϕ (E > 1.0 Mev), ϕ (E > 0.1 MeV), dpa].

The relative locations of the neutron sensors within the capsules are shown in Figure 4-2. The iron, nickel, copper, and cobalt-aluminum monitors, in wire form, were placed in holes drilled in spacers at several axial levels within the capsules. The cadmium-shielded neptunium and uranium fission monitors were accommodated within the dosimeter block located near the center of the capsule.

The use of passive monitors such as those listed in Table 6-6 does not yield a direct measure of the energy dependent flux level at the point of interest. Rather, the activation or fission process is a measure of the integrated effect that the time- and energy-dependent neutron flux has on the target material over the course of the irradiation period. An accurate assessment of the average neutron flux level incident on the various monitors may be derived from the activation measurements only if the irradiation parameters are well known. In particular, the following variables are of interest:

- The specific activity of each monitor.
- The operating history of the reactor.
- The energy response of the monitor.
- The neutron energy spectrum at the monitor location.
- The physical characteristics of the monitor.

The specific activity of each of the neutron monitors was determined using established ASTM procedures [19 through 32]. Following sample preparation and weighing, the activity of each monitor was determined by means of a lithium-drifted germanium, Ge(Li), gamma spectrometer. The irradiation history of the Sequoyah Unit 2 reactor during Cycles 1 through 5 was obtained from NUREG-0020, "Licensed Operating Reactors Status Summary Report" for the applicable period.

The irradiation history applicable to Capsule X is given in Table 6-7. Measured and saturated reaction product specific activities as well as measured full power reaction rates are listed in Table 6-8. Reaction rate values were derived using the pertinent data from Tables 6-6 and 6-7.

Values of key fast neutron exposure parameters were derived from the measured reaction rates using the FERRET least squares adjustment code [33]. The FERRET approach used the measured reaction rate data and the calculated neutron energy spectrum at the the center of the surveillance capsule as input and proceeded to adjust a priori (calculated) group fluxes to produce a best fit (in a least squares sense) to the reaction rate data. The exposure parameters along with associated uncertainties where then obtained from the adjusted spectra.

In the FERRET evaluations, a log-normal least-squares algorithm weights both the a priori values and the measured data in accordance with the assigned uncertainties and correlations. In general, the measured values f are linearly related to the flux ϕ by some response matrix A:

$$f^{(s,\alpha)} = \sum_g A_{ig}^{(s)} \phi_g^{(\alpha)}$$

where i indexes the measured values belonging to a single data set s, g designates the energy group and α delineates spectra that may be simultaneously adjusted. For example,

$$R_i = \sum_g \sigma_{ig} \phi_g$$

relates a set of measured reaction rates R_i to a single spectrum ϕ_g by the multigroup cross section σ_{ig}. (In this case, FERRET also adjusts the cross-sections.) The log-normal approach automatically accounts for the physical constraint of positive fluxes, even with the large assigned uncertainties.

In the FERRET analysis of the dosimetry data, the continuous quantities (i.e., fluxes and cross-sections) were approximated in 53 groups. The calculated fluxes from the discrete ordinates analysis were expanded into the FERRET group structure using the SAND-II code [34]. This procedure was carried out by first expanding the a priori spectrum into the SAND-II 620 group structure using a SPLINE interpolation procedure for interpolation in regions where group boundaries do not coincide. The 620-point spectrum was then easily collapsed to the group scheme used in FERRET.

The cross-sections were also collapsed into the 53 energy-group structure using SAND II with calculated spectra (as expanded to 620 groups) as weighting functions. The cross sections were taken from the ENDF/B-V dosimetry file. Uncertainty estimates and 53 x 53 covariance matrices were constructed for each cross section. Correlations between cross sections were neglected due to data and code limitations, but are expected to be unimportant.

For each set of data or a priori values, the inverse of the corresponding relative covariance matrix M is used as a statistical weight. In some cases, as for the cross sections, a multigroup covariance matrix is used. More often, a simple parameterized form is used:

$$M_{gg'} = R_N^2 + R_g R_{g'} P_{gg'}$$

where R_N specifies an overall fractional normalization uncertainty (i.e., complete correlation) for the corresponding set of values. The fractional uncertainties R_g specify additional random uncertainties for group g that are correlated with a correlation matrix:

$$P_{gg'} = (1 - \theta)\ \delta_{gg'} + \theta \exp\left[\frac{-(g-g')^2}{2\gamma^2}\right]$$

The first term specifies purely random uncertainties while the second term describes short-range correlations over a range γ (θ specifies the strength of the latter term).

For the a priori calculated fluxes, a short-range correlation of $\gamma = 6$ groups was used. This choice implies that neighboring groups are strongly correlated when θ is close to 1. Strong long-range correlations (or anticorrelations) were justified based on information presented by R.E. Maerker[35]. Maerker's results are closely duplicated when $\gamma = 6$. For the integral reaction rate covariances, simple normalization and random uncertainties were combined as deduced from experimental uncertainties.

Results of the FERRET evaluation of the Capsule X dosimetry are given in Table 6-9. The data summarized in Table 6-9 indicated that the capsule received an integrated exposure of 1.11 x 10^{19} n/cm^2 (E > 1.0 MeV) with an associated 1 σ uncertainty of $\pm$ 8%. Also reported are capsule exposures in terms of fluence (E > 0.1 MeV) and iron atom displacements (dpa). Summaries of the fit of the adjusted spectrum are provided in Table 6-10. In general, excellent results were achieved in the fits of the adjusted spectrum to the individual experimental reaction rates. The adjusted spectrum itself is tabulated in Table 6-11 for the FERRET 53 energy group structure.

A summary of the measured and calculated neutron exposure of Capsule X is presented in Table 6-12. The agreement between calculation and measurement falls within $\pm$ 6% for all fast neutron exposure parameters listed. The thermal neutron exposure calculated for the exposure period undepredicted the measured value by approximately a factor of two.

Neutron exposure projections at key locations on the pressure vessel inner radius are given in Table 6-13. Along with the current (5.36 EFPY) exposure derived from the Capsule X measurements, projections are also provided for an exposure period of 16 EFPY and to end of vessel design life (32 EFPY). In the evaluation of the future exposure of the reactor pressure vessel the exposure rates averaged over the first five cycles of operation were employed.

In the calculation of exposure gradients for use in the development of heatup and cooldown curves for the Sequoyah Unit 2 reactor coolant system, exposure projections to 16 EFPY and 32 EFPY were also evaluated. Data based on both a fluence (E > 1.0 MeV) slope and a plant specific dpa slope through the vessel wall are provided in Table 6-14. In order to access RT_{NDT} vs. fluence trend curves, dpa equivalent fast neutron fluence levels for the 1/4T and 3/4T positions were defined by the following relations:

$$\phi' (1/4T) = \phi \text{ (Surface) } \left\{\frac{\text{dpa } (1/4T)}{\text{dpa (Surface)}}\right\}$$

$$\phi' (3/4T) = \phi \text{ (Surface) } \left\{\frac{\text{dpa } (3/4T)}{\text{dpa (Surface)}}\right\}$$

Using this approach results in the dpa equivalent fluence values listed in Table 6-14.

In Table 6-15 updated lead factors are listed for each of the Sequoyah Unit 2 surveillance capsules. These data may be used as a guide in establishing future withdrawal schedules for the remaining capsules.

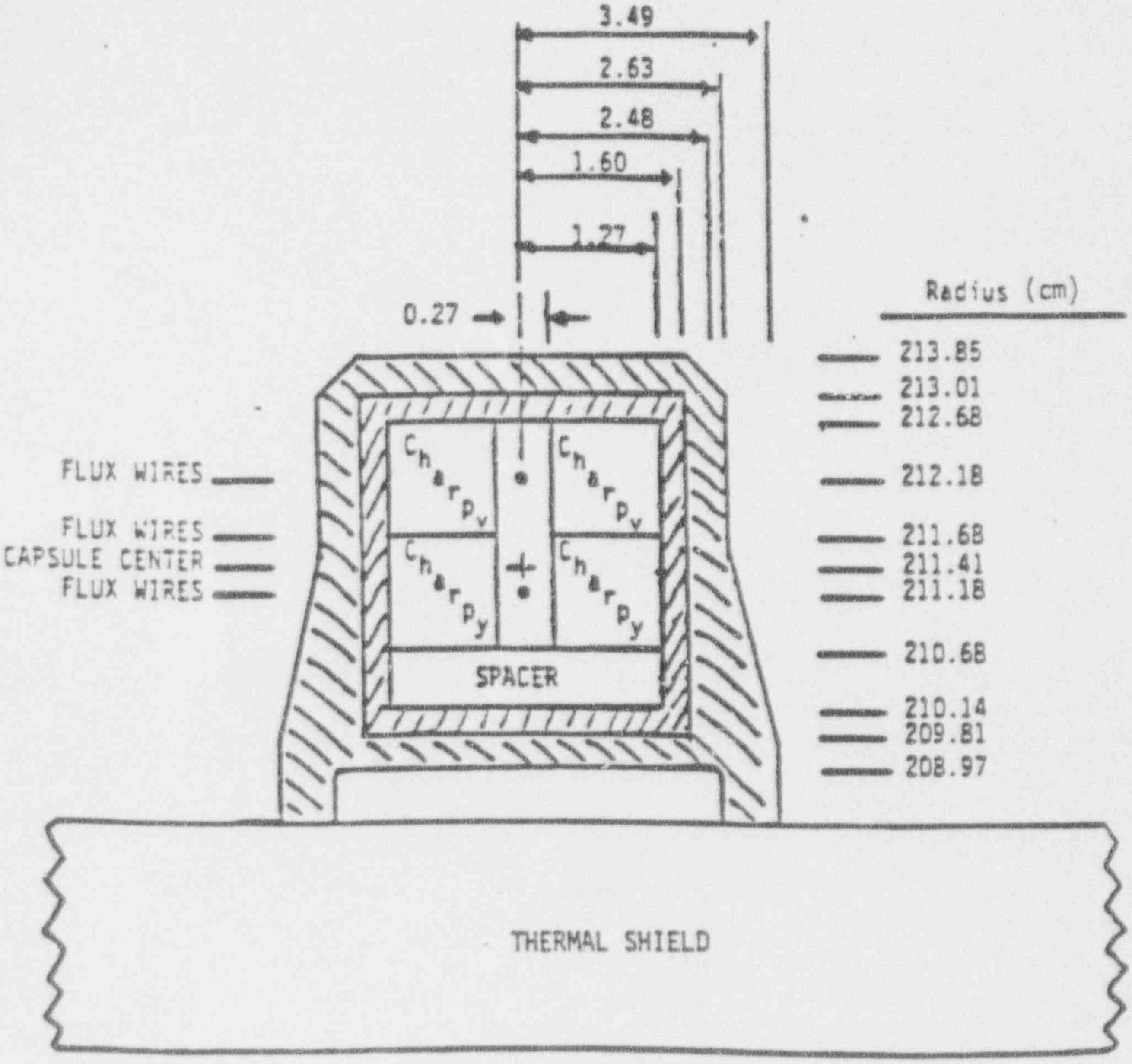

Figure 6-1. Plan View of a Reactor Vessel Surveillance Capsule

TABLE 6-1

CALCULATED FAST NEUTRON EXPOSURE PARAMETERS
AT THE SURVEILLANCE CAPSULE CENTER

	ϕ(E > 1.0MeV) [n/cm^2-sec]		ϕ(E > 0.1Mev) [n/cm^2-sec]		Iron Displacement Rate [dpa/sec]	
	4.0°	40.0°	4.0°	40.0°	4.0°	40.0°
DESIGN BASIS	2.82×10^{11}	9.05×10^{10}	8.15×10^{10}	3.04×10^{11}	4.58×10^{-11}	1.55×10^{-10}
CYCLE 1	2.12×10^{10}	6.82×10^{10}	6.13×10^{10}	2.29×10^{11}	3.43×10^{-11}	1.17×10^{-10}
CYCLE 2	2.13×10^{10}	8.19×10^{10}	6.16×10^{10}	2.75×10^{10}	3.45×10^{-11}	1.40×10^{-10}
CYCLE 3	2.53×10^{10}	5.01×10^{10}	7.31×10^{10}	1.68×10^{10}	4.10×10^{-11}	8.57×10^{-11}
CYCLE 4	1.77×10^{10}	6.17×10^{10}	5.12×10^{10}	2.07×10^{10}	2.87×10^{-11}	1.06×10^{-10}
CYCLE 5	1.73×10^{10}	5.81×10^{10}	5.00×10^{10}	1.95×10^{10}	2.80×10^{-11}	9.94×10^{-11}

TABLE 6-2

CALCULATED FAST NEUTRON EXPOSURE RATES AT
THE PRESSURE VESSEL CLAD/BASE METAL INTERFACE

$\phi(E > 1.0MeV)$ [n/cm^2-sec]

	0.0°	15.0°	30.0°	45.0°
DESIGN BASIS	8.43×10^{09}	1.36×10^{10}	1.72×10^{10}	2.68×10^{10}
CYCLE 1	6.46×10^{09}	1.04×10^{10}	1.31×10^{10}	2.03×10^{10}
CYCLE 2	6.52×10^{09}	1.13×10^{10}	1.50×10^{10}	2.36×10^{10}
CYCLE 3	7.43×10^{09}	1.13×10^{10}	1.06×10^{10}	1.49×10^{10}
CYCLE 4	5.40×10^{09}	8.99×10^{09}	1.16×10^{10}	1.79×10^{10}
CYCLE 5	5.43×10^{09}	9.37×10^{09}	1.15×10^{10}	1.73×10^{10}

$\phi(E > 0.1MeV)$ [n/cm^2-sec]

	0.0°	15.0°	30.0°	45.0°
DESIGN BASIS	2.11×10^{10}	3.41×10^{10}	4.34×10^{10}	6.96×10^{10}
CYCLE 1	1.62×10^{10}	2.61×10^{10}	3.30×10^{10}	5.28×10^{10}
CYCLE 2	1.63×10^{10}	2.84×10^{10}	3.78×10^{10}	6.14×10^{10}
CYCLE 3	1.86×10^{10}	2.84×10^{10}	2.67×10^{10}	3.87×10^{10}
CYCLE 4	1.35×10^{10}	2.26×10^{10}	2.92×10^{10}	4.65×10^{10}
CYCLE 5	1.36×10^{10}	2.35×10^{10}	2.90×10^{10}	4.50×10^{10}

Iron Atom Displacement Rate [dpa/sec]

	0.0°	15.0°	30.0°	45.0°
DESIGN BASIS	1.37×10^{-11}	2.19×10^{-11}	2.73×10^{-11}	4.26×10^{-11}
CYCLE 1	1.05×10^{-11}	1.67×10^{-11}	2.08×10^{-11}	3.23×10^{-11}
CYCLE 2	1.06×10^{-11}	1.82×10^{-11}	2.39×10^{-11}	3.75×10^{-11}
CYCLE 3	1.21×10^{-11}	1.82×10^{-11}	1.69×10^{-11}	2.37×10^{-11}
CYCLE 4	8.80×10^{-12}	1.45×10^{-11}	1.84×10^{-11}	2.85×10^{-11}
CYCLE 5	8.85×10^{-12}	1.51×10^{-11}	1.83×10^{-11}	2.75×10^{-11}

TABLE 6-3

RELATIVE RADIAL DISTRIBUTIONS OF NEUTRON FLUX (E > 1.0 MeV) WITHIN THE PRESSURE VESSEL WALL

Radius (cm)	0°	15°	30°	45°
220.27 (1)	1.00	1.00	1.00	1.00
220.64	0.977	0.978	0.979	0.977
221.66	0.884	0.887	0.889	0.885
222.99	0.758	0.762	0.765	0.756
224.31	0.641	0.644	0.648	0.637
225.63	0.537	0.540	0.545	0.534
226.95	0.448	0.451	0.455	0.443
228.28	0.372	0.373	0.379	0.367
229.60	0.309	0.310	0.315	0.303
230.92	0.255	0.257	0.261	0.250
232.25	0.211	0.212	0.216	0.206
233.57	0.174	0.175	0.178	0.169
234.89	0.143	0.144	0.147	0.138
236.22	0.117	0.118	0.121	0.113
237.54	0.0961	0.0963	0.0989	0.0912
238.86	0.0783	0.0783	0.0807	0.0736
240.19	0.0635	0.0632	0.0656	0.0584
241.51	0.0511	0.0501	0.0519	0.0454
242.17 (2)	0.0483	0.0469	0.0487	0.0422

NOTES: 1) Base Metal Inner Radius
2) Base Metal Outer Radius

TABLE 6-4

RELATIVE RADIAL DISTRIBUTIONS OF NEUTRON FLUX (E > 0.1 MeV) WITHIN THE PRESSURE VESSEL WALL

Radius (cm)	0°	15°	30°	45°
220.27(1)	1.00	1.00	1.00	1.00
220.64	1.00	1.00	1.00	1.00
221.66	1.00	0.996	1.00	0.994
222.99	0.965	0.958	0.968	0.953
224.31	0.916	0.906	0.919	0.898
225.63	0.861	0.849	0.865	0.838
226.95	0.803	0.790	0.809	0.777
228.28	0.746	0.732	0.752	0.717
229.60	0.689	0.675	0.695	0.657
230.92	0.633	0.619	0.640	0.600
232.25	0.578	0.565	0.586	0.544
233.57	0.525	0.513	0.534	0.490
234.89	0.474	0.463	0.483	0.437
236.22	0.424	0.414	0.433	0.387
237.54	0.375	0.367	0.385	0.338
238.86	0.328	0.322	0.338	0.291
240.19	0.283	0.277	0.292	0.244
241.51	0.239	0.232	0.245	0.196
242.17(2)	0.229	0.220	0.232	0.183

NOTES: 1) Base Metal Inner Radius
2) Base Metal Outer Radius

TABLE 6-5

RELATIVE RADIAL DISTRIBUTIONS OF IRON DISPLACEMENT RATE (dpa)
WITHIN THE PRESSURE VESSEL WALL

Radius (cm)	0°	15°	30°	45°
220.27[(1)]	1.00	1.00	1.00	1.00
220.64	0.983	0.983	0.984	0.983
221.66	0.913	0.914	0.918	0.915
222.99	0.818	0.819	0.827	0.820
224.31	0.728	0.728	0.739	0.730
225.63	0.647	0.646	0.659	0.647
226.95	0.574	0.573	0.587	0.573
228.28	0.510	0.507	0.523	0.507
229.60	0.453	0.450	0.466	0.449
230.92	0.402	0.399	0.414	0.397
232.25	0.356	0.353	0.368	0.349
233.57	0.315	0.312	0.327	0.307
234.89	0.277	0.275	0.289	0.269
236.22	0.243	0.241	0.254	0.233
237.54	0.212	0.210	0.222	0.201
238.86	0.182	0.181	0.192	0.170
240.19	0.155	0.154	0.164	0.141
241.51	0.131	0.128	0.137	0.113
242.17[(2)]	0.125	0.122	0.130	0.106

NOTES: 1) Base Metal Inner Radius
2) Base Metal Outer Radius

TABLE 6-6

NUCLEAR PARAMETERS FOR NEUTRON FLUX MONITORS

Monitor Material	Reaction of Interest	Target Weight Fraction	Response Range	Product Half-Life	Fission Yield (%)
Copper	$Cu^{63}(n,\alpha)Co^{60}$	0.6917	E > 4.7 MeV	5.272 yrs	
Iron	$Fe^{54}(n,p)Mn^{54}$	0.0582	E > 1.0 MeV	312.2 days	
Nickel	$Ni^{58}(n,p)Co^{58}$	0.6830	E > 1.0 MeV	70.90 days	
Uranium-238*	$U^{238}(n,f)Cs^{137}$	1.0	E > 0.4 MeV	30.12 yrs	5.99
Neptunium-237*	$Np^{237}(n,f)Cs^{137}$	1.0	E > 0.08 MeV	30.12 yrs	6.50
Cobalt-Aluminum*	$Co^{59}(n,\gamma)Co^{60}$	0.0015	0.4ev>E> 0.015 MeV	5.272 yrs	
Cobalt-Aluminum	$Co^{59}(n,\gamma)Co^{60}$	0.0015	E > 0.015 MeV	5.272 yrs	

*Denotes that monitor is cadmium shielded.

TABLE 6-7

MONTHLY THERMAL GENERATION DURING THE FIRST FIVE FUEL CYCLES
OF THE SEQUOYAH UNIT 2 REACTOR

MONTH	THERMAL GENERATION (MW-hr)	MONTH	THERMAL GENERATION (MW-hr)	MONTH	THERMAL GENERATION (MW-hr)	MONTH	THERMAL GENERATION (MW-hr)
11/81	3200	7/84	2105415	3/87	0	11/89	1474580
12/81	12713	8/84	1626829	4/87	0	12/89	2390942
1/82	244601	9/84	1471238	5/87	0	1/90	2369133
2/82	554637	10/84	0	6/87	0	2/90	2287291
3/82	942115	11/84	0	7/87	0	3/90	2491759
4/82	1611435	12/84	131366	8/87	0	4/90	2242121
5/82	943376	1/85	2002236	9/87	0	5/90	2509824
6/82	1918281	2/85	2069227	10/87	0	6/90	2437716
7/82	2498077	3/85	2532201	11/87	0	7/90	2487333
8/82	2386212	4/85	2449796	12/87	0	8/90	2046158
9/82	2079585	5/85	1401909	1/88	0	9/90	397459
10/82	2282698	6/85	2444832	2/88	0	10/90	0
11/82	957633	7/85	2535401	3/88	0	11/90	180336
12/82	32105	8/85	1693363	4/88	0	12/90	2415061
1/83	2203657	9/85	0	5/88	780704	1/91	2316660
2/83	2240493	10/85	0	6/88	820272	2/91	2287530
3/83	2422686	11/85	0	7/88	2050019	3/91	2525809
4/83	2411559	12/85	0	8/88	2459410	4/91	2449233
5/83	2490822	1/86	0	9/88	1870207	5/91	2534992
6/83	2216622	2/86	0	10/88	1625160	6/91	2414990
7/83	1415930	3/86	0	11/88	1533273	7/91	2533273
8/83	0	4/86	0	12/88	1458074	8/91	2533075
9/83	0	5/86	0	1/89	1014187	9/91	2452746
10/83	950094	6/86	0	2/89	0	10/91	2538138
11/83	1375955	7/86	0	3/89	0	11/91	1567577
12/83	2535658	8/86	0	4/89	98400	12/91	2498839
1/84	2535537	9/86	0	5/89	2208995	1/92	2526794
2/84	2077520	10/86	0	6/89	2433673	2/92	1840863
3/84	2535289	11/86	0	7/89	1959789	3/92	793075
4/84	2449814	12/86	0	8/89	2532338		
5/84	2287795	1/87	0	9/89	2451049		
6/84	2360139	2/87	0	10/89	2122206		

TABLE 6-8
MEASURED SENSOR ACTIVITIES AND REACTION RATES

Monitor and Axial Location	Measured Activity (dis/sec-gm)	Saturated Activity (dis/sec-gm)	Capsule Center Reaction Rate (RPS/NUCLEUS)
Cu-63 (n,α) Co-60			
Top-Middle	1.12×10^5	2.85×10^5	
Middle	1.13×10^5	2.88×10^5	
Bottom-Middle	1.15×10^5	2.93×10^5	
Average	1.13×10^5	2.89×10^5	4.23×10^{-17}
Fe-54(n,p) Mn-54			
Top	1.63×10^6	2.50×10^6	
Middle	1.61×10^6	2.47×10^6	
Bottom-Middle	1.65×10^6	2.53×10^6	
Bottom	1.64×10^6	2.52×10^6	
Average	1.63×10^6	2.50×10^6	4.22×10^{-15}
Ni-58 (n,p) Co-58			
Top	1.46×10^7	3.35×10^7	
Middle	1.45×10^7	3.33×10^7	
Bottom	1.52×10^7	3.49×10^7	
Average	1.48×10^7	3.39×10^7	5.70×10^{-15}
U-238 (n,f) Cs-137 (Cd)			
Middle	3.72×10^5	3.40×10^6	2.26×10^{-14}

TABLE 6-8

MEASURED SENSOR ACTIVITIES AND REACTION RATES - cont'd

Monitor and Axial Location	Measured Activity (dis/sec-gm)	Saturated Activity (dis/sec-gm)	Capsule Center Reaction Rate (RPS/NUCLEUS)
Np-237(n,f) Cs-137 (Cd)			
Middle	3.21×10^{6}	2.94×10^{7}	1.78×10^{-13}
Co-59 (n,γ) Co-60			
Top	1.88×10^{7}	4.78×10^{7}	
Bottom	1.86×10^{7}	4.73×10^{7}	
Average	1.87×10^{7}	4.76×10^{7}	3.27×10^{-12}
Co-59 (n,γ) Co-60 (Cd)			
Top	7.82×10^{6}	1.99×10^{7}	
Bottom	7.43×10^{6}	1.89×10^{7}	
Average	7.63×10^{6}	1.94×10^{7}	1.47×10^{-12}

TABLE 6-9

SUMMARY OF NEUTRON DOSIMETRY RESULTS

	TIME AVERAGED EXPOSURE RATES	
ϕ (E > 1.0 MeV) {n/cm^2-sec}	6.56×10^{10}	± 8%
ϕ (E > 0.1 MeV) {n/cm^2-sec}	2.25×10^{11}	± 15%
dpa/sec	1.10×10^{-10}	± 10%
ϕ (E < 0.414 eV) {n/cm^2-sec}	7.50×10^{10}	± 20%
	INTEGRATED CAPSULE EXPOSURE	
Φ (E > 1.0 MeV) {n/cm^2}	1.11×10^{19}	± 8%
Φ (E > 0.1 MeV) {n/cm^2}	3.81×10^{19}	± 15%
dpa	1.86×10^{-2}	± 10%
Φ (E < 0.414 eV) {n/cm^2}	1.27×10^{19}	± 20%

NOTE: Total Irradiation Time = 5.36 EFPY

TABLE 6-10

COMPARISON OF MEASURED AND FERRET CALCULATED REACTION RATES AT THE SURVEILLANCE CAPSULE CENTER

Reaction	Measured	Adjusted Calculation	C/M
Cu-63 (n,α) Co-60	4.23×10^{-17}	4.25×10^{-17}	1.00
Fe-54 (n,p) Mn-54	4.22×10^{-15}	4.23×10^{-15}	1.00
Ni-58 (n,p) Co-58	5.70×10^{-15}	5.70×10^{-15}	1.00
U-238 (n,f) Cs-137 (Cd)	2.26×10^{-14}	2.19×10^{-14}	0.97
Np-237 (n,f) Cs-137 (Cd)	1.78×10^{-13}	1.81×10^{-13}	1.02
Co-59 (n,γ) Co-60	3.27×10^{-12}	3.25×10^{-12}	1.00
Co-59 (n,γ) Co-60 (Cd)	1.47×10^{-12}	1.47×10^{-12}	1.00

TABLE 6-11

ADJUSTED NEUTRON ENERGY SPECTRUM AT THE SURVEILLANCE CAPSULE CENTER

Group	Energy (Mev)	Adjusted Flux (n/cm^2-sec)	Group	Energy (Mev)	Adjusted Flux (n/cm^2-sec)
1	1.73×10^{1}	3.61×10^{6}	28	9.12×10^{-3}	9.46×10^{9}
2	1.49×10^{1}	8.79×10^{6}	29	5.53×10^{-3}	1.19×10^{10}
3	1.35×10^{1}	4.03×10^{7}	30	3.36×10^{-3}	3.70×10^{9}
4	1.16×10^{1}	1.02×10^{8}	31	2.84×10^{-3}	3.53×10^{9}
5	1.00×10^{1}	2.47×10^{8}	32	2.40×10^{-3}	3.42×10^{9}
6	8.61×10^{0}	4.47×10^{8}	33	2.04×10^{-3}	9.95×10^{9}
7	7.41×10^{0}	1.08×10^{9}	34	1.23×10^{-3}	9.69×10^{9}
8	6.07×10^{0}	1.57×10^{9}	35	7.49×10^{-4}	9.39×10^{9}
9	4.97×10^{0}	3.28×10^{9}	36	4.54×10^{-4}	9.16×10^{9}
10	3.68×10^{0}	4.18×10^{9}	37	2.75×10^{-4}	9.71×10^{9}
11	2.87×10^{0}	8.38×10^{9}	38	1.67×10^{-4}	1.10×10^{10}
12	2.23×10^{0}	1.06×10^{10}	39	1.01×10^{-4}	1.05×10^{10}
13	1.74×10^{0}	1.38×10^{10}	40	6.14×10^{-5}	1.05×10^{10}
14	1.35×10^{0}	1.38×10^{10}	41	3.73×10^{-5}	1.02×10^{10}
15	1.11×10^{0}	2.36×10^{10}	42	2.26×10^{-5}	9.96×10^{9}
16	8.21×10^{-1}	2.50×10^{10}	43	1.37×10^{-5}	9.71×10^{9}
17	6.39×10^{-1}	2.46×10^{10}	44	8.32×10^{-6}	9.32×10^{9}
18	4.98×10^{-1}	1.74×10^{10}	45	5.04×10^{-6}	8.75×10^{9}
19	3.88×10^{-1}	2.30×10^{10}	46	3.06×10^{-6}	8.30×10^{9}
20	3.02×10^{-1}	2.54×10^{10}	47	1.86×10^{-6}	7.76×10^{9}
21	1.83×10^{-1}	2.41×10^{10}	48	1.13×10^{-6}	6.09×10^{9}
22	1.11×10^{-1}	1.90×10^{10}	49	6.83×10^{-7}	7.30×10^{9}
23	6.74×10^{-2}	1.38×10^{10}	50	4.14×10^{-7}	1.20×10^{10}
24	4.09×10^{-2}	8.30×10^{9}	51	2.51×10^{-7}	1.24×10^{10}
25	2.55×10^{-2}	9.98×10^{9}	52	1.52×10^{-7}	1.24×10^{10}
26	1.99×10^{-2}	5.43×10^{9}	53	9.24×10^{-8}	3.82×10^{10}
27	1.50×10^{-2}	7.36×10^{9}			

NOTE: Tabulated energy levels represent the upper energy of each group.

TABLE 6-12

COMPARISON OF CALCULATED AND MEASURED
EXPOSURE LEVELS FOR CAPSULE X

	Calculated	Measured	C/M
$\Phi(E > 1.0\ MeV)\ \{n/cm^2\}$	1.07×10^{19}	1.11×10^{19}	0.96
$\Phi(E > 0.1\ MeV)\ \{n/cm^2\}$	3.60×10^{19}	3.81×10^{19}	0.94
dpa	1.83×10^{-2}	1.86×10^{-2}	0.98
$\Phi(E < 0.414\ eV)\ \{n/cm^2\}$	6.33×10^{18}	1.27×10^{19}	0.50

TABLE 6-13
NEUTRON EXPOSURE PROJECTIONS AT KEY LOCATIONS
ON THE PRESSURE VESSEL CLAD/BASE METAL INTERFACE

5.36 EFPY

	0°	15°	30°	45°
Φ (E > 1.0 Mev) [n/cm2]	1.09×10^{18}	1.78×10^{18}	2.14×10^{18}	3.25×10^{18}
Φ (E > 0.1 MeV) [n/cm2]	2.73×10^{18}	4.47×10^{18}	5.39×10^{18}	8.45×10^{18}
Iron Atom Displacements [dpa]	1.78×10^{-3}	2.87×10^{-3}	3.40×10^{-3}	5.17×10^{-3}

16.0 EFPY

	0°	15°	30°	45°
Φ (E > 1.0 Mev) [n/cm2]	3.25×10^{18}	5.34×10^{18}	6.39×10^{18}	9.69×10^{18}
Φ (E > 0.1 MeV) [n/cm2]	8.13×10^{18}	1.34×10^{19}	1.61×10^{19}	2.52×10^{19}
Iron Atom Displacements [dpa]	5.30×10^{-3}	8.60×10^{-3}	1.02×10^{-2}	1.54×10^{-2}

32.0 EFPY

	0°	15°	30°	45°
Φ (E > 1.0 Mev) [n/cm2]	6.50×10^{18}	1.07×10^{19}	1.28×10^{19}	1.94×10^{19}
Φ (E > 0.1 MeV) [n/cm2]	1.63×10^{19}	2.69×10^{19}	3.23×10^{19}	5.04×10^{19}
Iron Atom Displacements [dpa]	1.06×10^{-2}	1.72×10^{-2}	2.04×10^{-2}	3.08×10^{-2}

TABLE 6-14

NEUTRON EXPOSURE VALUES AT 1/4T AND 3/4T LOCATIONS FOR 16 AND 32 EFPY

16 EFPY

	NEUTRON FLUENCE (E > 1.0 MeV) SLOPE (n/cm^2)			dpa SLOPE (equivalent n/cm^2)		
	Surface	1/4 T	3/4 T	Surface	1/4 T	3/4 T
0°	3.25×10^{18}	1.72×10^{18}	3.54×10^{17}	3.25×10^{18}	2.08×10^{18}	7.54×10^{17}
15°	5.34×10^{18}	2.84×10^{18}	5.87×10^{17}	5.34×10^{18}	3.41×10^{18}	1.23×10^{18}
30°	6.39×10^{18}	3.43×10^{18}	7.22×10^{17}	6.39×10^{18}	4.17×10^{18}	1.55×10^{18}
45°	9.69×10^{18}	5.10×10^{18}	1.02×10^{18}	9.69×10^{18}	6.20×10^{18}	2.14×10^{18}

32 EFPY

	NEUTRON FLUENCE (E > 1.0 MeV) SLOPE (n/cm^2)			dpa SLOPE (equivalent n/cm^2)		
	Surface	1/4 T	3/4 T	Surface	1/4 T	3/4 T
0°	6.50×10^{18}	3.44×10^{18}	7.08×10^{17}	6.50×10^{18}	4.16×10^{18}	1.51×10^{18}
15°	1.07×10^{19}	5.68×10^{18}	1.17×10^{18}	1.07×10^{19}	6.82×10^{18}	2.46×10^{18}
30°	1.28×10^{19}	6.86×10^{18}	1.44×10^{18}	1.28×10^{19}	8.33×10^{18}	3.09×10^{18}
45°	1.94×10^{19}	1.02×10^{19}	2.03×10^{18}	1.94×10^{19}	1.24×10^{19}	4.28×10^{18}

TABLE 6-15

UPDATED LEAD FACTORS FOR SEQUOYAH UNIT 2 SURVEILLANCE CAPSULES

Capsule	Lead Factor
T	3.36[a]
U	3.41[a]
X	3.42[b]
Y	3.42[b]
S	1.10[b]
V	1.10[b]
W	1.10[b]
Z	1.10[b]

(a) Plant specific evaluation based on end of Cycle 1 calculated fluence.

(b) Plant specific evaluation based on end of Cycle 5 calculated fluence.

SECTION 7.0
SURVEILLANCE CAPSULE REMOVAL SCHEDULE

The following removal schedule meets ASTM E185-82 and is recommended for future capsules to be removed from the Sequoyah Unit 2 reactor vessel:

Capsule	Location (deg.)	Capsule Lead Factor	Removal Time [(b)]	Estimated Fluence (n/cm^2)
T	40	3.36	1.04 (Removed)[(a)]	2.20×10^{18} (Actual)
U	140	3.41	2.93 (Removed)[(a)]	6.43×10^{18} (Actual)
X	220	3.42	5.36 (Removed)[(a)]	1.11×10^{19} (Actual)
Y	320	3.42	9.50	1.97×10^{19} (c)
S	4	1.10	EOL	2.13×10^{19}
V	176	1.10	Standby	---
W	184	1.10	Standby	---
Z	356	1.10	Standby	---

(a) Plant Specific Evaluation

(b) Effective Full Power Years (EFPY) from plant startup.

(c) Approximate EOL (32 EFPY) fluence at the reactor vessel inner wall location.

SECTION 8.0
REFERENCES

1. S.E. Yanichko et al., "Tennessee Valley Authority Sequoyah Unit No. 2 Reactor Vessel Radiation Surveillance Program," WCAP-8513, November 1975.

2. Code of Federal Regulations, 10CFR50, Appendix G, "Fracture Toughness Requirements", and Appendix H, "Reactor Vessel Material Surveillance Program Requirements," U.S. Nuclear Regulatory Commission, Washington, D.C.

3. Regulatory Guide 1.99, Proposed Revision 2, "Radiation Damage to Reactor Vessel Materials", U.S. Nuclear Regulatory Commission, February, 1986.

4. Section III of the ASME Boiler and Pressure Vessel Code, Appendix G, "Protection Against Nonductile Failure."

5. ASTM E208, "Standard Test Method for Conducting Drop-Weight Test to Determine Nil-Ductility Transition Temperature of Ferritic Steels."

6. ASTM E185-82, "Standard Practice for Conducting Surveillance Tests for Light-Water Cooled Nuclear Power Reactor Vessels, E706 (IF)."

7. ASTM E23-88, "Standard Test Methods for Notched Bar Impact Testing of Metallic Materials."

8. ASTM A370-89, "Standard Test Methods and Definitions for Mechanical Testing of Steel Products."

9. ASTM E8-89b, "Standard Test Methods of Tension Testing of Metallic Materials."

10. ASTM E21-79 (1988), "Standard Practice for Elevated Temperature Tension Tests of Metallic Materials."

11. ASTM E83-85, "Standard Practice for Verification and Classification of Extensometers."

12. R. G. Soltesz, R. K. Disney, J. Jedruch, and S. L. Ziegler, "Nuclear Rocket Shielding Methods, Modification, Updating and Input Data Preparation. Vol. 5--Two-Dimensional Discrete Ordinates Transport Technique", WANL-PR(LL)-034, Vol. 5, August 1970.

13. "ORNL RSCI Data Library Collection DLC-76 SAILOR Coupled Self-Shielded, 47 Neutron, 20 Gamma-Ray, P3, Cross Section Library for Light Water Reactors".

14. R. W. Miller, et. al., "The Core Physics Characteristics of the Sequoyah Unit 2 Nuclear Power Plant - Cycle 1", WCAP-9516, May 1979. (Proprietary)

15. J. Macrae, et. al., "The Nuclear Design of the Sequoyah Unit 2 Nuclear Power Plant - Cycle 2", WCAP-10400, September 1983. (Proprietary)

16. M. J. Poploski, et. al., "Nuclear Parameters and Operations Package for Sequoyah Unit 2 - Cycle 3", WCAP-10753, December 1984. (Proprietary)

17. M. J. Poploski, et. al., "Nuclear Parameters and Operations Package for Sequoyah Unit 2 - Cycle 4", WCAP-12160, May 1989. (Proprietary)

18. M. M. Baker, et. al., "Nuclear Parameters and Operations Package for Sequoyah Unit 2 - Cycle 5", WCAP-12713, November 1990. (Proprietary)

19. ASTM Designation E482-89, "Standard Guide for Application of Neutron Transport Methods for Reactor Vessel Surveillance", in ASTM Standards, Section 12, American Society for Testing and Materials, Philadelphia, PA, 1991.

20. ASTM Designation E560-84, "Standard Recommended Practice for Extrapolating Reactor Vessel Surveillance Dosimetry Results", in ASTM Standards, Section 12, American Society for Testing and Materials, Philadelphia, PA, 1991.

21. ASTM Designation E693-79, "Standard Practice for Characterizing Neutron Exposures in Ferritic Steels in Terms of Displacements per Atom (dpa)", in ASTM Standards, Section 12, American Society for Testing and Materials, Philadelphia, PA, 1991.

22. ASTM Designation E706-87, "Standard Master Matrix for Light-Water Reactor Pressure Vessel Surveillance Standard", in ASTM Standards, Section 12, American Society for Testing and Materials, Philadelphia, PA, 1991.

23. ASTM Designation E853-87, "Standard Practice for Analysis and Interpretation of Light-Water Reactor Surveillance Results", in ASTM Standards, Section 12, American Society for Testing and Materials, Philadelphia, PA, 1991.

24. ASTM Designation E261-90, "Standard Method for Determining Neutron Flux, Fluence, and Spectra by Radioactivation Techniques", in ASTM Standards, Section 12, American Society for Testing and Materials, Philadelphia, PA, 1991.

25. ASTM Designation E262-86, "Standard Method for Measuring Thermal Neutron Flux by Radioactivation Techniques", in ASTM Standards, Section 12, American Society for Testing and Materials, Philadelphia, PA, 1991.

26. ASTM Designation E263-88, "Standard Method for Determining Fast-Neutron Flux Density by Radioactivation of Iron", in ASTM Standards, Section 12, American Society for Testing and Materials, Philadelphia, PA, 1991.

27. ASTM Designation E264-87, "Standard Method for Determining Fast-Neutron Flux Density by Radioactivation of Nickel", in ASTM Standards, Section 12, American Society for Testing and Materials, Philadelphia, PA, 1991.

28. ASTM Designation E481-86, "Standard Method for Measuring Neutron-Flux Density by Radioactivation of Cobalt and Silver", in ASTM Standards, Section 12, American Society for Testing and Materials, Philadelphia, PA, 1991.

29. ASTM Designation E523-87, "Standard Method for Determining Fast-Neutron Flux Density by Radioactivation of Copper", in ASTM Standards, Section 12, American Society for Testing and Materials, Philadelphia, PA, 1991.

30. ASTM Designation E704-90, "Standard Method for Measuring Reaction Rates by Radioactivation of Uranium-238", in ASTM Standards, Section 12, American Society for Testing and Materials, Philadelphia, PA, 1991.

31. ASTM Designation E705-90, "Standard Method for Measuring Fast-Neutron Flux Density by Radioactivation of Neptunium-237", in ASTM Standards, Section 12, American Society for Testing and Materials, Philadelphia, PA, 1991.

32. ASTM Designation E1005-84, "Standard Method for Application and Analysis of Radiometric Monitors for Reactor Vessel Surveillance", in ASTM Standards, Section 12, American Society for Testing and Materials, Philadelphia, PA, 1991.

33. F. A. Schmittroth, FERRET Data Analysis Core, HEDL-TME 79-40, Hanford Engineering Development Laboratory, Richland, WA, September 1979.

34. W. N. McElroy, S. Berg and T. Crocket, A Computer-Automated Iterative Method of Neutron Flux Spectra Determined by Foil Activation, AFWL-TR-7-41, Vol. I-IV, Air Force Weapons Laboratory, Kirkland AFB, NM, July 1967.

35. EPRI-NP-2188, "Development and Demonstration of an Advanced Methodology for LWR Dosimetry Applications", R. E. Maerker, et al., 1981.

36. R. S. Boggs, et al, "Analysis of Capsule T From the Tennessee Valley Authority Sequoyah Unit 2 Reactor Vessel Radiation Surveillance Program", WCAP-10509, April 1984. (Westinghouse Class 3 Non-Proprietary)

37. Southwest Research Institute Nondestructive Evaluation Science and Technology Division, "Reactor Vessel Material Surveillance Program for Sequoyah Unit 2: Analysis of Capsule U", Final Report SwRI Project 17-8851 TVA Contract 85PJH-964430, January 1990.

APPENDIX A

Load-Time Records for Charpy Specimen Tests

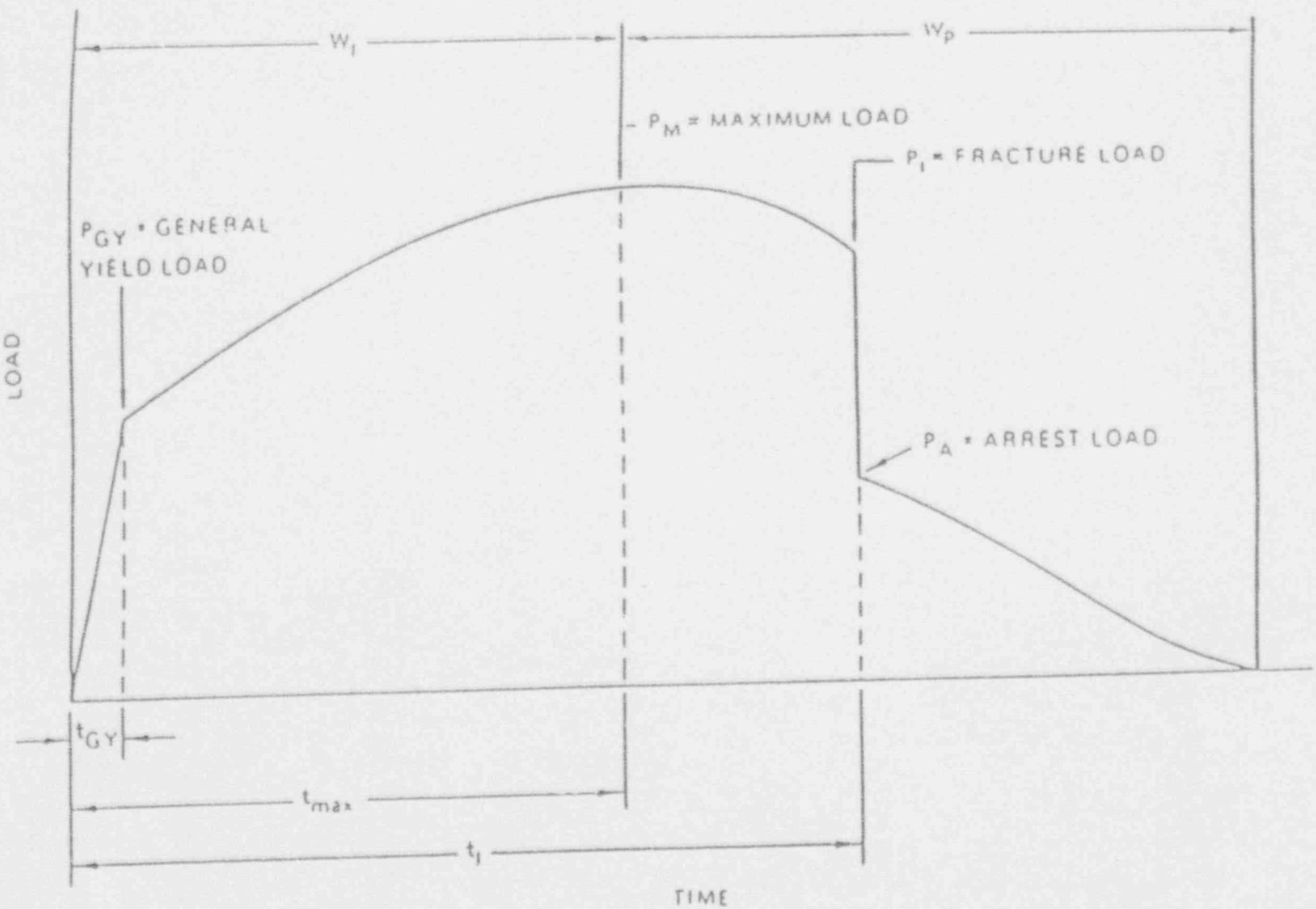

Figure A-1. Idealized load-time record

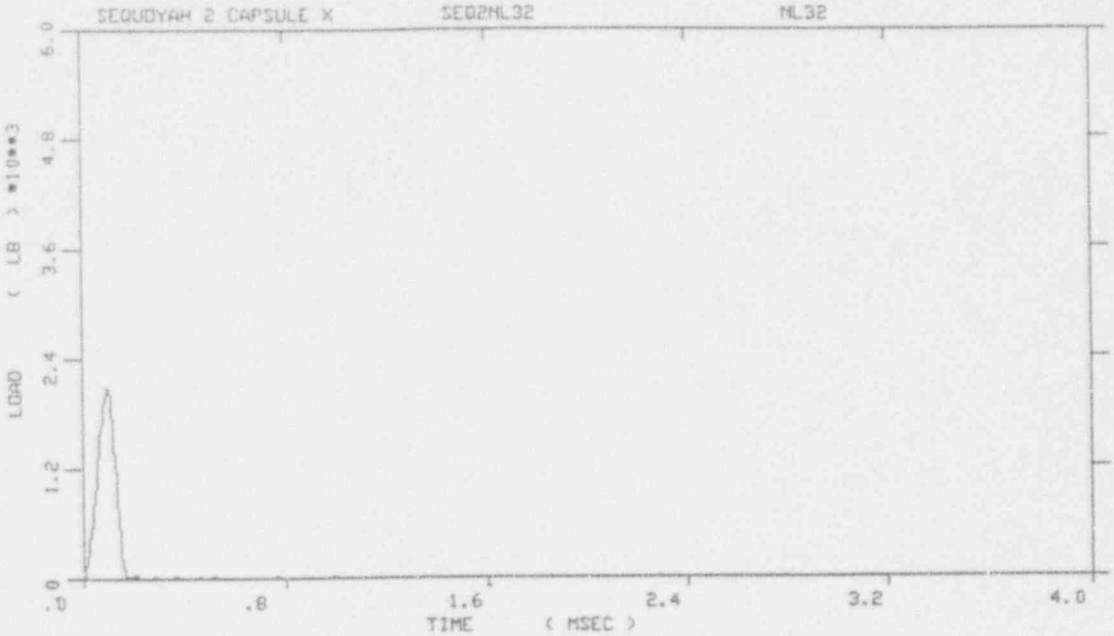

Sequoyah 2 Capsule X

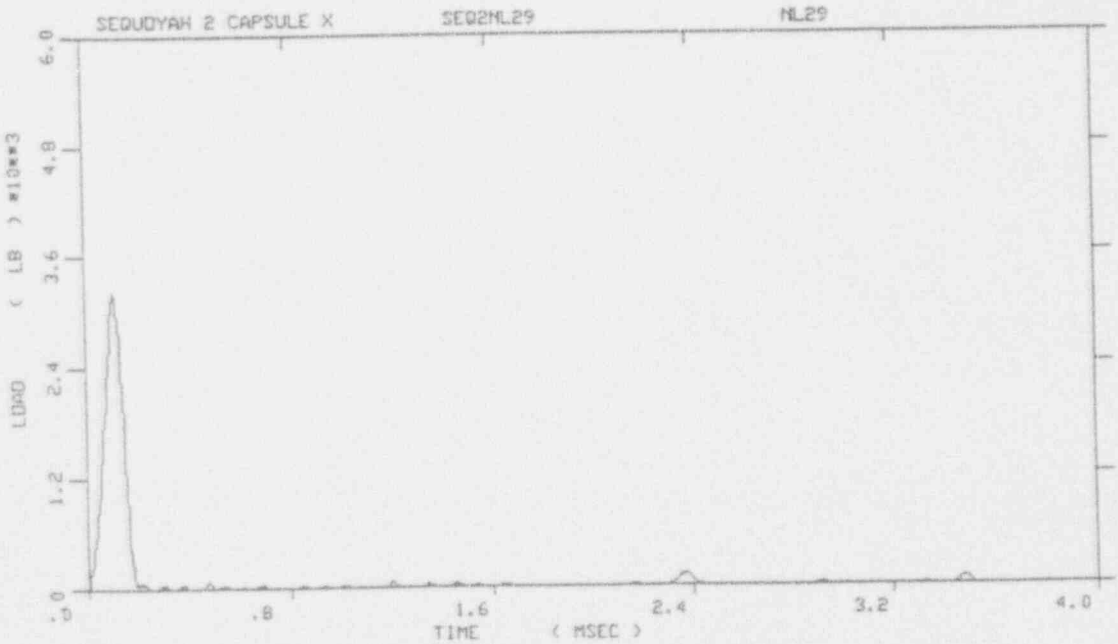

Sequoyah 2 Capsule X

Figure A-2. Load-time records for Specimens NL32 and NL29

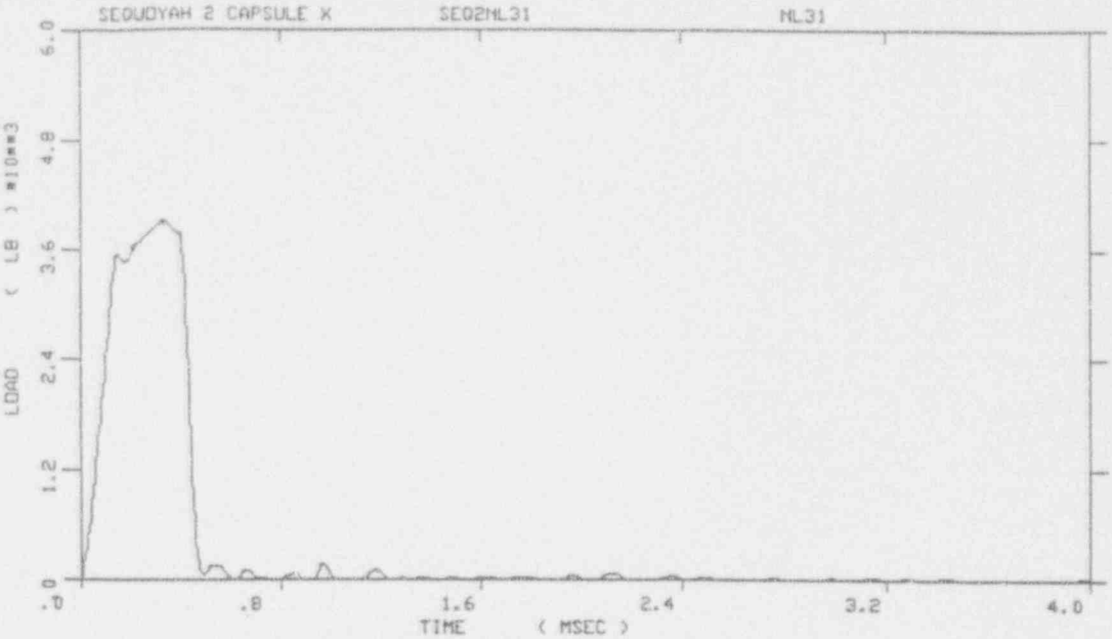

Sequoyah 2 Capsule X

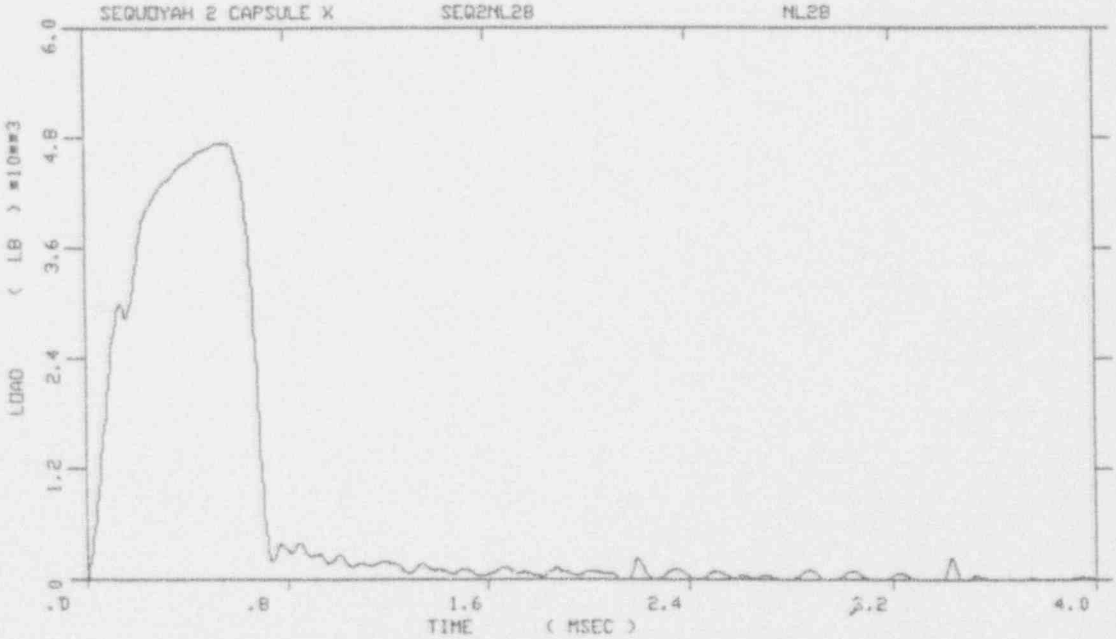

Sequoyah 2 Capsule X

Figure A-3. Load-time records for Specimens NL31 and NL28

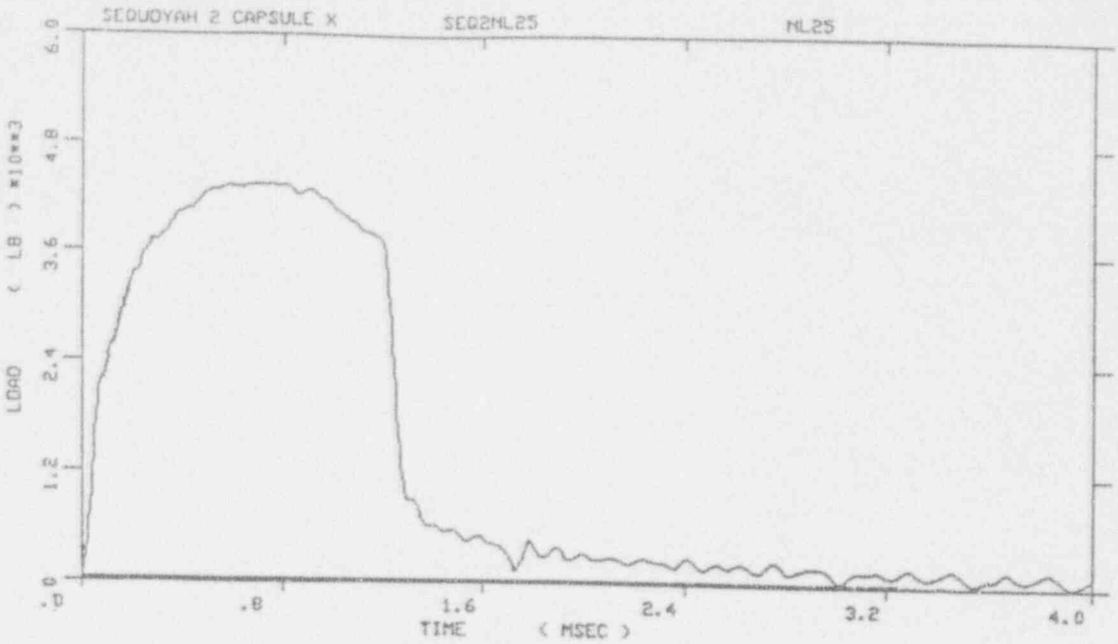

Sequoyah 2 Capsule X

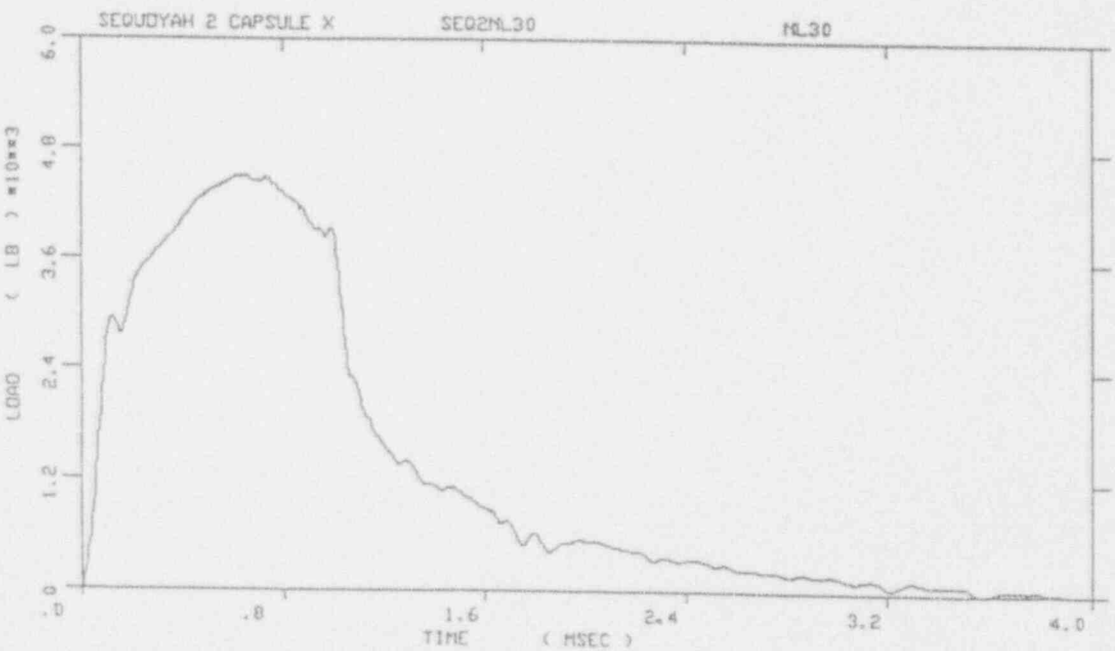

Sequoyah 2 Capsule X

Figure A-4. Load-time records for Specimens NL25 and NL30

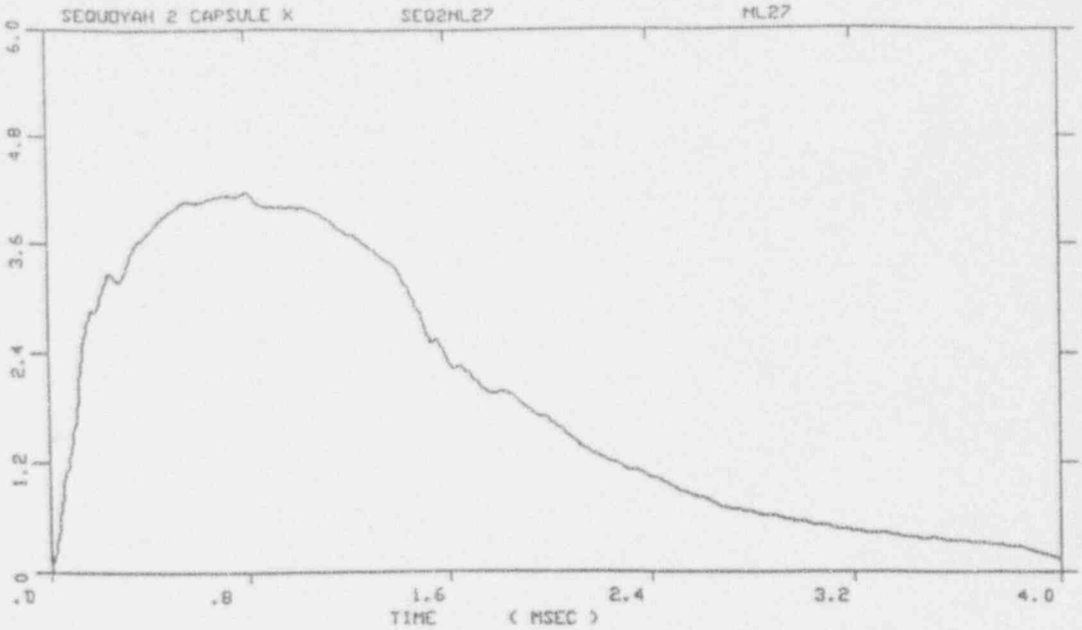

Sequoyah 2 Capsule X

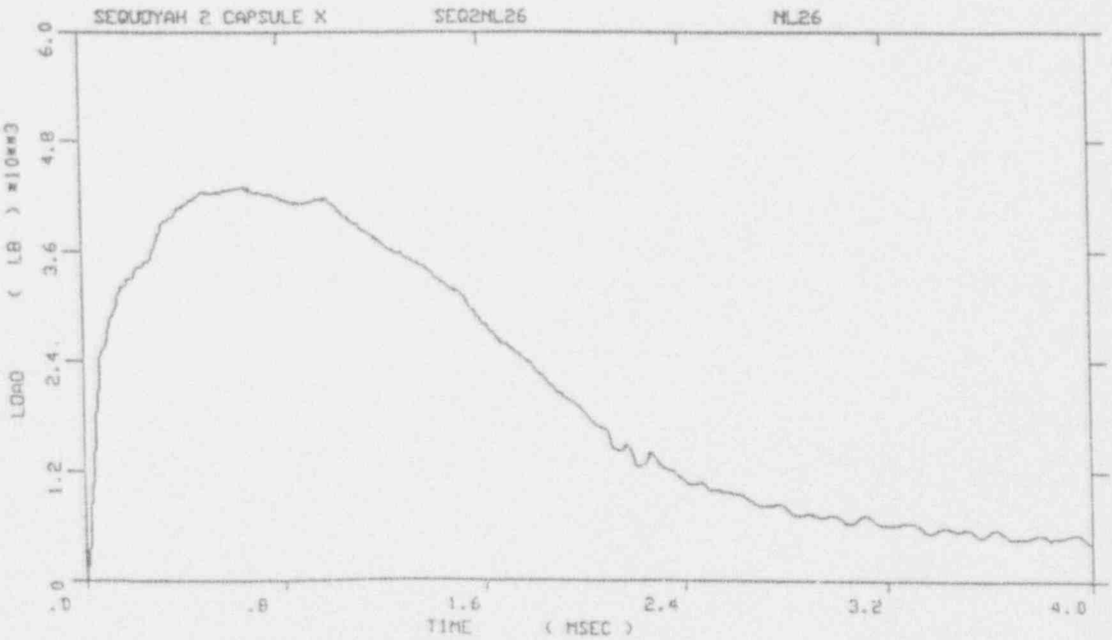

Sequoyah 2 Capsule X

Figure A-5. Load-time records for Specimens NL27 and NL26

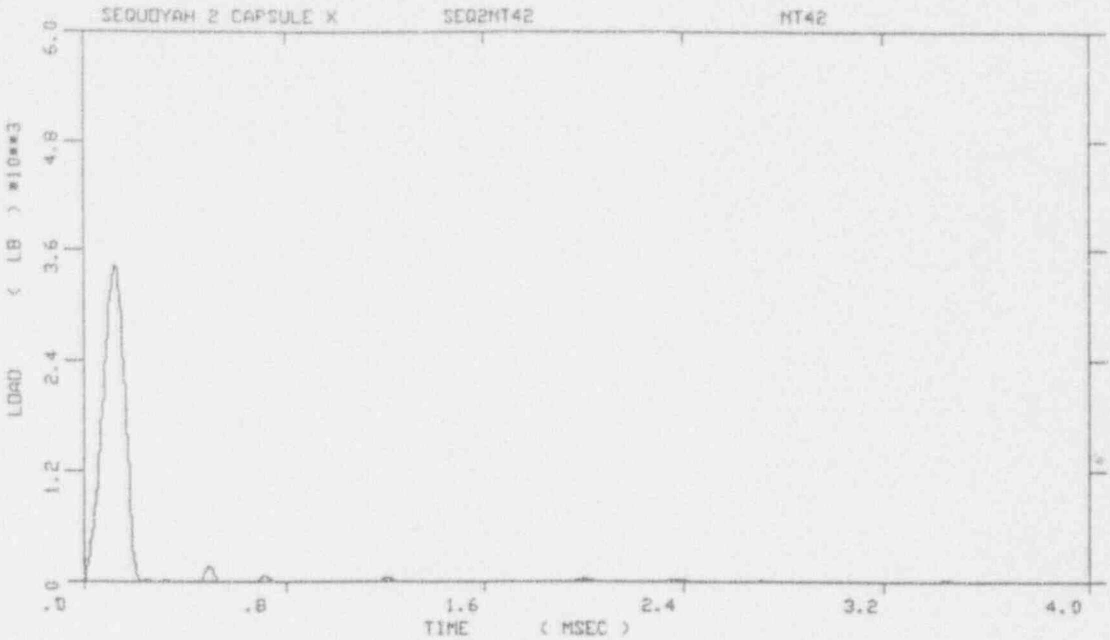

Sequoyah 2 Capsule X

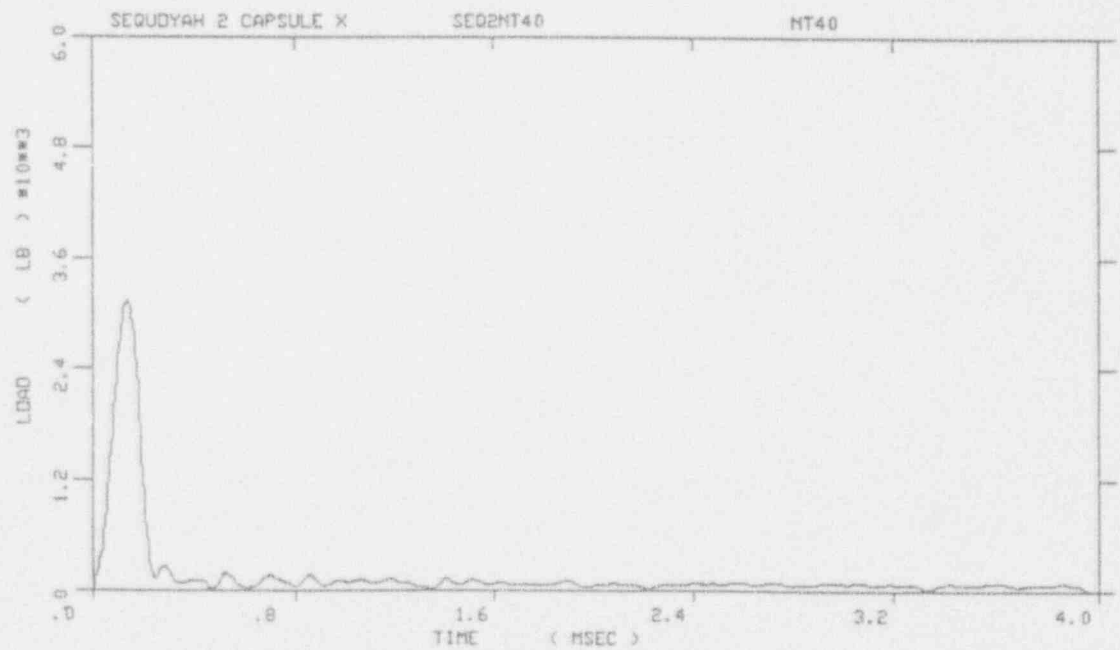

Sequoyah 2 Capsule X

Figure A-6. Load-time records for Specimens NT42 and NT40

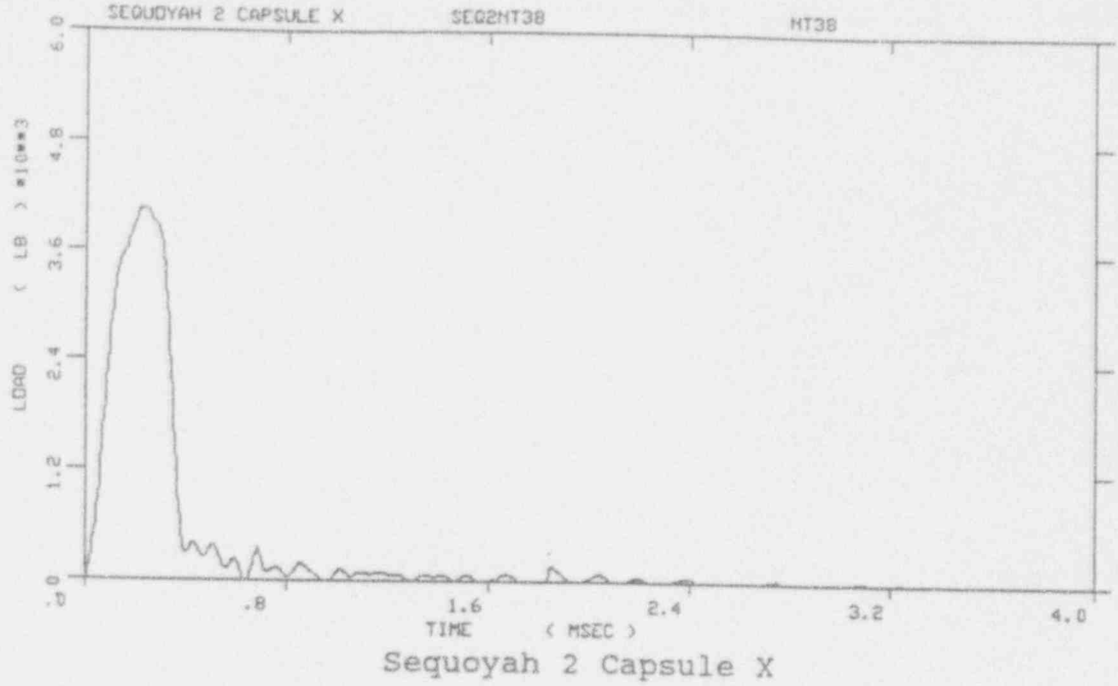

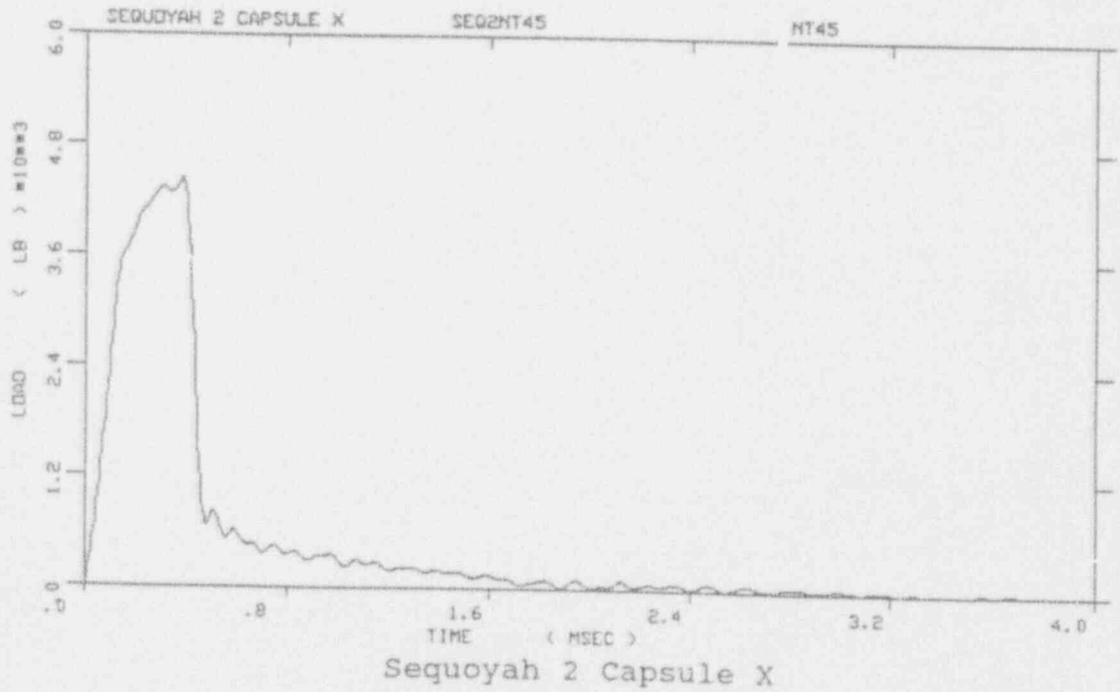

Figure A-7. Load-time records for Specimens NT38 and NT45

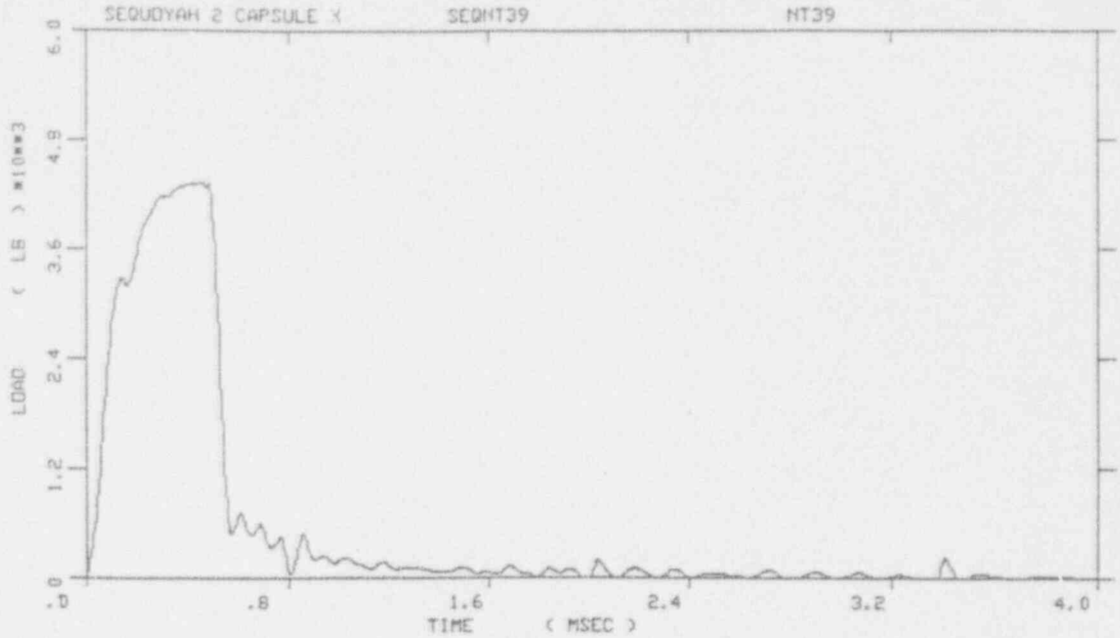

Sequoyah 2 Capsule X

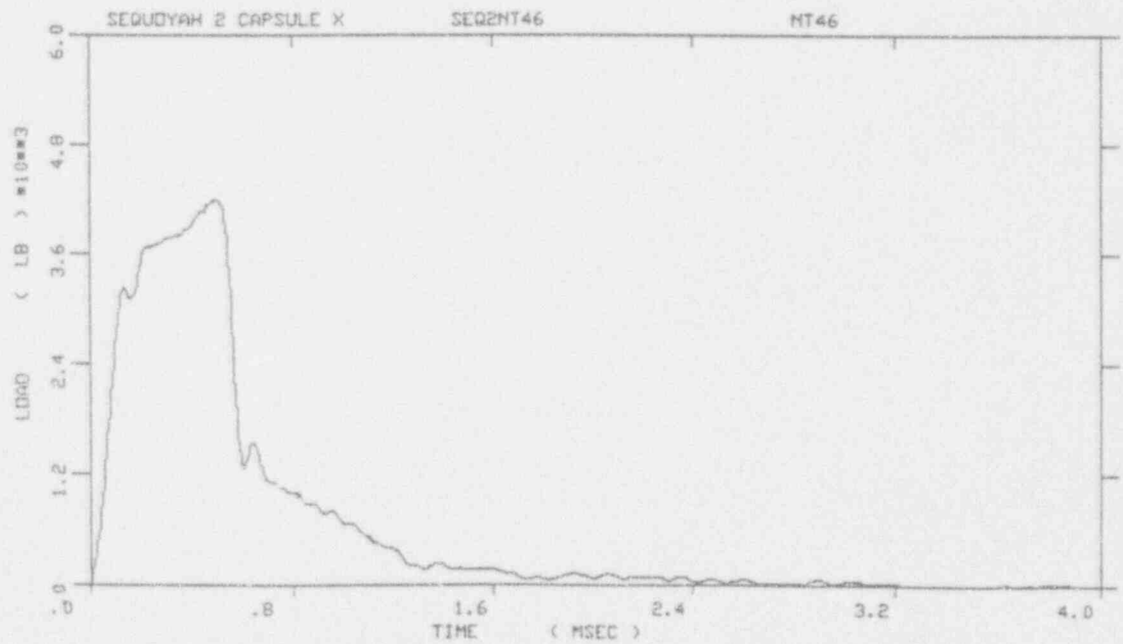

Sequoyah 2 Capsule X

Figure A-8. Load-time records for Specimens NT39 and NT46

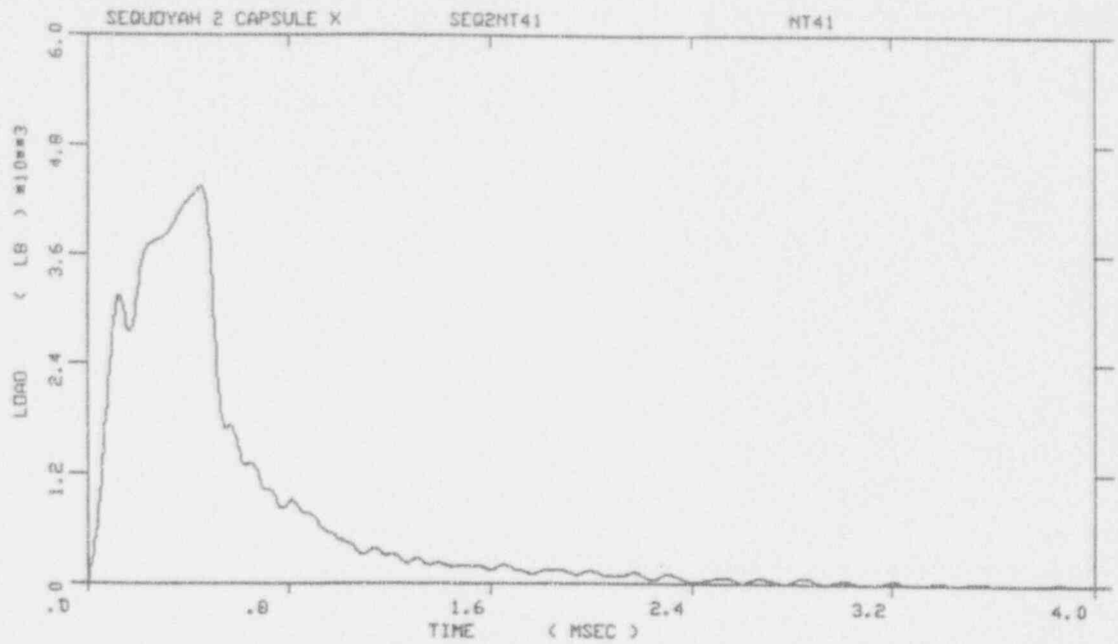

Sequoyah 2 Capsule X

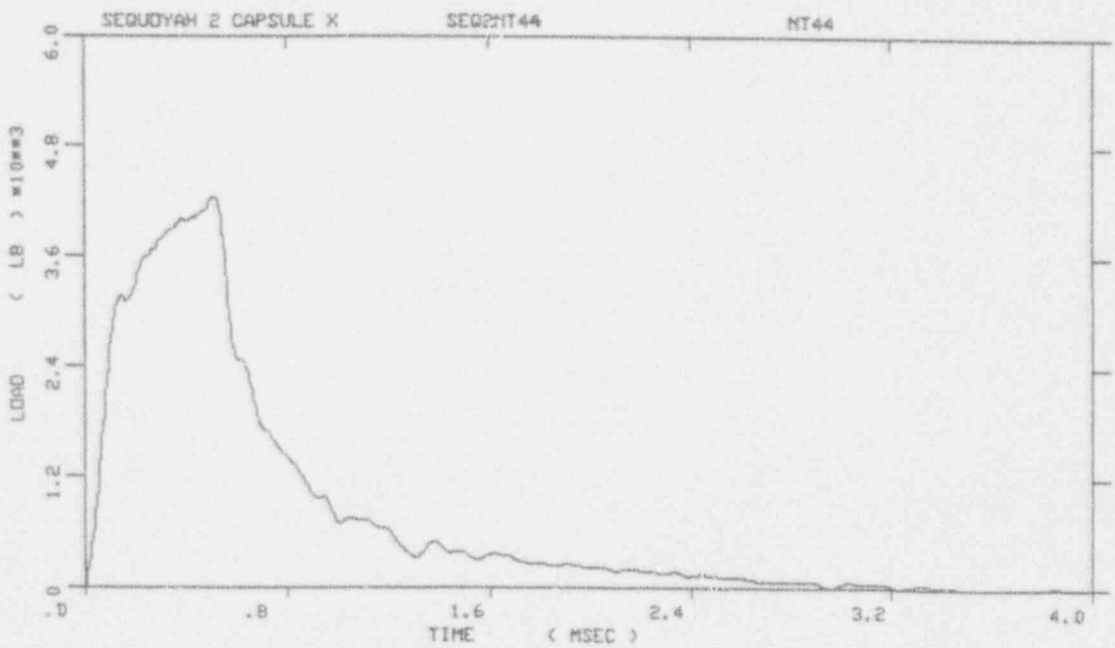

Sequoyah 2 Capsule X

Figure A-9. Load-time records for Specimens NT41 and NT44

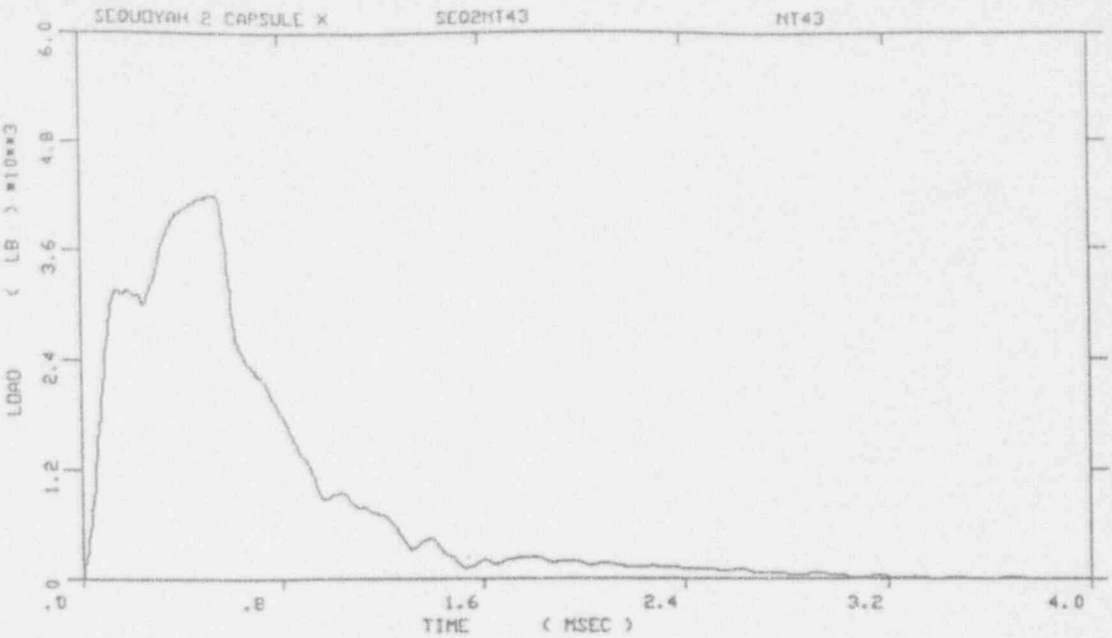

Sequoyah 2 Capsule X

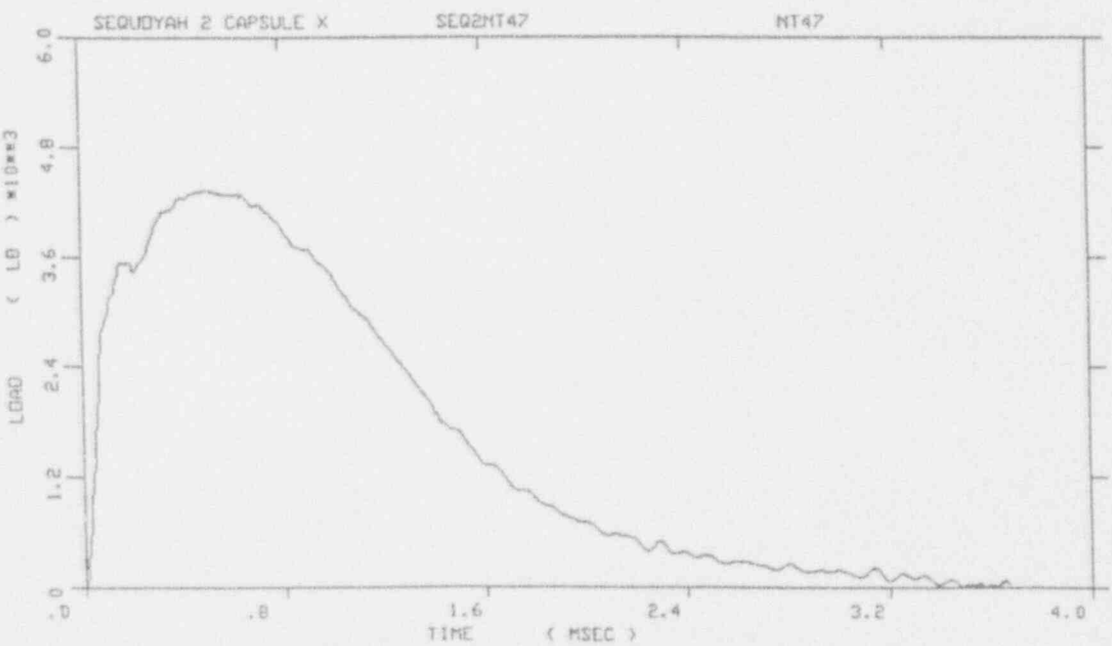

Sequoyah 2 Capsule X

Figure A-10. Load-time records for Specimens NT43 and NT47

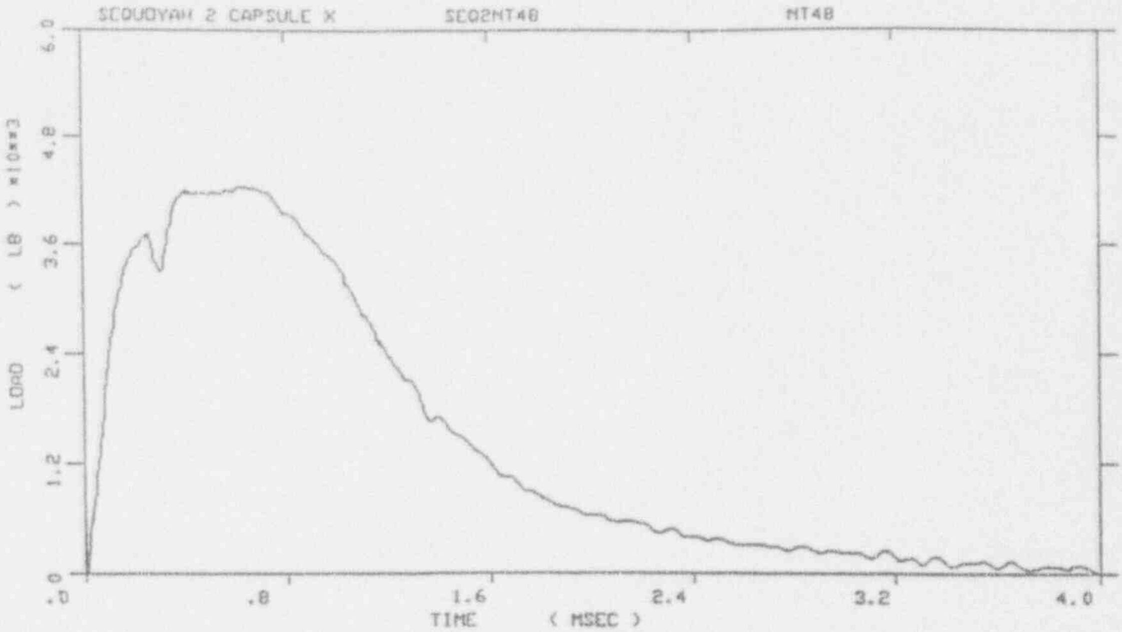

Sequoyah 2 Capsule X

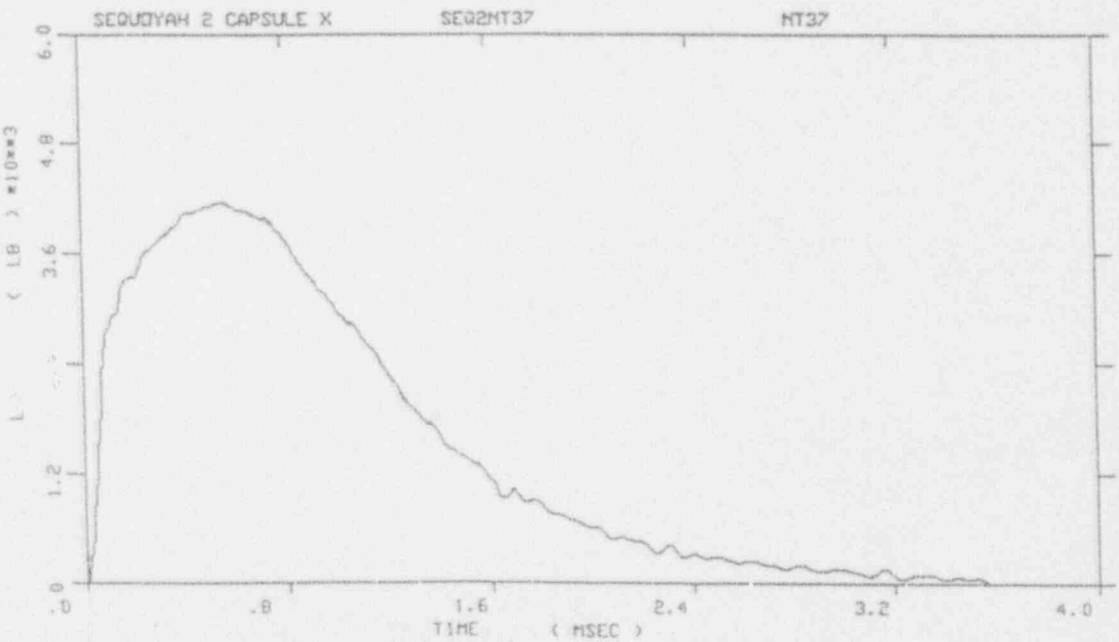

Sequoyah 2 Capsule X

Figure A-11. Load-time records for Specimens NT48 and NT37

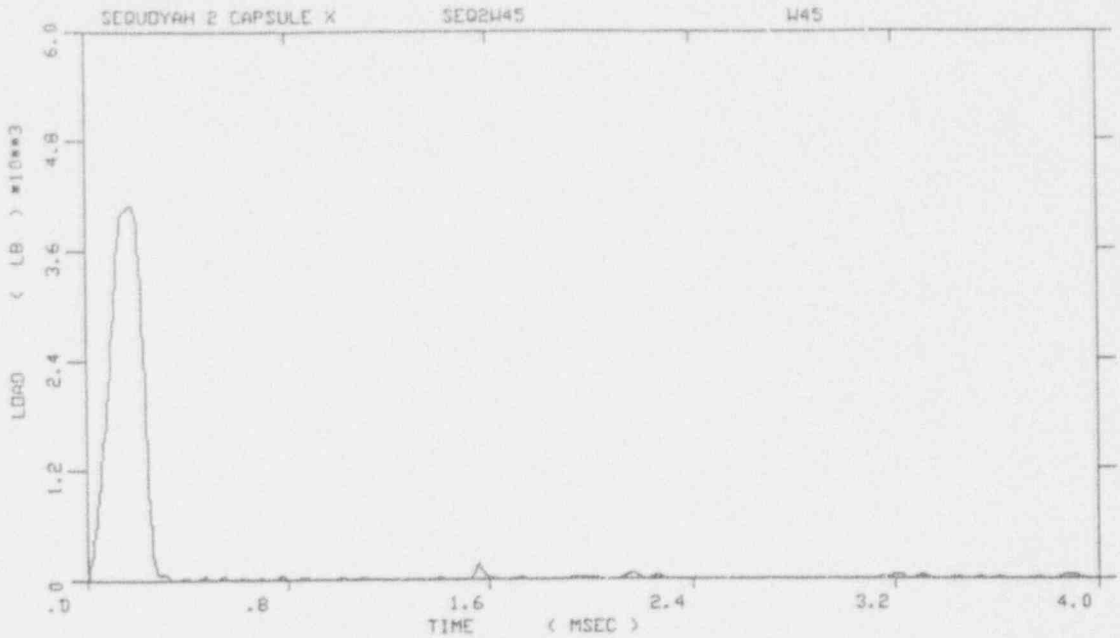

Sequoyah 2 Capsule X

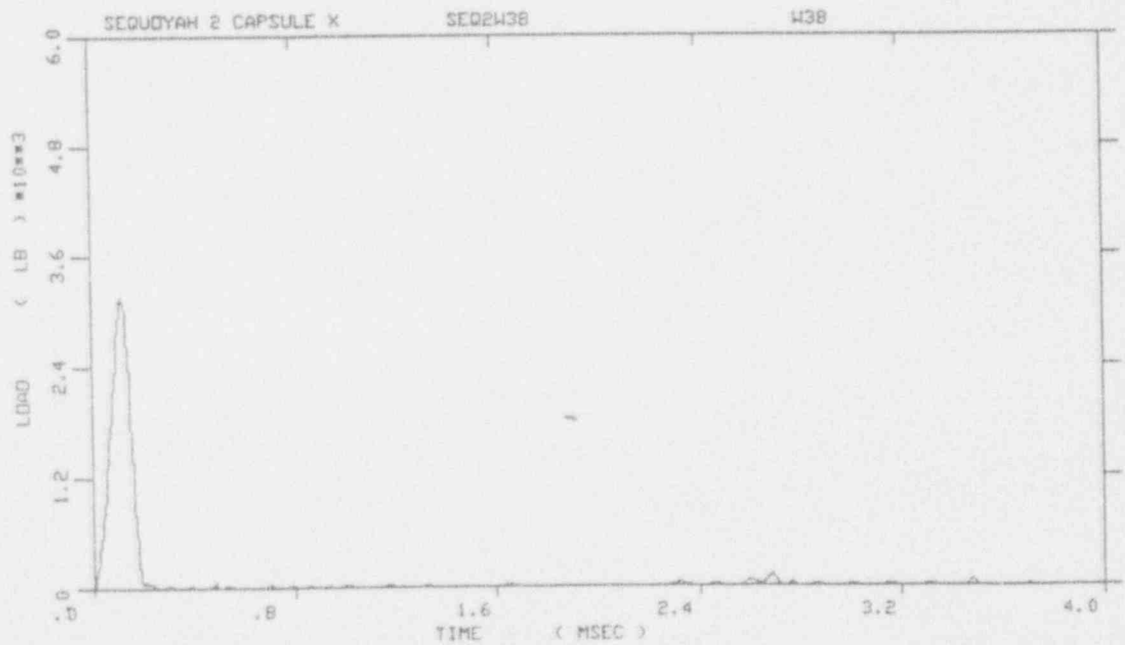

Sequoyah 2 Capsule X

Figure A-12. Load-time records for Specimens W45 and W38

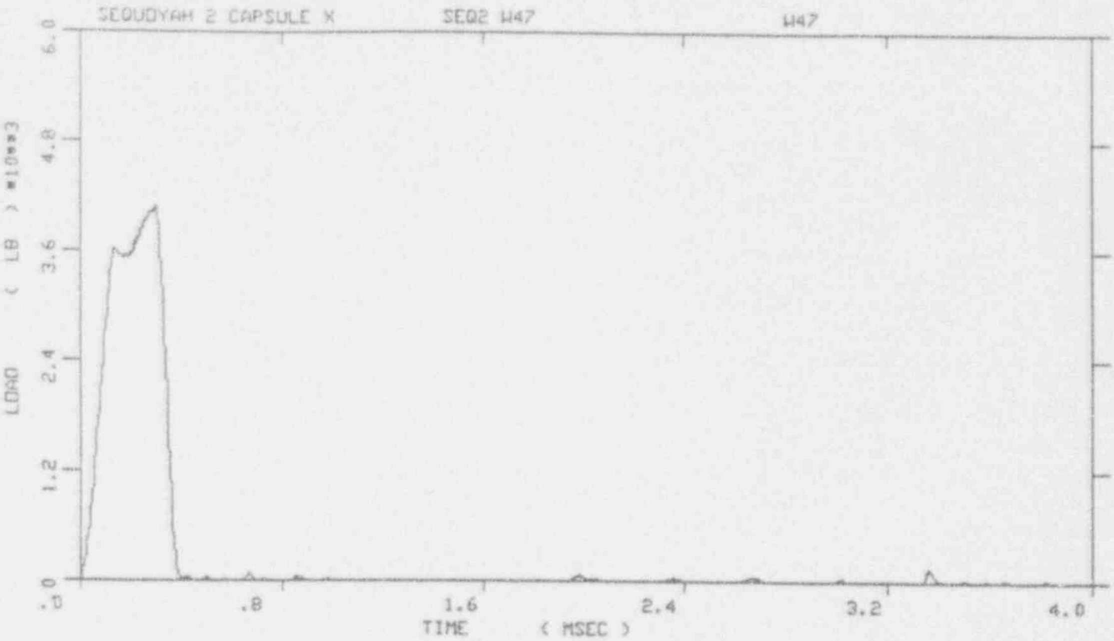

Sequoyah 2 Capsule X

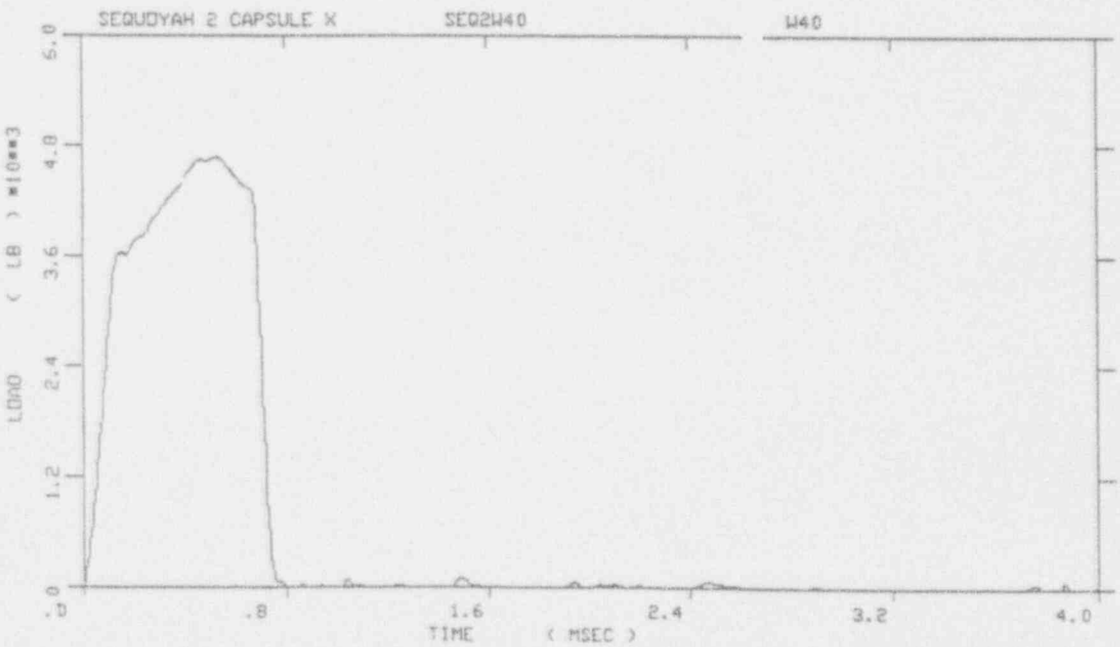

Sequoyah 2 Capsule X

Figure A-13. Load-time records for Specimens W47 and W40

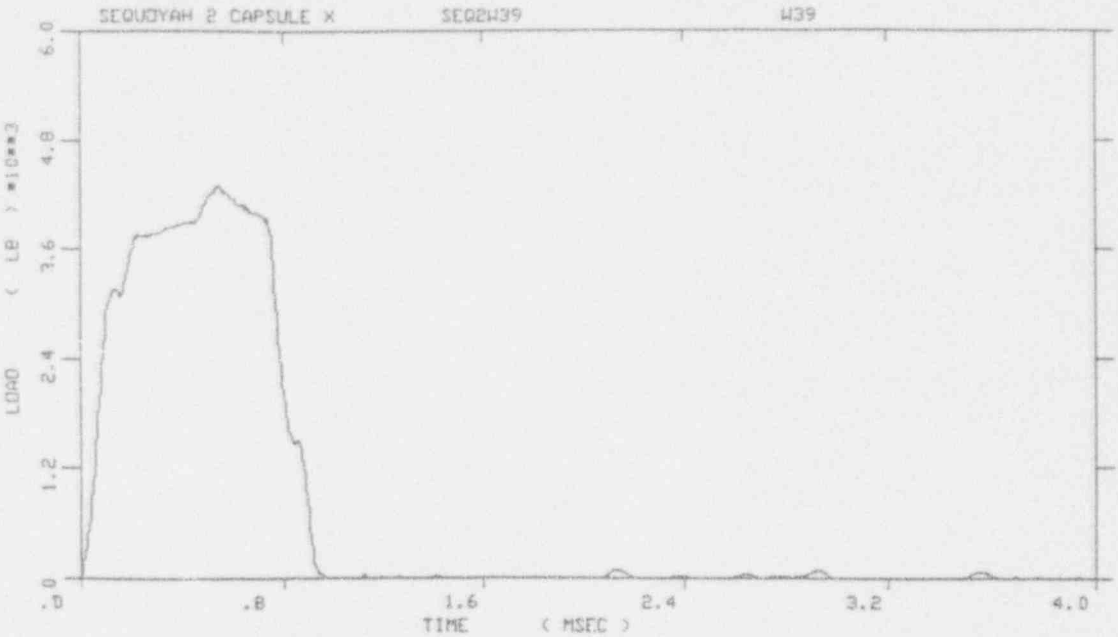

Sequoyah 2 Capsule X

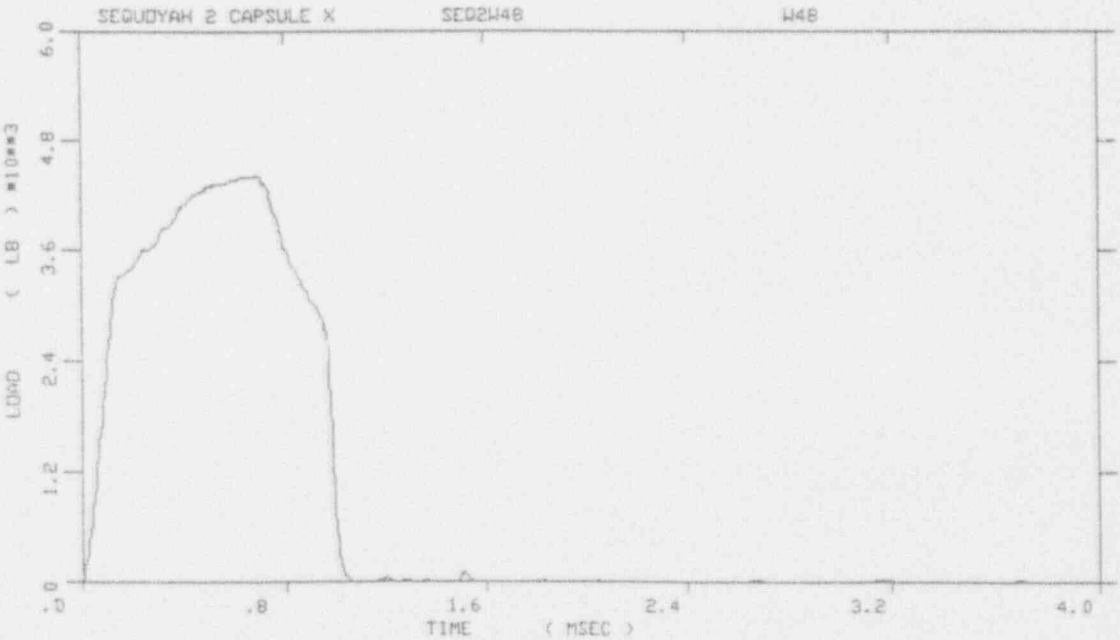

Sequoyah 2 Capsule X

Figure A-14. Load-time records for Specimens W39 and W48

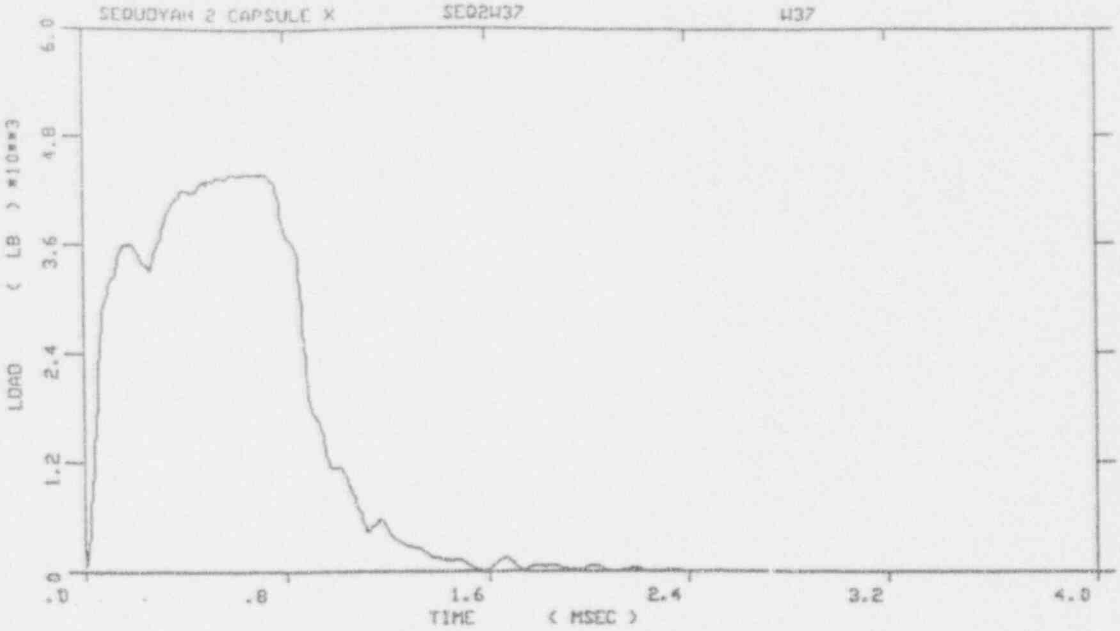

Sequoyah 2 Capsule X

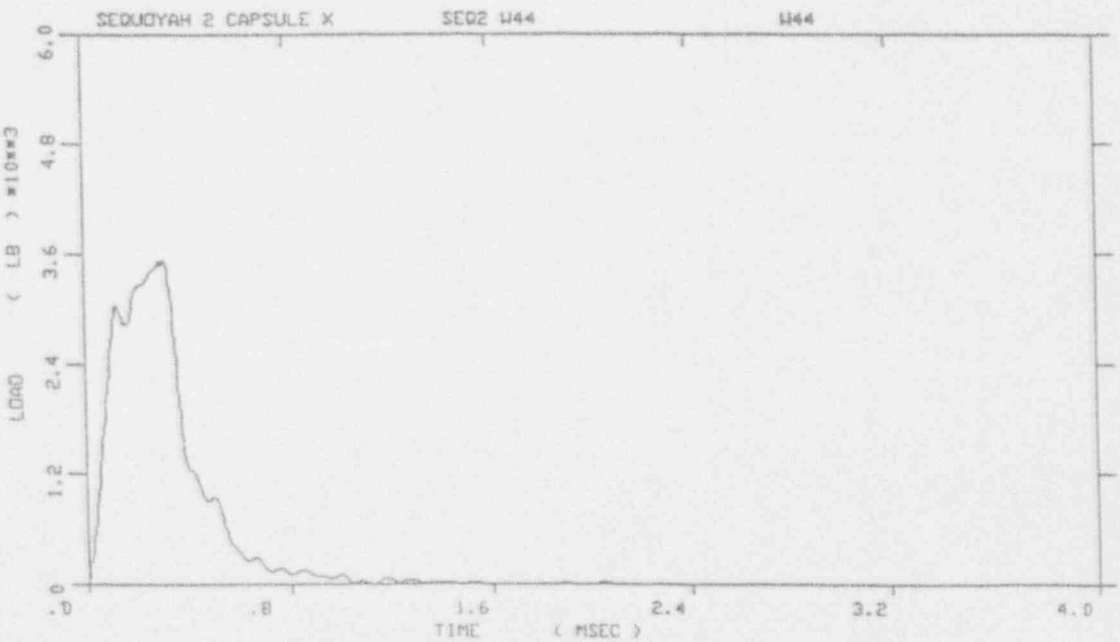

Sequoyah 2 Capsule X

Figure A-15. Load-time records for Specimens W37 and W44

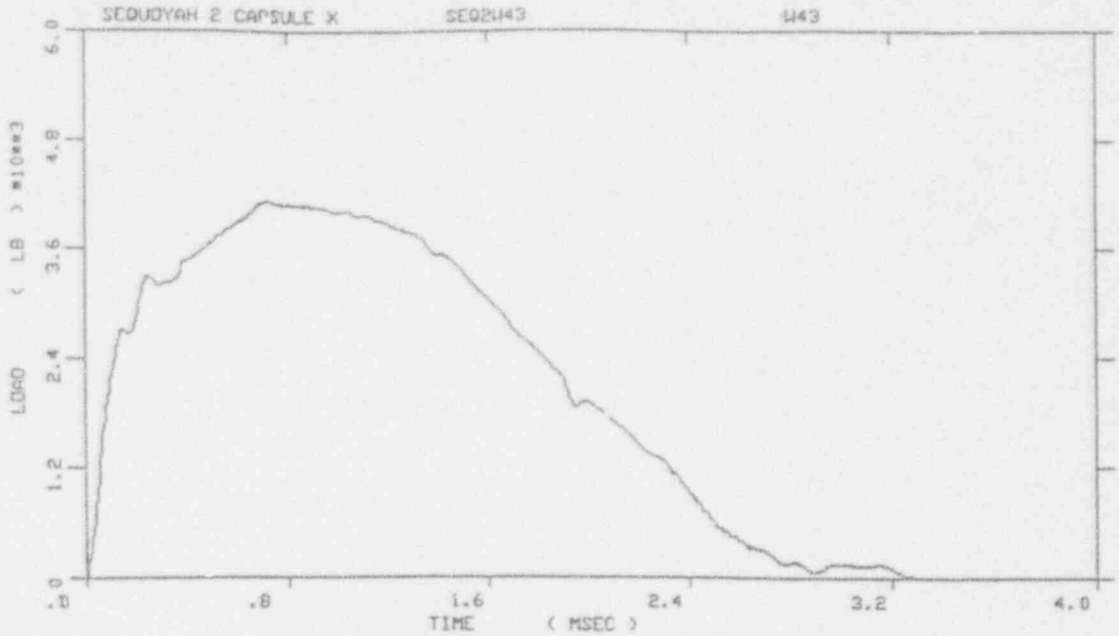

Sequoyah 2 Capsule X

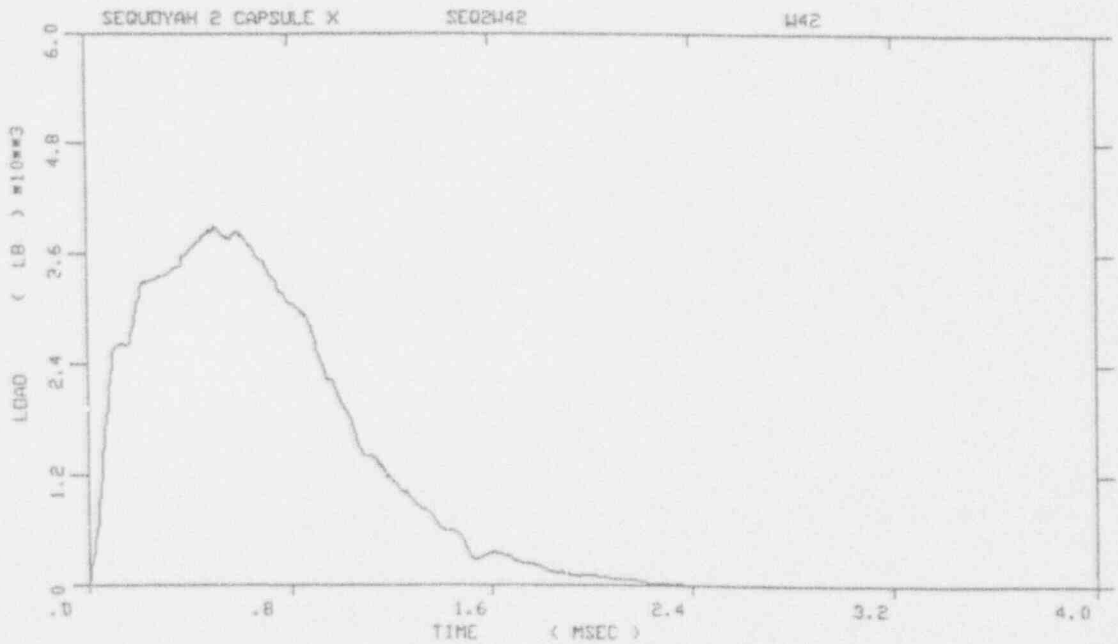

Sequoyah 2 Capsule X

Figure A-16. Load-time records for Specimens W43 and W42

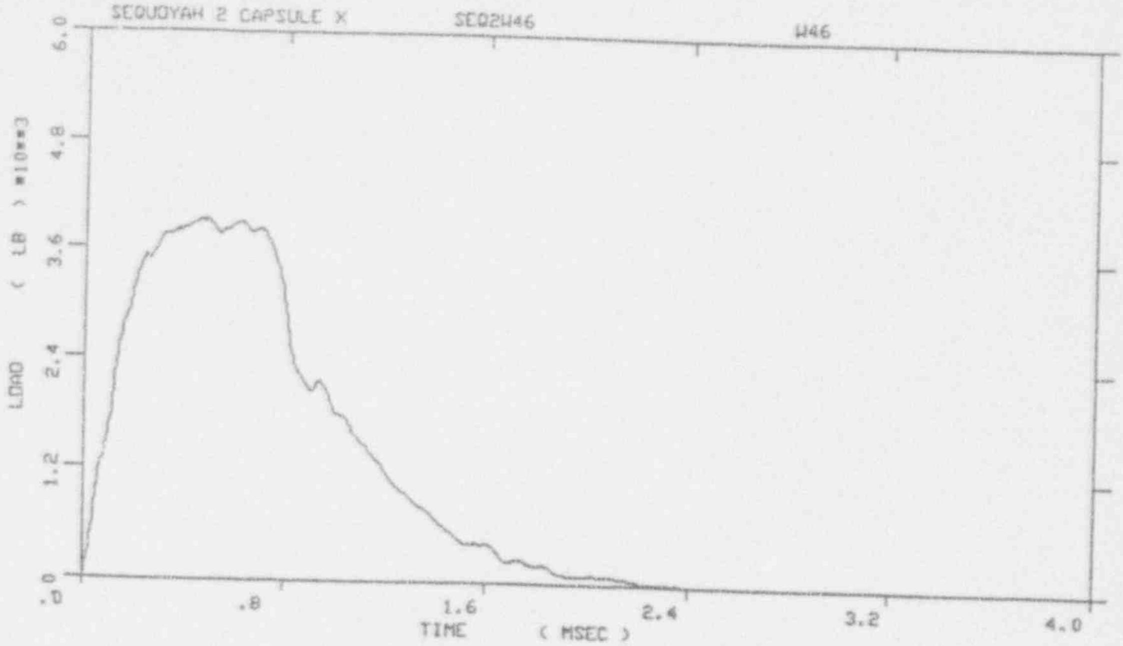

Sequoyah 2 Capsule X

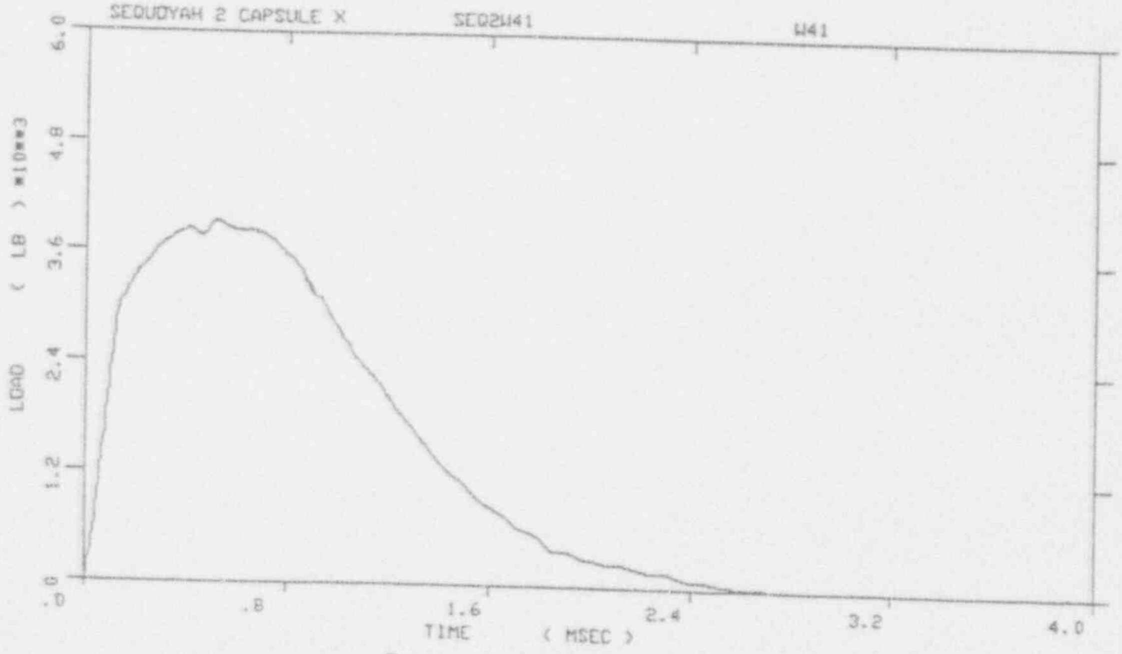

Sequoyah 2 Capsule X

Figure A-17. Load-time records for Specimens W46 and W41

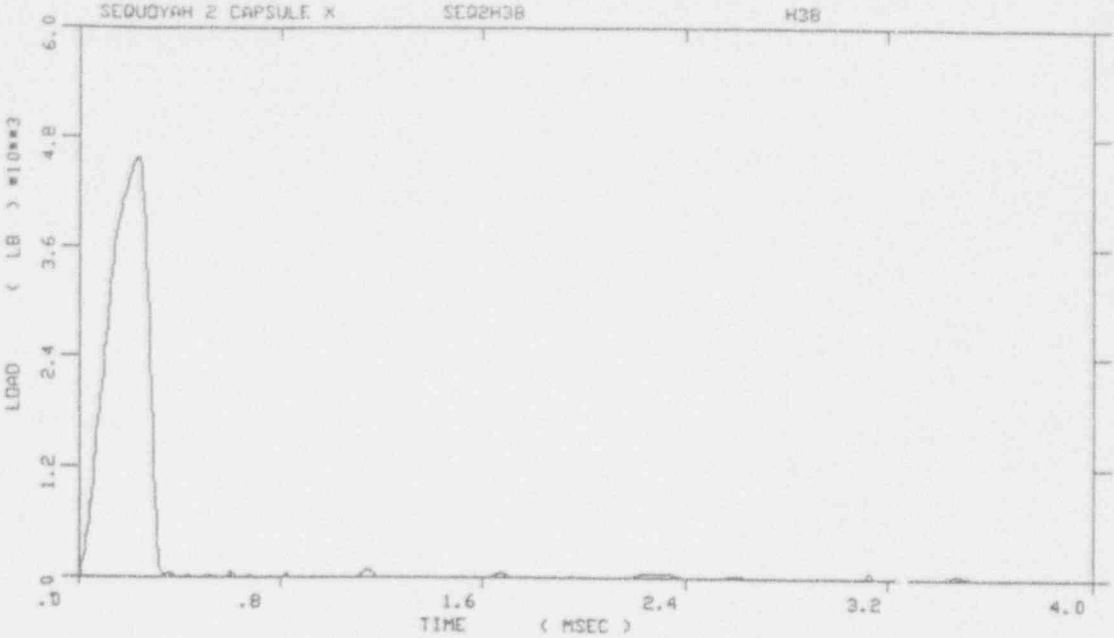

Sequoyah 2 Capsule X

H40
diagram is not available
due to computer malfunction

Figure A-18. Load-time records for Specimens H38 and H40

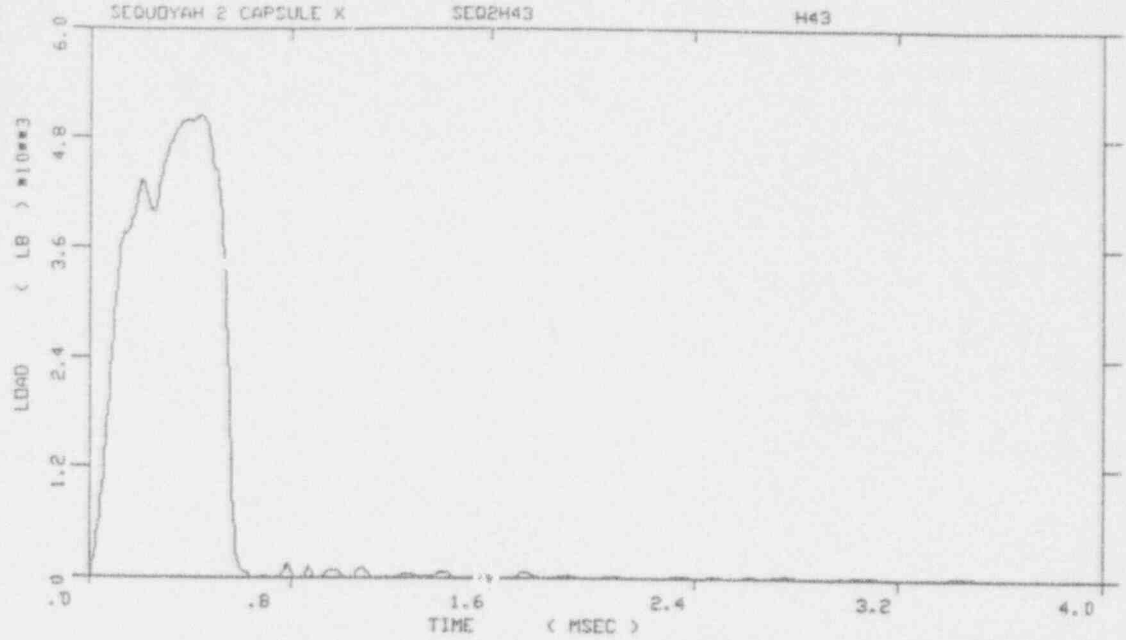

Sequoyah 2 Capsule X

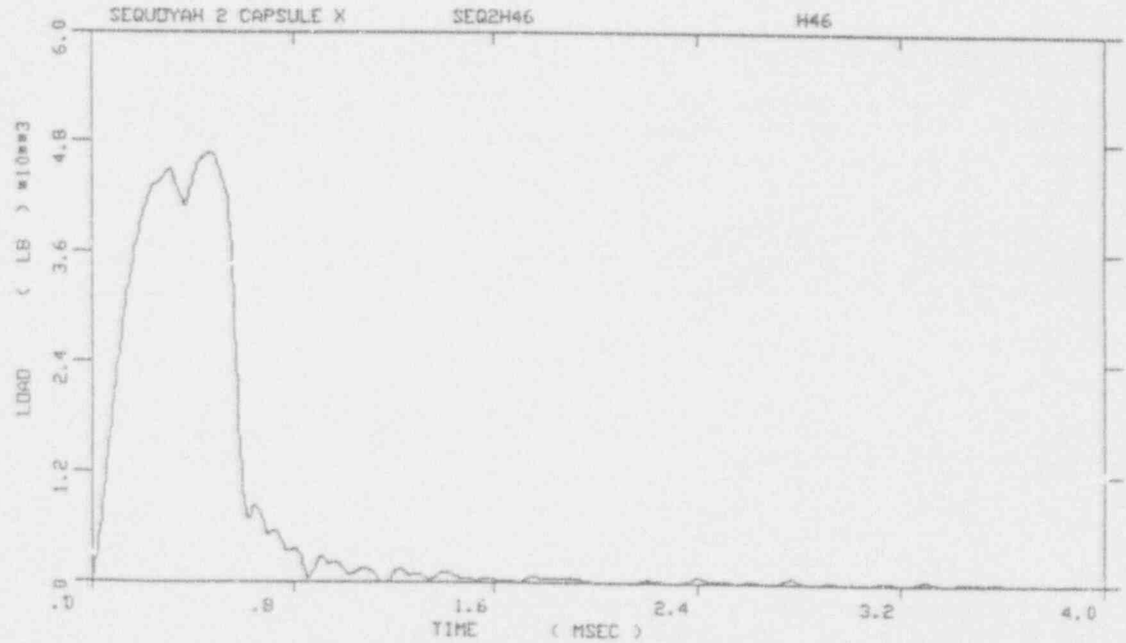

Sequoyah 2 Capsule X

Figure A-19. Load-time records for Specimens H43 and H46

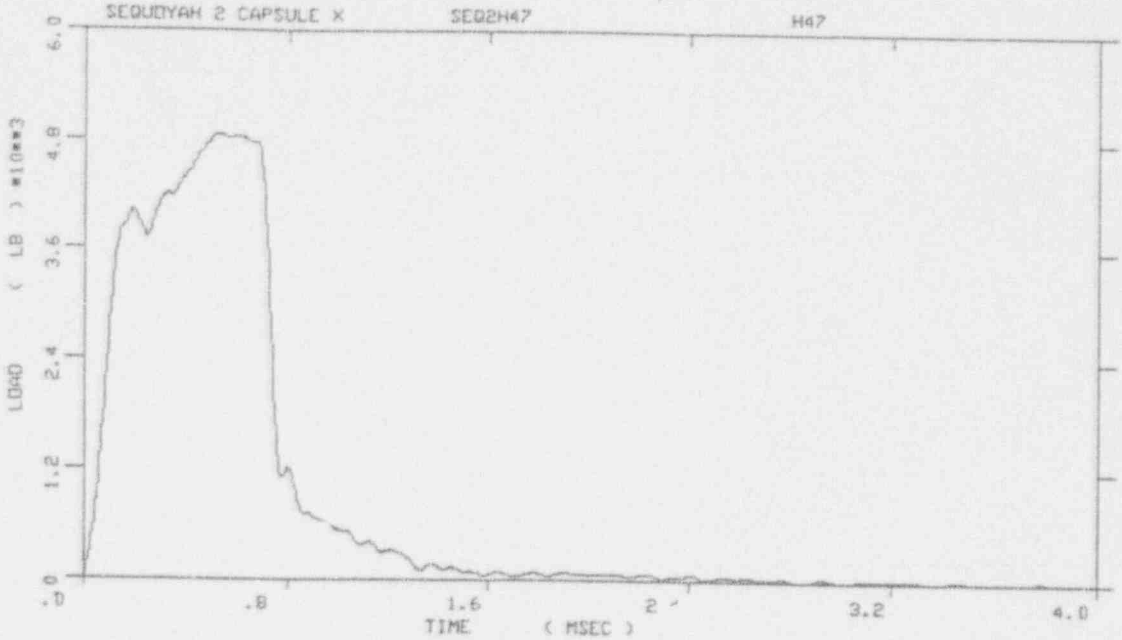

Sequoyah 2 Capsule X

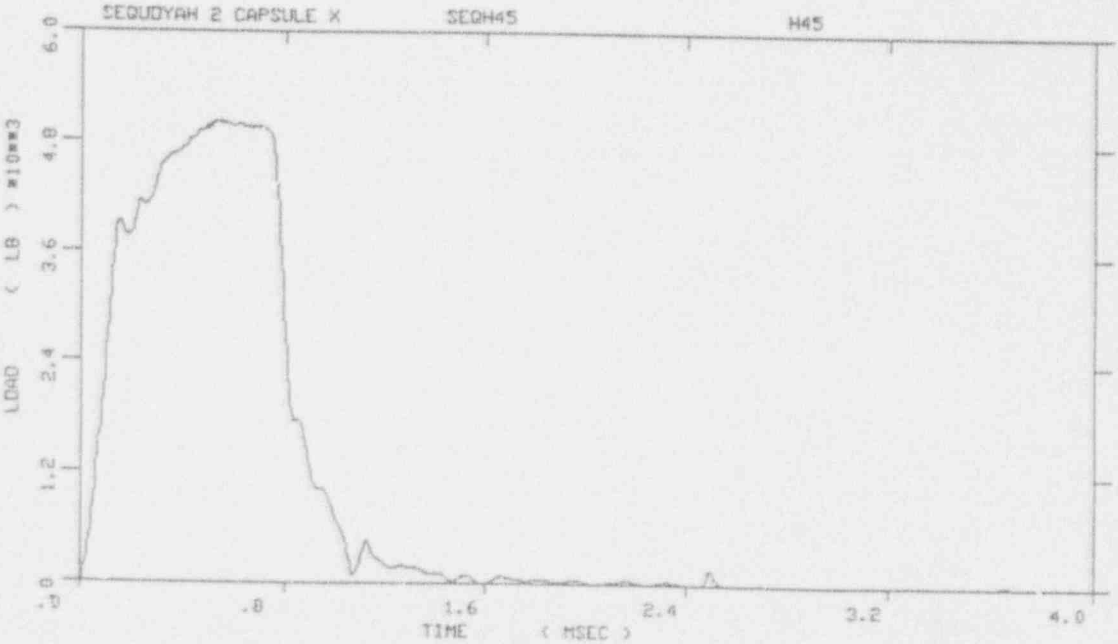

Sequoyah 2 Capsule X

Figure A-20. Load-time records for Spec. [illegible] and H45

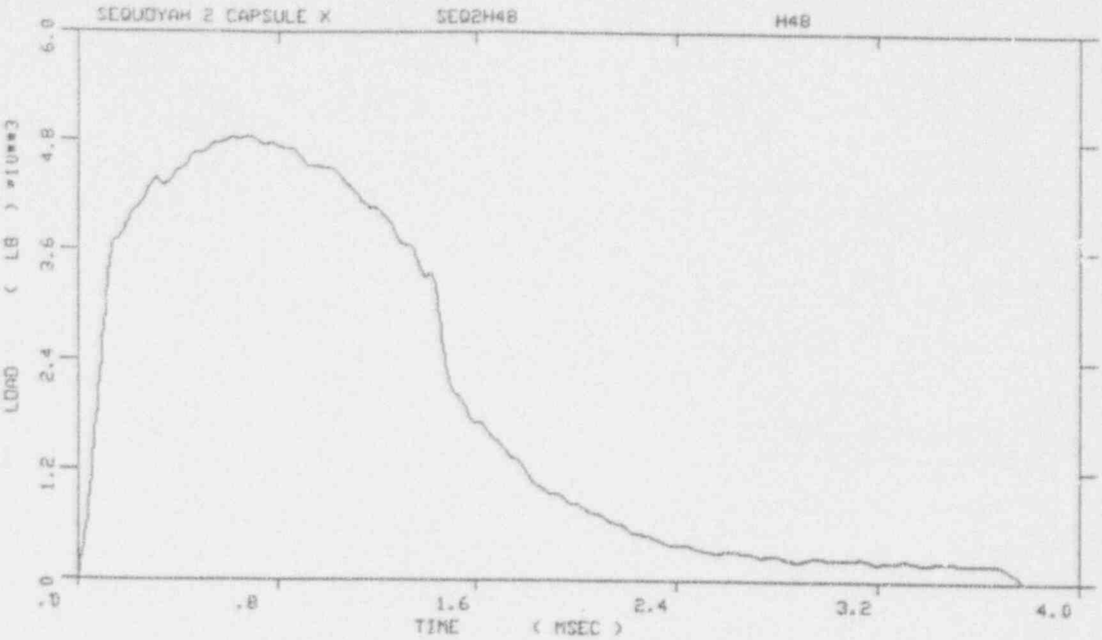

Sequoyah 2 Capsule X

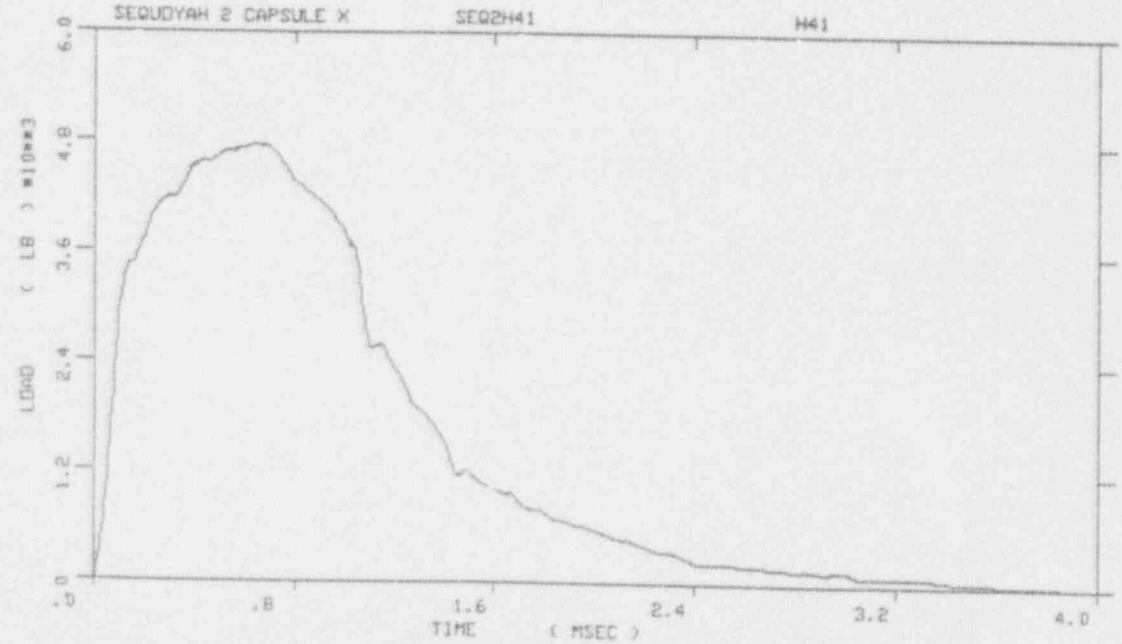

Sequoyah 2 Capsule X

Figure A-21. Load-time records for Specimens H48 and H41

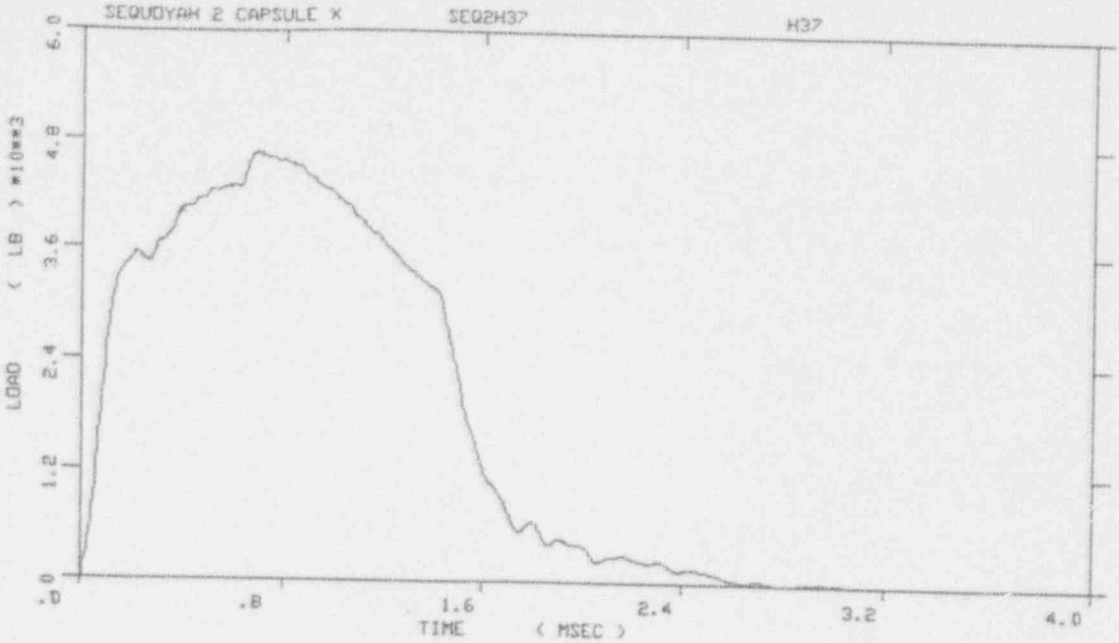

Sequoyah 2 Capsule X

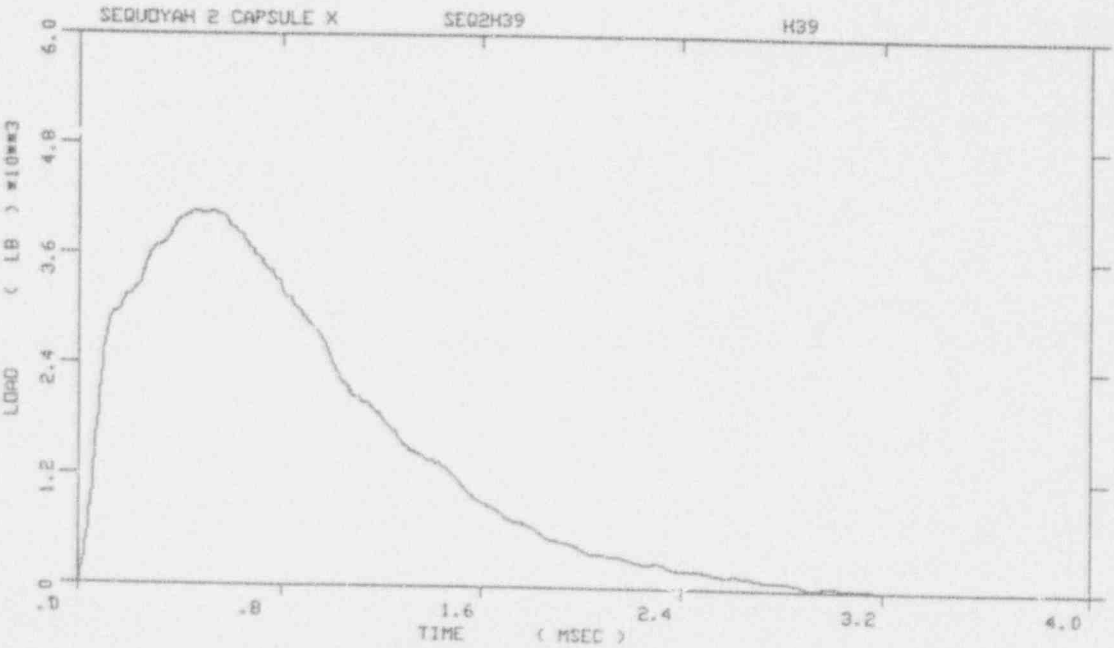

Sequoyah 2 Capsule X

Figure A-22. Load-time records for Specimens H37 and H39

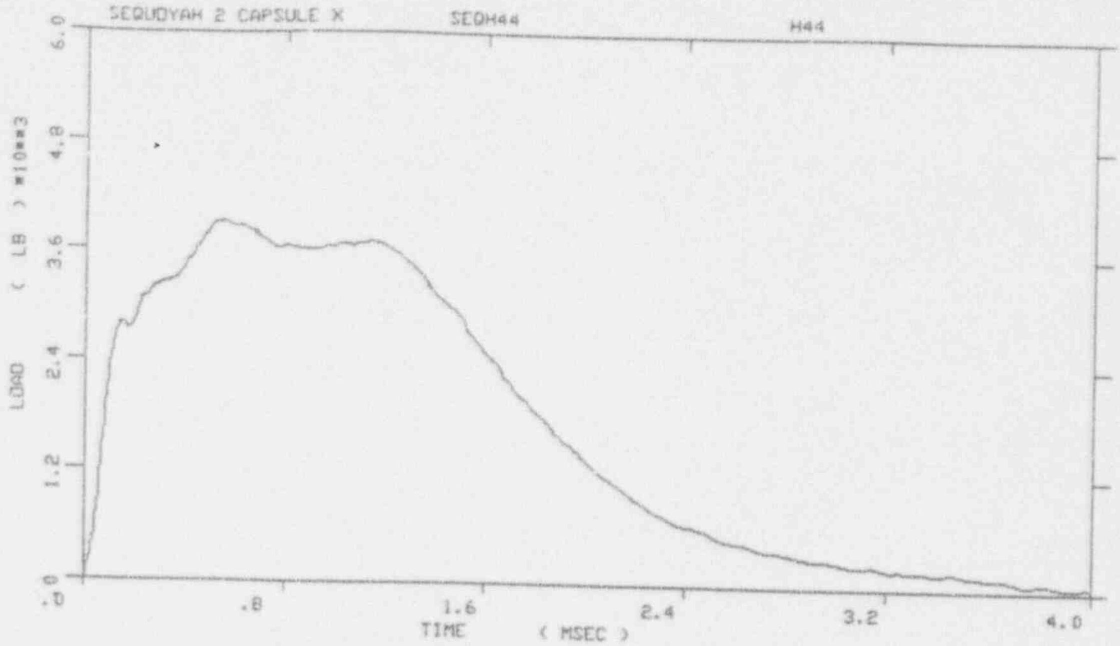

Sequoyah 2 Capsule X

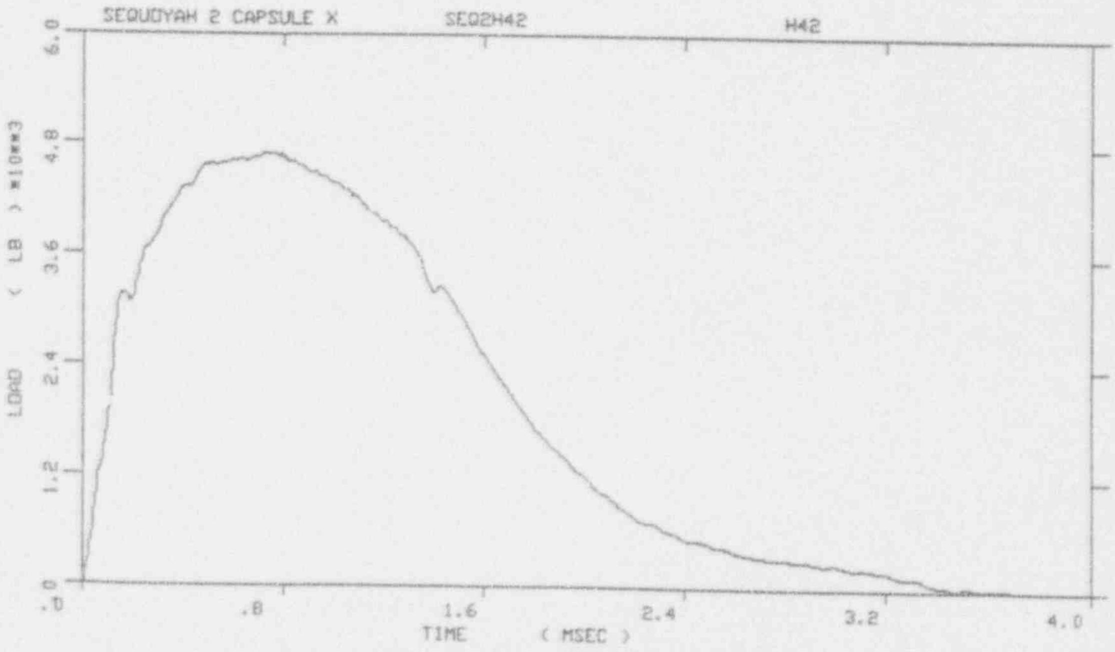

Sequoyah 2 Capsule X

Figure A-23. Load-time records for Specimens H44 and H42